Coagulation of Emulsion Polymers

Margarida Beatriz Fonseca Nunes Marques

Thesis to obtain the Master of Science Degree in

Chemical Engineering

Supervisors:

Prof.ª Maria do Rosário Gomes Ribeiro

Dr.ª Nida Sheibat Othman

Dr. Timothy McKenna

Examination Committee

Chairperson: Prof. Dr. João Carlos Moura Bordado

Supervisor: Prof.ª Maria do Rosário Gomes Ribeiro

Member of the Committee: Dr. Jorge Alberto Vigário Moniz dos Santos

December 2014

Acknowledgments

Foremost, I want to thank to my supervisor Prof. Dr.ª Maria do Rosário Ribeiro and Dr. Jorge Moniz dos Santos for accepting to examine my thesis. Many thanks also to Prof. Dr. João Bordado, president of the jury.

I'm extremely grateful to Dr.ª Nida Othman and Dr. Timothy McKenna for accepting me in their team and providing me all the conditions I needed to work.

I would like to thank to my colleague Ana Carolina Mendez for her kind support in my work. It was a great pleasure to work with you. Gracias Ana!

I am also indebted to all the LCPP and LAGEP personal for their steady support in the laboratory. I want to give a special thank you to Bárbara Rezende, Anthony Palmeira, Thiago Guimarães, Eliana Grant, Thaíssa Chaparro, Leila Santos, Aarón Sanz, Teresa Pinto and Andreia Nunes for providing me great moments during my stay in Lyon.

I cannot forget to thank all my friends in Portugal for the support through these last months.

Lastly, and most important, I want to thank to my parents for their endless love and constant support throughout my academic career.

Abstract

This thesis is a contribution to the study of coagulation of latexes produced by emulsion polymerization, more particularly the coagulation of polystyrene latexes, which were stabilized with sodium dodecyl sulfate (SDS). The stability of these polymer particles was analyzed by turbidity measurements. This research project was divided in two parts.

The first part was dedicated to the acquisition of experimental data about the influence of the particle size, solid content and particle size distribution on backscattering of light. The data was acquired in Turbiscan^{TM}Lab and Turbiscan^{TM}On Line and the results show that the backscattering increases with particle size and solid content and is more sensitive to bigger particles when two latexes with different particle sizes are mixed. The use of Turbiscan^{TM}On Line with the simple force of gravity to analyze latexes with a high solid content is not advisable, since they do not flow properly.

In the second part, the coagulation between polystyrene particles was provoked by electrolyte addition with the aim of analyze the effect of SDS concentration, solid content and particle size on Hamaker constant. The results show that this constant is sensitive to the slope of the curves of stability in function of electrolyte concentration, logW vs C_E. To complement this project, it were analyzed two more polystyrene latexes stabilized with a clay, in which the effect of the clay concentration on Hamaker constant was studied. It was observed again the sensitivity of this constant to the slope.

Key words: Emulsion polymerization, sodium dodecyl sulfate, turbidity, coagulation, slope, Hamaker constant.

.

Resumo

Este projecto, dividido em duas partes, pretende dar um contributo ao estudo da coagulação de latexes produzidos por polimerização em emulsão, mais particularmente da coagulação de latexes de polistireno, estabilizados com dodecil sulfato de sódio (SDS). A estabilidade das partículas foi analisada através de métodos de medição de turbidez.

A primeira parte foi dedicada à aquisição de dados experimentais sobre a influência do tamanho de partículas, do conteúdo de sólidos e da distribuição de tamanho de partículas na retrodifusão da luz. Para tal, foram utilizados o Turbiscan^{TM}Lab e Turbiscan^{TM}On Line. Os resultados mostram que a retrodifusão aumenta com o tamanho das partículas e com o conteúdo de sólidos, e é mais sensível às partículas de maiores dimensões quando dois latexes com diferentes tamanhos são misturados. O uso do Turbiscan^{TM}On Line para analisar latexes com conteúdo de sólidos mais elevado não é recomendável uma vez que estes não fluem apropriadamente.

Na segunda parte, a coagulação entre as partículas foi induzida através de várias adições de sal tendo como objectivo analisar o efeito da concentração de SDS, do conteúdo de sólidos e do tamanho das partículas na constante de Hamaker. Os resultados mostram que esta constante é sensível ao declive das curvas da estabilidade em função da concentração de electrólito, LogW vs $LogC_E$. Para enriquecer este projecto, foram analisados mais dois latexes de polistireno estabilizados com uma argila, a partir dos quais foi analisado o efeito da sua concentração na constante de Hamaker. Foi observado novamente a sensibilidade desta constante ao declive.

Palavras Chave: Polimerização em emulsão, dodecil sulfato de sódio, turbidez, coagulação, declive, constante de Hamaker.

Contents

List of figures

List of tables

Notations

A	Hamaker constant (J)
CCC	Critical coagulation concentration (mol/dm^3)
C_E	Electrolyte Concentration (mol/dm^3)
C_i	Concentration of the ionic species (mol/dm^3)
C_0	Initial concentration of electrolyte (mol/dm^3)
d	Average diameter (m)
D_n	Number-average diameter (m)
D_p	Particle diameter (nm)
$D_{t,avg}$	Translational diffusion coefficient
D_v	Volume-average diameter (m)
$D_{v,50}$	Median for a volume distribution (µm)
Dw	Weight-average diameter (m)
D_Z	Z-average (nm)
e	Electron charge (C)
g	Asymmetry efficiency factor
h	Height of the Turbiscan^{TM}Lab cell (mm)
I	Ionic force (mol/dm^3)
k_B	Boltzmann constant (J/K)
l^*	Penetration distance of the photon into the dispersion (m)
L	Distance between the surfaces of the two particles (m)
m_i	Mass of i-thype particles/species (g)
m_j	Mass of j-thype particles/species (g)
M_{total}	Total mass obtained after using the Turbiscan^{TM}On Line (g)

n_d	Refractive index of dispersed phase
n_f	Refractive index of aqueous phase
N_A	Avogadro's number
n_i	Number of particles with diameter d_i
Q_M	Mass flow (g/s)
Q_s	Extinction efficiency factor
r	Particle radius (m)
R	Center-to-center separation (m)
r_i	Diameter of particle i in a two-body collision (m)
r_j	Diameter of particle j in a two-body collision (m)
T	Temperature (K)
t	Time (s)
V	Total potencial energy (J)
V_A	Attraction potencial energy (J)
V_{added}	Volume of electrolyte in the solution after each addition (L)
V_R	Repulsion potencial energy (J)
V_T	Total volume reactor (dm^3)
V_0	Initial volume of latex (L)
W	Stability ratio
W_{ij}	Funch's stability ratio
Z_i	Valence of the ionic species
Z+	Valence of the counterions

Greek symbols

β_{ij}	Coagulation rate between ith- and jth-type particles (m^3/s)
Δ	Stern layer thickness (m)

ϵ	Aqueous phase permittivity ($C^2/N.m^2$)
ϵ_0	Vacuum permittivity ($C^2/N.m^2$)
ϵ_r	Water permittivity ($C^2/N.m^2$)
ζ	Zeta potencial (V)
η	Aqueous phase viscosity (kg/m.s)
κ	Debye-Hückel parameter (m^{-1})
σ	Surface density charge ($\mu C/cm^2$)
τ	Turbidity (m^{-1})
ϕ	Volume fraction
ϕc	Critical volume fraction
Ψ	Surface potential (V)

Abbreviations

CMC	Critical micellar concentration
CSTR	Continuous stirred tank reactor
CTBA	Cetyltrimethylammonium bromide
[clay]	Clay concentration
DLS	Dynamic Light scattering
DLVO	Deryaguin-Landau-Verwey-Overbeek
EP	Emulsion polymerization
f(m,t)dm	Particle fraction of particles of mass m to m+dm at time t
KPS	Potassium perfulfate
MLS	Multiple light scattering
NIR	Near infrared
PFR	Plug flow reactor

PSD	Particle size distribution
QELS	Quasi-Elastic Light Scattering
RPM	Revolutions per minute
SDS	Sodium dodecyl sulfate
[SDS]	Concentration of sodium dodecyl sulfate
SC	Solid content
%BS	Percentage of backscattering
%TS	Percentage of transmission

Introduction

Scope & Aim

Emulsion Polymerization (EP) is an important polymerization process used to prepare colloidal polymer particles dispersed in a continuous medium, most often known as latexes or emulsion polymers. It was first implemented at an industrial scale during World War II to overcome the urgent need for synthetic rubber and is nowadays employed to produce for example paints, adhesives and coatings. One of the reasons why this process is preferred is because the reaction medium (water) facilitates agitation and ease of heat and mass transfer whilst being environmentally-friendly, as well as providing an inherently safe process. However, modeling and simulation of emulsion polymerization is a challenging task due to the complex physico-chemical sub-processes exist within the multi-phase process.

Coagulation is the process by which particles become destabilized and begin to clump together. Is really important to understand the factors that influence the coagulation in order to reduce or eliminate the coagulum, since this phenomenon may have an adverse effect on the product quality and causes large costs for product loss, cleaning and reactor downtime.

The objective of the present work is to study the effect of some parameters on turbidity and on coagulation using a different device, Turbiscan^{TM}. To do so, it were chosen various systems of polystyrene produced by EP of styrene, using potassium persulfate as initiator and sodium dodecyl sulfate as surfactant. It was chosen this system because it's the one which appears to be the most similar to an ideal system. The dispersions so produced are monodisperse and a range of particle sizes can be obtained.

Outline of the Manuscrit

This thesis comprises 3 chapters: Chapter 1, which corresponds to the bibliography review of the aspects of emulsion polymerization and coagulation most relevant to this work; Chapter 2, which deals with the material, equipments, latex selection and procedures used and Chapter 3 which concerns the experimental investigation and respective treatment and discussion.

Chapter 1. Literature Review: Emulsion Polymerization and Coagulation

1.1. Polymers

Polymers are found in a large variety of products and their versatility in terms of end-use properties is due to the variety and complexity of the microstructure of the polymeric material (polymer and additives). This microstructure refers to the molecular and morphological characteristics of the polymer, and will be determined by the process and type of chemistry used to produce the polymer and the additives used. Chemical composition, monomer sequence distribution, molecular weight distribution, polymer architecture, chain configuration and morphology are the molecular characteristics of the polymer. [1]

Polymers are very high molecular weight materials formed by smaller structural units bound together by covalent bonds. Some natural materials such as cellulose and natural rubber are polymers. Besides these natural polymers, there are a lot of synthetic polymers, which are made by combination of small molecules (monomers) and additives. The reaction of monomers to form a polymer is called polymerization. The molecular and morphological characteristics change with the formulation (monomers, catalysts, initiators, etc), the polymerization process (reactor, polymerization technique) and conditions (temperature, concentrations, time). [1] The current study will deal only with emulsion polymerization, and readers are referred to references [2], [3] and [4] for a discussion of other types of polymerization processes.

1.2. Emulsion Polymerization

Conventional emulsion polymerization (EP) is a heterogeneous process used to carry out free-radical polymerization reactions[1]. A classical batch recipe contains: water, monomer(s), surfactant(s) and water soluble initiator(s)[2]. This process leads to colloidal polymer particles dispersed in a continuous medium, most often water (see figure 1). These polymeric dispersions are called latexes, emulsion polymers, polymer dispersions or polymer colloids. [1], [5], [6]

This kind of polymerization was developed for the first time in the 1920's with the objective of the production of synthetic rubber latexes as an alternative to the use of natural rubber latexes in tyre manufacture. [5]

[1] There is a detailed explanation of free radical polymerization in the appendix I.

[2] For more details about these components see section 1.2.2.

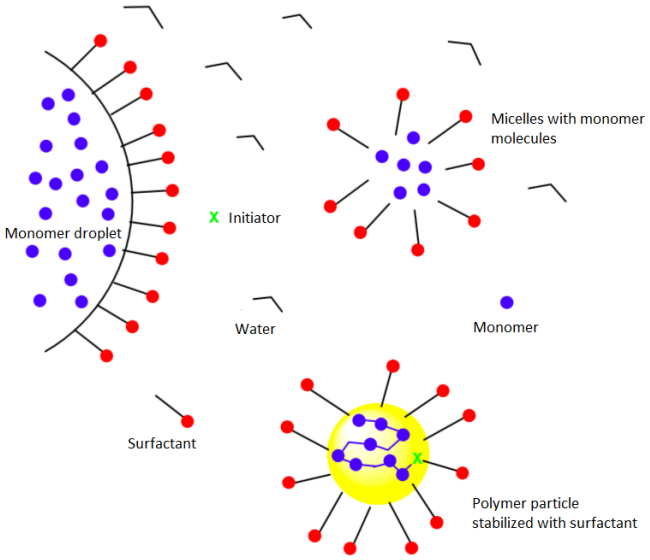

Figure 1: Emulsion polymerization. [Adapted from [7]]

1.2.1. Importance and advantages/disadvantages of emulsion polymerization

Among the different types of polymerization processes, EP is presently a very important process employed in industry to produce a different types of latexes with several uses such as paints and adhesives. [1]

Due to its multiphase nature and compartmentalization of the reaction sites, this kind of polymerization allows one to obtain high reaction rate (with respect to other types of free radical polymerization processes) and higher molecular weights at the same time. [1]

Latexes produced by emulsion polymerization can be commercialized either as aqueous dispersions sold “as-is” (or with additives) upon leaving the reactor, or as dry products in particle form. Both of these latexes are used in a large range of products, which can be seen in table 1. Carboxylated styrene-butadiene copolymers, acrylic and styrene acrylic latexes and vinyl acetate homopolymer and copolymers are examples of polymers classes used. [1]

Table 1: Synthetic emulsion polymers [1]

Latex	Applications
Carboxylated styrene-butadiene copolymers	Paper coating, carpet backing, adhesives, additives for mortar and bitumen
Acrylic and styrene acrylic latexes	Paints, adhesives, textiles, inks, leather treatment, paper coating
Vinyl acetate homopolymer and copolymers	Paints, adhesives for paper, wood and textiles

The advantage of an emulsion polymerization processes for many applications such as paper coatings, paints and adhesives is that very little post-reactor processing needs to be done.

EP is very important in different ways: makes products that can't be made by any other way; the resulting latexes have very low viscosity, even at high conversion – absolutely not the case with bulk polymerization – meaning that handling is easier, get better heat transfer, etc; most synthetic latexes are made with water as continuous medium, which is not toxic and acts as a good heat sink meaning that can tolerate fast reaction rates; often made in semi-batch processes so have lots of flexibility in terms of product slate.

Despite all the advantages of EP, there are some disadvantages. If it's necessary to recover the particles in dry form, they are often very small, so, the coagulation needs to be provoked. Also, the counterpart of having a low viscosity is that only 60% of the reactor space is actually polymer, the rest is water. This is acceptable for example for paints used as liquids, but not for dry products. Sometimes, there are issues related to particle stability and reactor stability that can be problematic.

1.2.2. Emulsion Polymerization components

As has been said before, EP is used to produce a large variety of polymers with different applications. The chemical composition is one of the factors that affect the form and properties of the final product. The components are added before or during the polymerization. There are two phases in an emulsion, the dispersed (oil) phase containing the monomers and other monomer-soluble components, and the continuous (aqueous) phase containing water-soluble components. [1], [5], [6], [7]

Next the main components of EP are briefly discussed.

a. Monomers and Comonomers

The choice of monomers should take into account the cost and the performance required for the intended application. The monomer cannot be completely miscible in water phase (otherwise it

would be a dispersion polymerization[3]) nor can it be completely insoluble (or conventional emulsion polymerization could not be proceeded). [5]

Most of the commercial emulsions use a system with more than one monomer (i.e., a comonomer system) with the aim of controlling the properties of the resulting polymer, called copolymer. Some examples of monomers used in EP are illustrated in figure below.

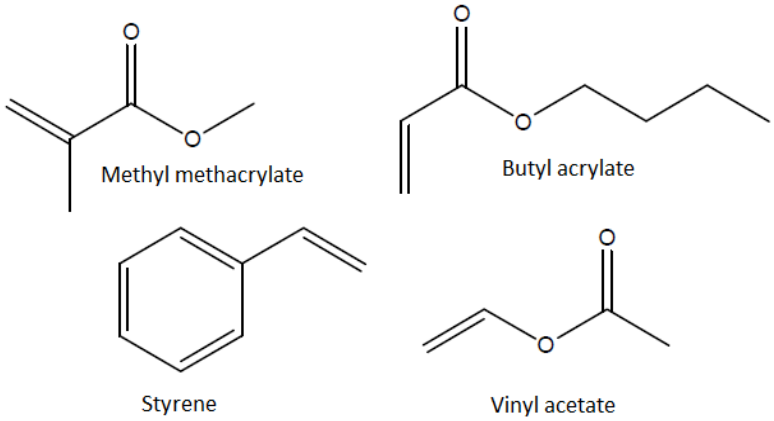

Figure 2: Examples of monomers used in emulsion polymerization.[Adapted from [7]]

b. Water

The water is the major component of the continuous phase[4]. Being a polar solvent, the solubility of monomers, which are non-polar, in water is limited allowing the dispersion of discrete monomer droplets. [5]

The use of water brings some advantages for the process, such as the extraction of large quantities of heat energy during polymerization due its high heat capacity and the rapid mixing and heat transfer resultant of its low viscosity. Furthermore, the water is inexpensive and has no negative effects on health or environment. [5]

c. Surfactants

The surfactant, also known as a stabilizer or emulsifier, is an amphiphilic molecule, which means that it has a hydrophobic and a hydrophilic section. This characteristic causes the partition between the two phases by adsorbing at the particle interface. When the surfactant is adsorbed at the

[3] Dispersion polymerization is an heterogeneous polymerization where the monomer is soluble in the continuous phase, but the resulting polymer is not.

[4] The other components of aqueous phase are initiator, surfactant and buffer.

interface, it keeps the particles separated since they are repelled due the electrostatic and/or steric stabilization mechanisms. [5], [7]

Since the surfactants are surface active, they lower the interfacial tension between the water and monomer phases, what allows an easier formation of smaller droplets, avoiding at the same time the coalescence. [5]

For all this reasons, the use of surfactant is very important to prepare more colloidally stable emulsions. The surfactant can also be used to control the particle size. However, the use of this component must be made very carefully, because adding too much surfactant could nucleate additional/unwanted particles and affect the water sensitivity of films formed from latexes.

The surfactants can be anionic (such as sodium dodecyl sulfate-SDS), cationic (such as cetyltrimethylammonium bromide-CTAB) or nonionic (such as the polyoxyethylenated alkylphenols). It's usual to mix anionic and nonionic surfactants in the same recipe to provide additional stability. Mixtures of anionic and cationic surfactants are to be avoided because they tend to coagulate. There are same surfactants that contain reactive groups that function as initiators (inisurfs) or chain transfer agents (transurfs). [5]

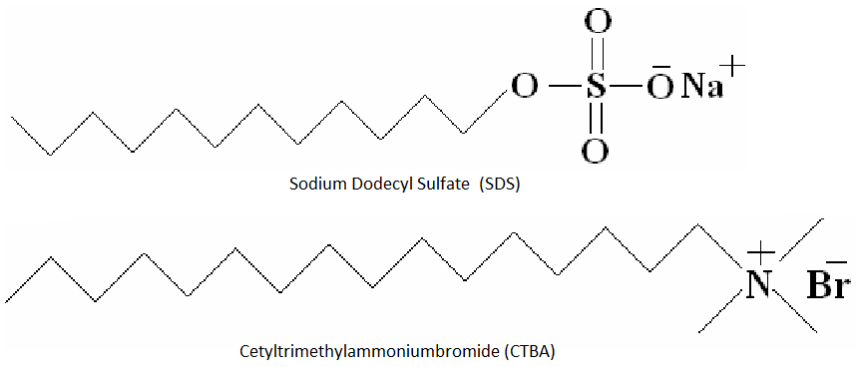

Figure 3: Examples of surfactants used in emulsion polymerization. [8] and [9]

d. Initiators

The initiator nucleates the particles and provides a radical flux during all the polymerization. The choice of initiator must take into account the partitioning between the oil and the aqueous phases and its half-time. [5]

Some initiators, e.g. persulfates are salts that dissociate and produce ionically charged radicals, and are water-soluble. Others are nonionic and have a range of water solubilities and there is also some that are strictly oil-soluble, such as, hydroperoxides and benzoyl peroxide, respectively.

The persulfates are very useful in EP and persulfate-initiated latexes have an enhanced anionic surface charge that promotes colloidal stability.

The components described above are the most important ones and are used in all EP reactions. However, there are other components that can be added to achieve the desired properties, such as crosslinkers (to improve chemical and mechanical properties), chain transfer agents (to control the molecular weight of the polymer), buffers (to moderate the pH of the aqueous phase and the stability of the particles), rheology modifiers (to control the viscosity) and others. [5]

1.2.3. Process description

The first theory of the mechanisms of EP is attributed to Harkins [10]. According to this theory, batch EP is divided into 3 intervals, comprising a particle formation stage (interval I) and two particle growth stages (intervals I and III). It is known that Harkins' model has some limitations. However, it is very useful for understanding the key steps of EP. This classical interval division can be seen in figure 4.

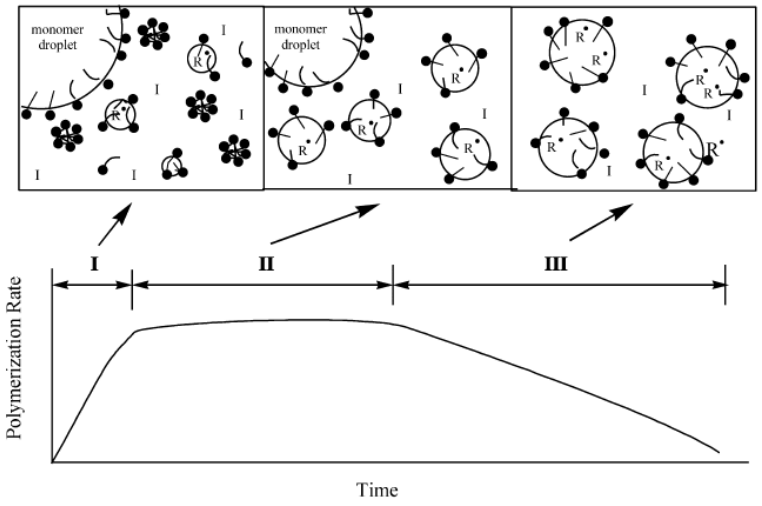

Figure 4: Intervals in emulsion polymerization. I corresponds to the initiator [12]

The initial reaction mixture consists of a continuous aqueous phase in which initiator, some surfactant, some monomer(s) (and eventually other components such as buffers, electrolytes or chain-transfer agents) are dissolved, and a dispersion of monomer droplets in which any hydrophobic species present in the reactor might be dissolved. Surfactants are amphiphilic species that can dissolved in the water to a limited degree, but beyond the critical micelle concentration (CMC) they form micelles (aggregates, in this case, of surfactant), which are structures where the hydrophobic part

of the molecule is oriented inwards, and the hydrophillic bits outward (see figure 5). The monomer actually partitions between the monomer droplets, the water and the micelles. [5],[6], [7]

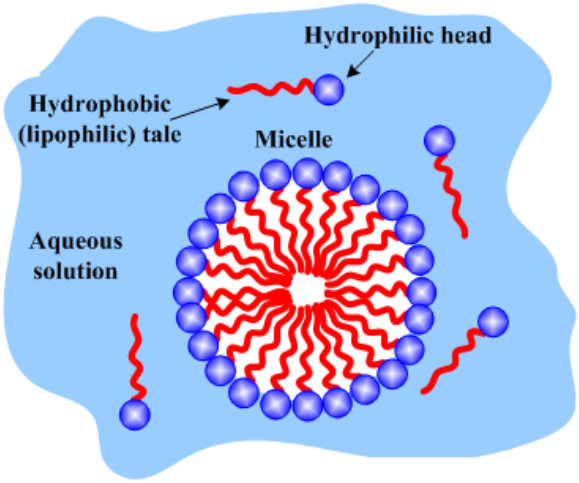

Figure 5: Hydrophobic and hydrophilic tale of a surfactant molecule and a the formation of a micelle. [Adpated from [11]]

As the initiator decomposes, primary radicals are generated which react with monomer dissolved in the aqueous phase to form oligoradicals. These oligoradicals continue to polymerize until they are too long to remain soluble in the water. In the Harkins model of micellar nucleation, the insoluble oligoradicals now look for a hydrophobic phase, and thus enter into the micelles containing dissolved monomer, or into polymer particles containing monomer. If the oligoradical enters a micelle, it immediately begins to polymerize and converts the micelle into a polymer particle. This is referred to as micellar nucleation. As the particles created this way grow, they need surfactant to stabilize the new surface. Thus particle growth can also consume some of the micelles present in the reactor. Micellar nucleation continues until all of the micelles are consumed. This point corresponds to the end of Interval I. [5], [6]

It is also possible that rather than penetrating a micelle or a polymer particle, the insoluble oligoradical can precipitate out of solution. If this happens, the precipitated chains can coagulate amongst themselves to form new polymer particles. This is referred to as homogeneous (coagulative) nucleation. This last mechanism can occur above or below the CMC and can thus be present throughout the reaction. [5], [6]

If we can neglect homogenous nucleation, the number of polymer particles will ideally remain fixed during intervals II and III. In addition it is difficult to swell the polymer particles beyond a certain point as well. This means that as long as there are monomer droplets in the reactor (i.e. interval II) the concentration of monomer in the particle is constant. A constant number of particles and a constant monomer concentration in the particles contribute to the fact that the reaction rate is said to remain constant during interval II. This stage ends when there are no more monomer droplets to saturate the aqueous phase and the latex particles. [5], [6]

During interval III, the concentrations of monomer in the aqueous phase and latex particles drop off. The rate of polymerization tends to lower due to the decrease of monomer concentration in the particles. [5], [6]

This process description is illustrated in figure 6. It's important to notice that this simple description of EP does not apply for every possible situation.

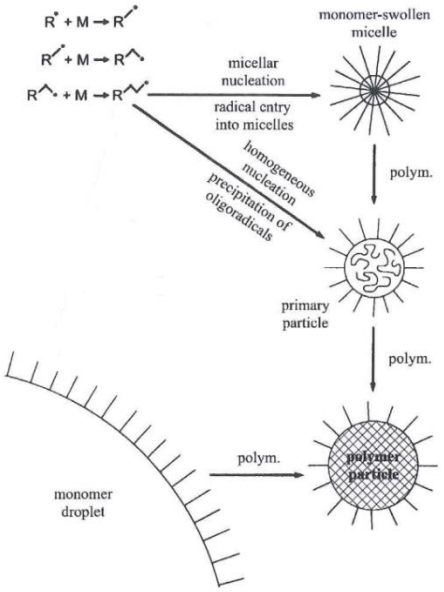

Figure 6: Nucleation mechanisms. [Adapetd from[5]]

1.2.4. Emulsion Polymerization processes

The microstructure of emulsion polymers is determined in the reactor. Thus, the reactor type used should be adequate to prepare many different grades in the same reactor and be adaptable to a large range of production rate. [1]

The semi-continuous, or semi-batch, stirred-tank reactor is the most used since it fulfils better the requirements. Batch, Semi-continuous and continuous reactors are shown in figure 7.

a) Batch

In this polymerization method all the components are added into a stirred reactor at the same time, i.e., no more material is added or removed during the reaction. To begin the polymerization, the reactor is heated.

Batch polymerizations are implemented in screening experiments on the laboratory-scale level. In large-scale, this method is used less often due the limitations in controlling the recipe and temperature. [1], [5]

b) Semi-Continuous/Semi-Batch

The semi-continuous, or semi-batch, method is the most widely used technology for emulsion polymerizations. The reaction takes place in a stirred-tank reactor. [1], [5]

In a typical semi-continuous process, there are two stages: the seeding stage and the feeding stage. In the first stage, a fraction of the formulation is charged in the reactor and heated. After this, the initiator is added. In this step, most of the polymer particles are formed. In the second stage, the rest of the monomer is continuously fed to the reactor (to supply monomer to the polymerizing particles) over some period of time. [1], [5]

The great advantage of this method is the flexibility. Varying the composition and amount of initial charge, as well as the composition and flow rates of the feeds, the temperature and polymer quality can be controlled. The main disadvantage is the relatively low productivity, which is compensated by using larger reactors (up to 60 m^3). [1], [5]

c) Continuous

In this process, the monomer emulsion is fed at a constant rate to a reactor in which the polymerization occurs and from which the final polymer is continuously removed.

The reactor conditions do not change with time, which means that the polymerization is run at steady state, so that the final product is consistent, unlike what happens in batch polymerizations. In addition, the production rates are higher and heat removal is more effectively controlled than in batch reactions. [1], [5]

The continuous polymerizations found in industry typically employ a cascade of up to 8 continuous stirred tank reactors (CSTRs). CSTRs are large tanks that are ideally well-mixed and are operated at constant overall conversions. It is very rare to find a continuous process using a tubular reactor for EP. This is because the high surface per unit volume of a tube, while good for heat transfer, tends to pose problems related to the destabilization of latexes. Plugging could lead to expensive and dangerous situations. [1], [5]

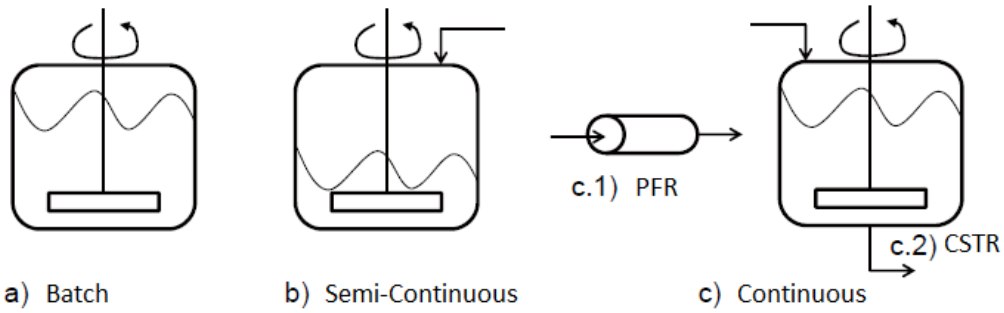

Figure 7: Reactors used in the manufacture of polymers with different modes of operation. [Adapted from [7]]

1.3. Colloidal stability – latex coagulation

Coagulation leads to the formation of larger particle aggregates from smaller particles and/or individual particles in a colloidal dispersion. Is of major importance to understand the factors that influence the coagulation in order to reduce or eliminate the coagulum. Colloidal stability is an important issue to master during an EP process. In the reaction or the plant, undesirable coagulation can be a problem when the latex is sheared through pumping or mixing; when the latex is frozen and then thawed; when additives are introduced into the latex and when the latex is stored for long periods of time at different temperatures. The formation of lumps due to coagulation can lead to reactor shut down, or degrade latex properties, plug lines and filters, and cost money since they need to be removed (if possible).[1], [5], [13], [14]

When latexes are formed by EP, the free energy at the interface between the colloidal particles and the continuous phase increases. This increase is significant in latexes with small particle sizes and large interfacial areas. The decrease of the interfacial free energy is thermodynamically favorable and causes the coagulation of latex, which is undesirable. One of the principal roles of the surfactant is to overcome this problem. [5]

The two major destabilization phenomena that affect the homogeneity of dispersions are particle migration (creaming, sedimentation) and particle size variation or aggregation (coalescence, flocculation). Unlike creaming and sedimentation, coalescence and flocculation are not reversible. Thus, it is very important to detect these phenomena at an early stage. [13], [14]

Currently, the techniques used to detect physical destabilization are the naked eye or analytical methods, which are more accurate and reliable, such as microscopy, spectroscopy, turbidity and particle size analysis.

1.3.1. Particle size and size distribution

The particle size distribution (PSD) of a latex is one of the main parameters that influences the final quality of latex. The PSD contributes to the surface aspects of films made from the latex, plays a role in the reaction kinetics, influences reaction stability, and can have an impact downstream on the way in which additives are absorbed, etc. High solid content latexes are an example of a product that requires an accurate control of the PSD, since their formulation usually requires a very well-defined PSD in order to maintain acceptable levels of viscosity.

The latex particles are not always uniform in size (monodisperse). It's common to find a distribution of particle diameters in the same latex. Bimodal and multimodal particle size distributions are the result of secondary nucleation. Figure 8 shows a typical representation of a PSD for a monodisperse sample in which the number percentage is a function of particle diameter.

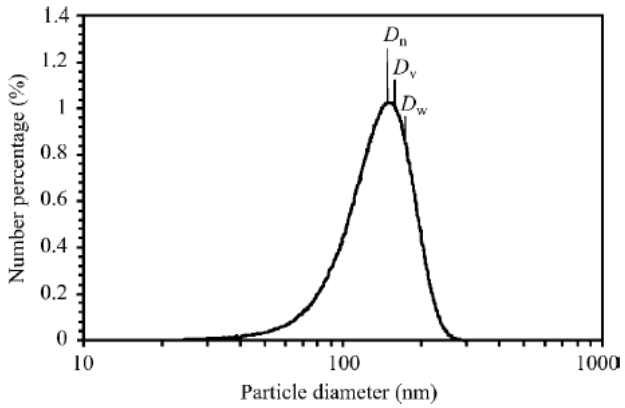

Figure 8: Typical particle size distribution for latex particles.[5]

The particle diameters are expressed in terms of averages, the most important being the number average diameter (D_n), the volume-average diameter (D_v) and the weight-average diameter (D_w). These three average diameters are calculated by the following equations: [5]

$$D_n = \frac{\sum n_i d_i}{\sum n_i} \quad (1)$$

$$D_v = \left(\frac{\sum n_i {d_i}^3}{\sum n_i}\right)^{1/3} \quad (2)$$

$$D_w = \frac{\sum n_i {d_i}^4}{\sum n_i {d_i}^3} \quad (3)$$

Where n_i is the number of particles with diameter d_i.

There are three major group techniques that can be used to measure the particle size and PSD. These techniques are based on microscopy (optical microscopy, electron microscopy, flow ultramicroscopy, dark field microscopy), light scattering (dynamic light scattering - DLS, laser diffraction) or on the movement of the particles (fractional creaming, disc centrifuge sedimentation, microfiltration, hydrodynamic chromatography, electrozone sensing). The choice of method to use depends on the size range of interest, the effort required, and the accuracy desired. [5]

If the stability of the particles is controlled during the formation and growth of the polymer particles, it's possible to control the particle size and the PSD. To do so, it's necessary to quantify the role of the concentration and the types of surfactant and initiator species in providing the desired polymer characteristics. This influence of the surfactant and initiator species can be predicted through mathematical models that describe coagulation rates between polymer particles as a function of the particle size and operation conditions. [15], [16]

The electrostatic stabilization model (described in section 1.3.2) and balance populations can be used to describe the distribution of particle size. In this approach, coagulation rate between the particles, β, must be determined for particles of different sizes. The model must accurately predict the coagulation based on their particle size to well represent the mean diameter, the mean number of particles of the latex and the PSD. For systems where the coagulation of particles is the only phenomenon that affects the density function, the balance populations, or the evolution of the PSD, is determined by[5]: [16]

$$\frac{\partial f(m_i,t)}{\partial t} = -\frac{f(m_i,t)}{V_T}\int_{m_0}^{m_f}\beta(m_i,m_j)f(m_i,t)dm_j + \frac{1}{2V_T}\int_{m_0}^{m_i-m_0}\beta(m_i-m_j,m_j)f(m_i-m_j,t)f(m_j,t)dm_j \qquad (4)$$

Where f(m,t)dm, V_T and $\beta(m_i,m_j)$ corresponds to the fraction of particles with mass between m and m+dm (or density function); the reaction volume and the coagulation rate between two particles of masses m_i and m_j, respectively. The best way to determine β is to use the DLVO theory.

1.3.2. Electrostatic stabilization Model- DLVO theory

The colloidal properties of polymer latexes are determined by interactions between particles. If the latex is stabilized with ionic surfactants or/and charged groups on the surface of the particles (e.g., sulfate groups from initiators), the stabilization mechanism is based on the creation of electrostatic repulsive forces between polymer particles. The ionic species adsorb onto the particle surface, form a charged layer near the surface. The surface charges are in equilibrium with counterions in both inner

[5] Valid only if coagulation occurs through 2-body collisions.

and diffuse regions of the electrical double layer. These regions are called Stern region and Gouy-Chapman region, respectively. In the Stern region the counterions are strongly adsorbed onto ions of the particle surface. On the other hand, in the Gouy-Chapman region the counterions are freely distributed due to the lower attractive force between surface ions and counterions. [15], [16]

Deryaguin, Landau, Verwey and Oberbeek (DLVO) used the representation described above to establish the DLVO theory with the aim to determine the interaction energy between two charged particles. This theory is applied to electrically charged surfaces submerged in a diluted solution of salts.

According to this theory, the total potential energy of interaction (V) can be determined as the sum of the attraction energy (V_A) and the repulsion energy (V_R): [15], [16]

$$V = V_A + V_R \qquad (5)$$

The attractive forces between polymer particles come from the interaction between the temporary dipole on one molecule and the induced on a neighboring one. The attractive energy is proportional to the semiempirical Hamaker constant, A, which depends on the polymer, the polarizability of atoms or molecules and the medium in which the particles are dispersed. This energy between two particles of radium r_i and r_j can be determined by the following equation according to Hamaker: [15], [16]

$$V_A = -\frac{A}{6}\left[\frac{2r_i r_j}{R^2 - \left(r_i + r_j\right)^2} + \frac{2r_i r_j}{R^2 - \left(r_i - r_j\right)^2} + ln\left(\frac{R^2 - \left(r_i + r_j\right)^2}{R^2 - \left(r_i - r_j\right)^2}\right)\right] \qquad (6)$$

Where R is the distance between the center of the particles.

The repulsive energy potential is calculated by the following equation proposed by Hogg et al, which depends on zeta potential, ζ, of each particle, on the Debye-Hückel parameter, κ, on the distance between the surfaces of the two particles, L, and on the permittivity ε. [15], [16]

$$V_R = \frac{\epsilon r_i r_j (\zeta_i{}^2 + \zeta_j{}^2)}{4(r_i + r_j)}\left\{\frac{2\zeta_i\zeta_j}{\zeta_i{}^2 + \zeta_j{}^2} ln\left(\frac{1 + \exp(-\kappa L)}{1 - \exp(-\kappa L)}\right) + \ln(1 - \exp(-\kappa L))\right\} \qquad (7)$$

The permittivity constant of the aqueous phase, ε, is a function of the permittivity constant of vacuum, ε_0, and water, ε_r. [15], [16]

$$\epsilon = 4\pi\epsilon_0\epsilon_r \qquad (8)$$

The distance between the surfaces of the two particles and the Debye-Hückel parameter are given by: [15], [16]

$$L = R - \left(r_i + r_j\right) \quad (9)$$

$$\kappa = \left(\frac{8\pi N_A I e^2}{\epsilon k_B T}\right)^{0.5} \quad (10)$$

Where N_A is the Avogadro's number, I the ionic force (equation 11), *e* the electron charge, k_B the Boltzmann constant and T the temperature.

$$I = \sum_{i=1}^{n} C_i {z_i}^2 \quad (11)$$

C_i and z_i are the concentration and the valence of the ionic species, respectively.

The zeta potentials are determined as a function of the surface potential, ψ, and the Stern layer thickness, Δ, by the following equations: [15], [16]

$$\zeta = \frac{2k_B T}{z_+ e} ln\left[\frac{\exp(\lambda_4) + 1}{\exp(\lambda_4) - 1}\right] \quad (12)$$

$$\lambda_4 = k\Delta + ln\left[\frac{\exp(\lambda_5) + 1}{\exp(\lambda_5) - 1}\right] \quad (13)$$

$$\lambda_5 = \frac{z_+ e\psi}{2k_B T} \quad (14)$$

Where the z_+ corresponds to the valence of the counterions.

The surface potential, Ψ, is proportional to the surface charge density, σ. If κr is lower than 1, spherical surfaces may be approximated to plate surfaces and use the approach proposed by Verwey and Overbeek (equation 15). On the other hand, if the product κr is higher than 1, spherical geometry has to be assumed and the surfaces potentials are calculated by the equation 16. R corresponds to the particle radius. [15], [16]

$$\psi = \frac{4\pi r\sigma}{\epsilon(1 + kr)} \quad (15)$$

$$\psi = \frac{2k_BT}{e}\sinh^{-1}\left(\frac{2\pi re\sigma}{\epsilon k k_BT}\right) \quad (16)$$

Finally, the coagulation rate of two particles of size i and j (β_{ij}) is related to Funch's stability ratio (W_{ij}): [15], [16]

$$W_{ij} = 2(r_i + r_j)\int_0^{\infty} \frac{\exp\left(\frac{V}{k_BT}\right)}{R^2} dR \quad (17)$$

$$\beta_{ij} = \beta_{ji} = \frac{2k_BT}{3\eta W_{ij}}\frac{(r_i + r_j)^2}{r_i r_j} \quad (18)$$

Where η is the viscosity of the medium.

The Hamaker constant is the only parameter that can be adjustable for the determination of the force balance between the polymer particles and the coagulation rates calculated in the DLVO model. This is why it's possible to use the model and experimental data to fit reasonable values for A. Since the Hamaker constant is related to attractive forces between the polymer particles, low values of this constant correspond to a higher stability of polymer particles due to the decrease of the attractive forces. [15], [16]

1.3.3. Turbidity

The models can be validated with experiments in which coagulation between polymer particles is induced by electrolyte addition. The stability/instability of polymer latexes can be evaluated with turbidity measurements using, for example, a device called Turbiscan™ Lab.

The Turbiscan™ technology was introduced more than 15 years ago with the aim to analyze quickly and accurately the stability of concentrated dispersions such as emulsions, suspensions and foams. The Turbiscan™Lab is the spearhead of the Turbiscan™ range to make this kind of measurements. [17]

The Turbiscan™ uses multiple light scattering (MLS) to characterize concentrated liquid dispersions without dilution. The multiple light scattering consists of sending photons into the sample, using a pulsed near infrared light source (NIR, λ=880 nm). [17], [18]

The most important item in the Turbiscan™ Lab is a detection head which moves up and down along a flat-bottom cylindrical glass cell, where the sample is inserted. It is in this head that is located the NIR light source and two synchronous detectors, which can be seen in figure 9. The photons, after being scattered many times by the particles in the dispersion, emerge from the sample and are detected by the two detectors. The transmission detector (0º from light source) receives the light which goes through the sample, and the backscattering detector (135º from light source) receives

the light scattered backward by the sample. With the Turbiscan^{TM}Lab it's possible to regulate the temperature between 4 and 60ºC. [13], [14], [17], [18]

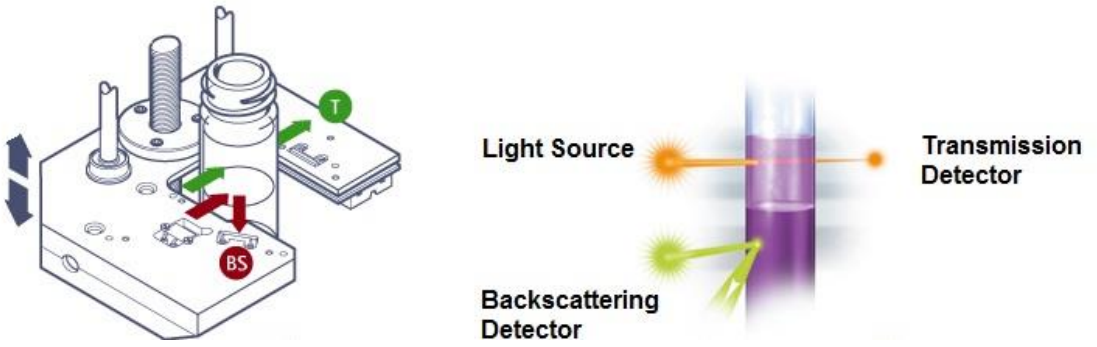

Figure 9: Principle of Turbiscan^{TM} measurement. [Adapted from [17], [18]]

With Turbiscan^{TM}Lab, it's possible to choose two modes of measurements:

❖ Scan mode: The detection head scans the entire glass cell (from height = 0 to 55 mm) at various programmed times, acquiring transmission and backscattering data every 40µm. This mode is the most complete for the detection of migration phenomena, such as creaming and sedimentation. [17], [18]

Creaming is an instability phenomenon that occurs when the density of the dispersed phase is lower than the density of the continuous phase. It may be coupled to the flocculation (irreversible and consists in aggregation of particles) or coalescence (irreversible, leads to the merging of interfaces and the creation of a single drop). Both this phenomenon lead to an increase in particle size, which is easily recognized by the Turbiscan^{TM} because it causes a decrease in backscattering along the entire height of the sample. Creaming is also easy to detected because it provokes an increase in backscattering in the top of the cell. [17], [18]

On the other hand, sedimentation occurs when the density of the continuous phase is lower than the density of the dispersed phase. Sedimentation makes that the backscattering increases in the bottom of the cell. [17], [18]

All these phenomenon can be seen in figure 10.

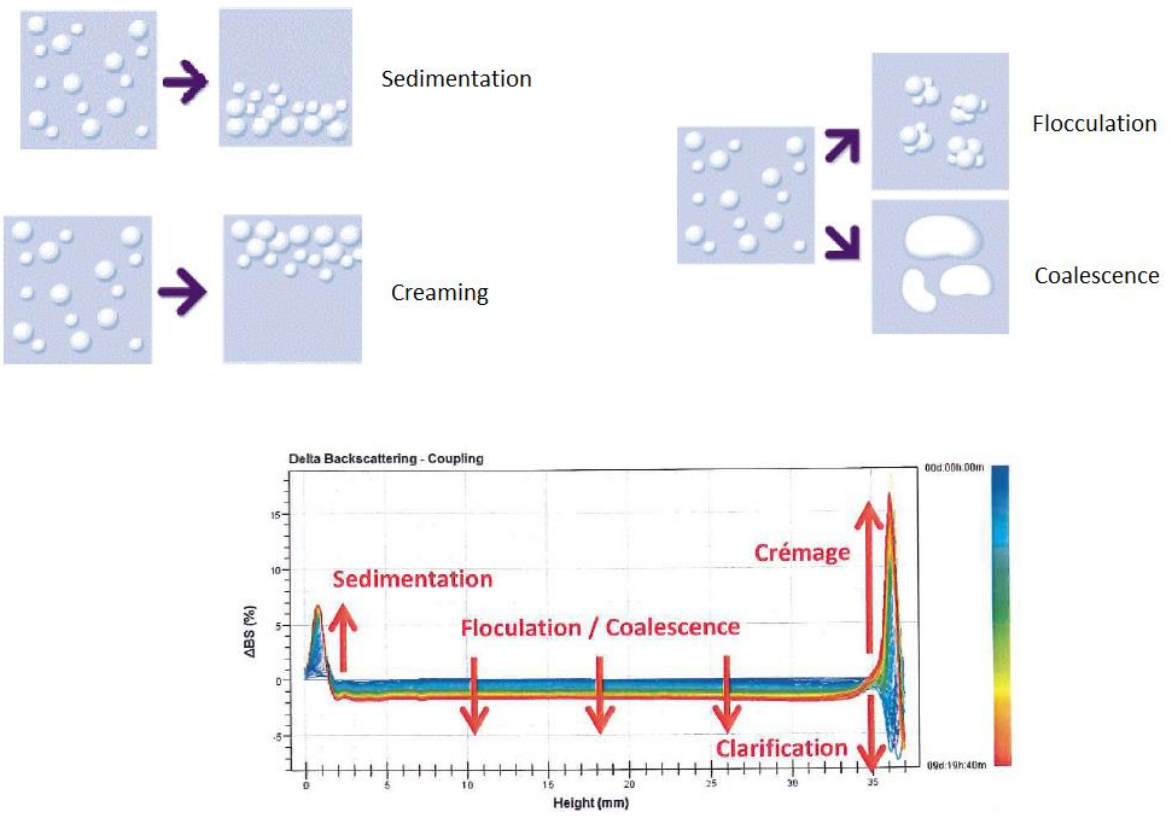

Figure 10: Sedimentation, creaming, flocculation and coalescence phenomenon. Turbiscan™ profile (Delta backscattering as a function of the height of the cell) that shows the different instabilities. [Adapted from [18]]

In industry, the products do not generally undergo a single instability phenomenon but several at the same time. The Turbiscan™Lab reflects the macroscopic view of the stability of concentrated dispersions, making possible to determine the instabilities phenomenon that are taking place in the product.

❖ Fixed mode: In this mode the height of the acquisition is set by the user and the device performs until one measure per 0.1 seconds. This mode is useful in quality control to assess the reproducibility of a lot compared to another or to analyze a very fast instability phenomenon (eg foams). [17], [18]

The backscattered flux measured with Turbiscan™ depends on the penetration distance of the photon into the dispersion, l^*: [13], [14], [17], [18], [19]

$$BS = \frac{1}{\sqrt{l^*}} \quad (19)$$

According to Mie theory, l^* is inversely proportional to the particle volume fraction, Φ, and proportional to their average diameter, d: [13], [14], [17], [18], [19]

$$l^*(\Phi, \mathrm{d}) = \frac{2d}{3\Phi(1-\mathrm{g})Q_s} \quad (20)$$

The parameters g and Q_s corresponds to the asymmetry and extinction efficiency factors, respectively, and both depend on the average diameter, the wavelength of incident radiation and the refractive index of the dispersed and continuous medium.

The backscattered flux is therefore proportional to Φ and Q_s and inversely proportional to d.

Measurement of stability ratio:

The stability ratio, W, in homo-coagulation processes is given by the ratio of the rate of rapid to slow coagulation processes (equation 21), where τ is the turbidity and C_E the electrolyte concentration. The point of separation between the slow and the fast coagulation corresponds to an electrolyte concentration, C_E, called critical coagulation concentration (CCC). [15], [16], [20]

$$W = \frac{(d\tau/dt)_{0,CE>CCC}}{(d\tau/dt)_{0,CE}} \quad (21)$$

If the electrolyte concentration is higher than CCC, the electrostatic repulsive forces are canceled and rapid coagulation occurs due the Brownian motion of the polymer particles. On the other hand, if the electrolyte concentration is below the CCC, coagulation is slower. [15], [16], [20]

Figure 11 shows the experimental stability ratio versus electrolyte concentration curves for a system comprising butyl-acrylate and methyl methacrylate. In order to calculate the stability ratio, it's necessary to determine first the CCC. This concentration was obtained from the intercept with abscissa of the logW-logC_E plot. [15], [16], [20]

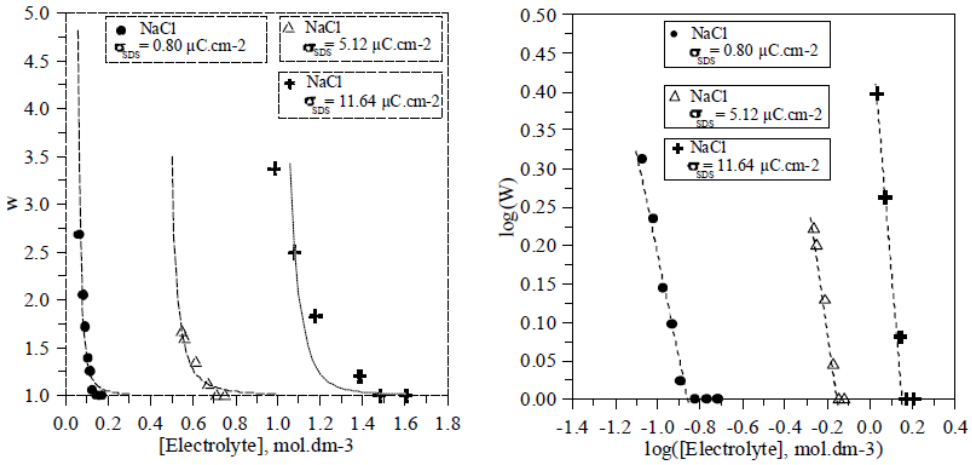

Figure 11: Experimental and theoretical dependence of W on the C_E for a system butyl acrylate-methyl methacrylate stabilized with SDS at three different concentrations. [15], [16]

Measurement of Hamaker constant:

According to Reerink and Overbeek [21] and Romero-Cano [22], the slope of the graph LogW vs $LogC_E$ allows the calculation of Hamaker constant using the following equation if is used a symmetrical electrolyte:

$$A = \sqrt{\frac{1.73 \times 10^{-57}(dlogW/dlogC_E)^2}{r^2 CCC}} \qquad (22)$$

Known features

From literature [13], [14], [16] and [23] it is known that the intensity of the light backscattered by the sample depends on three parameters: the diameter of the particles, their volume fraction (SC(%v/v)) and the relative refractive index between the dispersed and continuous phases. Therefore, any change due to a variation of the particle size (flocculation, coalescence) or a local variation of the volume fraction (creaming, sedimentation) is detected by the optical device.

Figure 12 shows the variation of the backscattering level as a function of the particle diameter for a fixed volume fraction of latex particles.

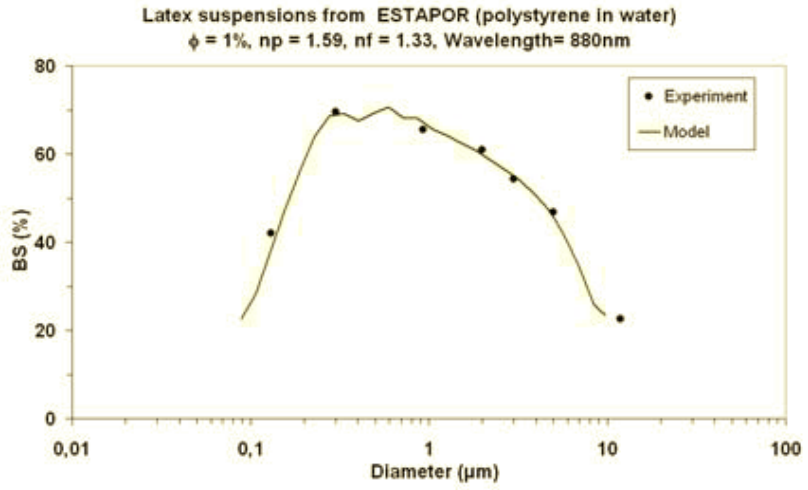

Figure 12: Backscattering level versus diameter for latex particles at 1%.[16]

The curve obtained is a bell shaped curve, where the top is related to the wavelength of the incident light (880 nm). For particles smaller than the wavelength of the incident light, the backscattering increases when the particle size increases. For particles bigger than the wavelength of the incident light an increase in size leads to a decrease in backscattering.

In the figure below, the variation of transmission and backscattering levels are shown as a function of the volume fraction for a fixed diameter of latex particles.

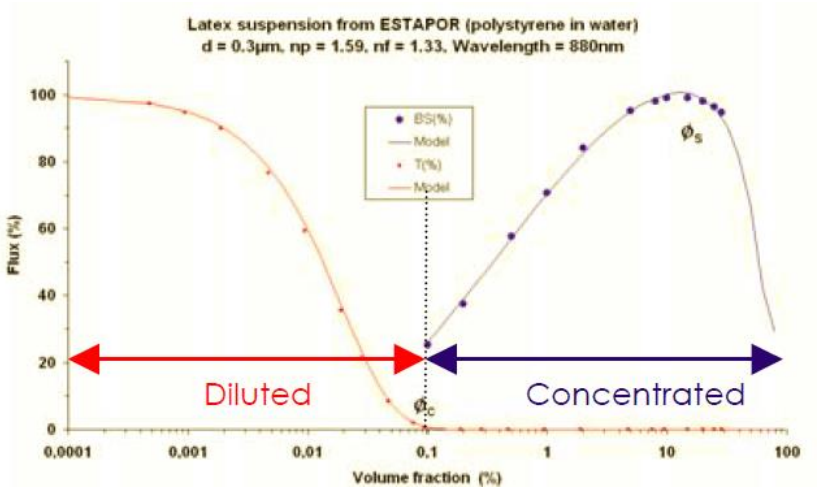

Figure 13: Transmission and Backscattering levels versus volume fraction for latexes with 300 nm of diameter. [16]

If the concentration (or volume fraction or solid content by volume) of particles is smaller than the critical concentration ϕ_c, the product can be considered as diluted and the transmission level decreases with an increase in concentration. On the other hand, when the concentration is higher than the critical concentration ($\phi > \phi_c$), there is no transmission signal (opaque product) and the backscattering level increases with an increase of the volume fraction. The backscattering level starts to decrease as the distance between particles is smaller than the wavelength of incident light when the concentration of particles becomes too high ($\phi > \phi_c$). Usually, this phenomenon is observed when the particles are small (< 1µm) and is called dependent diffusion.

1.4. Conclusions

Emulsion polymerization is a very complex heterogeneous process, from which is produced colloidal polymer particles dispersed in continuous medium, called latexes. These latexes are essential components in many of the commercial applications encountered daily.

Latex coagulation is really important to study, since the formation of coagulum can bring serious problems in reactors, plants or in the final products. The stability of polymer can be evaluated using turbidity measurements and/or creating a model (based on DLVO theory). These turbidity measurements can be performed in Turbiscan^{TM}Lab, where the coagulation is induced by electrolyte addition in order to calculate the values of critical coagulation concentration (CCC) and consequently, values of Hamaker constant, A. This constant is the only parameter that can be adjustable to determine the force balance between the polymer particles and the coagulation rates calculated in the DLVO model. So, reasonable values for A can be fitted using the experimental data and model.

Chapter 2. Experimental Part

In this chapter are inserted the materials, equipments, latex selection and procedures used to study the effect of particle size, solid content and particle size distribution on turbidity and the influence of the surfactant concentration, solid content and particle size on coagulation.

2.1. Materials

Styrene monomer (with inhibitor) was supplied by Acros Organics with a purity of 99%. Sodium dodecyl sulfate (99%, Acros Organics, and 98,5%, Sigma-Aldrich) was used as surfactant and potassium persulfate (99%, Sigma-Aldrich) as initiator. Sodium chloride (99,5%, Acros Organics) was used for the coagulation studies. To clean the latex was used a Dowex MR-3 (mixed bed ion-exchange resin), supplied by Sigma- Aldrich, and a glass wool used as a filter and supplied by Roth. The clay used corresponds to Laponite®($Na^{+}_{0.7}[(Si_8Mg_{5.5}Li_{0.3})O_{20}\ (OH)_4]^{0.7-}$) which is a layered silicate manufactured from naturally occurring inorganic mineral sources and it is used to improve the performance and properties of a wide range of industrial and consumer products, such as surface coatings, household cleaners and personal care products. [24], [25] Deionized water was used through the work.

2.2. Equipment

All the reactions were carried out in a 1L jacketed glass reactor equipped with a 3-blade impeller. The pre-emulsion was put in a glass tank. The temperature of the reactor solution was controlled using a circulating water bath from huber. In order to keep the emulsion well mixed, was used a stirrer from Ika. To circulate the water from the bath and pre-emulsion were used two pumps.

All the components were weighed with a balance from Ohaus.

The solid content was measured using a Thermo-balance from Mettler.

The conductivity was measured with a conductivity module from Metrohm.

To measure the PSD was used the Mastersizer®3000 from Malvern and the average particle sizes were determined using the Zetasizer®Nano ZS from Malvern also. The turbidity measures were performed in Turbiscan™Lab and Turbiscan™On Line. The coagulation studies were performed only with Turbiscan™Lab.

The addition of electrolyte in the latex to provoke coagulation was made using microliter pipettes.

Zetasizer®Nano ZS

The Zetasizer®Nano ZS is a widely used system for measure the size, electrophoretic mobility of proteins, zeta potential of colloids and nanoparticles, molecular weights and optionally the measurement of protein mobility and microrheology of protein and polymer solutions.

The particle size is measured using dynamic light scattering (DLS), sometimes referred to as Quasi-Elastic Light Scattering (QELS), which is a non-invasive and well-established technique that measures the diffusion of particles moving under Brownian motion, and converts this to size and a size distribution using the Stokes-Einstein relationship. DLS results are expressed in terms of the Z-average. According to [24] the Z-Average is close to $D_{v,50}$[6] and is calculated from DLS data by: $D_Z \approx k_B T/3\pi\eta D_{t,avg}$, where K_B, T, η and $D_{t,avg}$, corresponds to the Boltzmann's constant , temperature, viscosity and translational diffusion coefficient (by DLS), respectively. [27]

The measurement range of particle size (diameter) is between the 0.3 nm and 10 μm. [27]

Mastersizer®3000

The Mastersizer®3000 uses the technique of laser diffraction to measure particle size distributions by measuring the angular variation in intensity of light scattered as a laser beam passes through a dispersed particulate sample. This data is then analyzed to calculate the size of the particles that created the scattering pattern.[27]

Particles with diameters between 0.01 and 3500μm can be measured with Mastersizer®. [27]

Figure 14: Zetasizer®Nano ZS and Mastersizer®3000. [27]

[6] For particle size distributions the median is called the D_{50}. The D_{50} is the size in microns that splits the distribution with half above and half below this diameter. The $D_{v,50}$ is the median for a volume distribution. [26]

Turbiscan™

The turbidity measurements were performed in the Turbiscan™Lab and Turbiscan™ On Line, both from Formulaction, which can be seen in figure 15 and 17. In figure 16, the Tursbica™Lab is installed to perform the coagulation studies, in which a stirrer from IKA and a glass impeller were used.

Figure 15: Turbiscan™Lab and Turbiscan™On Line[28]

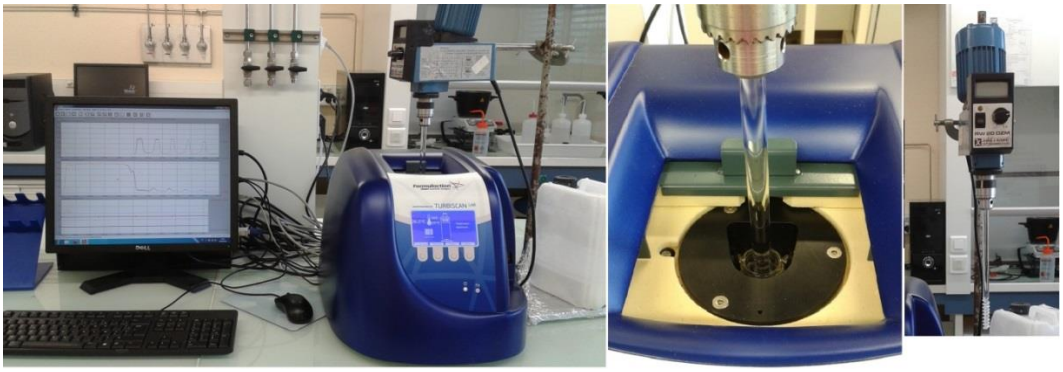

Figure 16: Turbiscan™Lab with a stirrer, to mix well the latex during the coagulation studies, and a computer to acquire and treat the data.

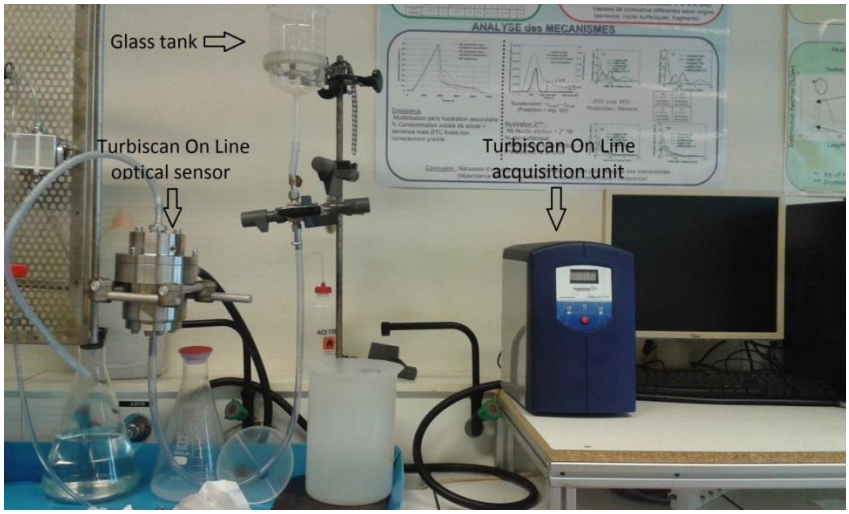

Figure 17: Turbiscan™Online installation with a glass tank, the optical sensor and the acquisition unit. The computer is used to receive and treat the data.

2.3. Polymerization experiments

2.3.1. Experimental procedure

Figure 18 depicts the polymerization unit used to perform all the reactions. The procedure described into the next two paragraphs was always the same.

Figure 18: Polymerization unit. 1-Reactor, 2- Pré-emulsion tank, 3-Stirrer+impeller, 4-Condenser, 5-Pump responsible for forwarding the pre emulsion to the reactor, 6- Pump responsible for forwarding the water from the bath to the reactor jacket.

After performing a reaction and cleaning the reactor, it is important fill it with water. So, the first step was to empty the reactor. After this, deionized water was introduced into the reactor and the agitation was switched on and kept at 400rpm. The sodium dodecyl sulfate (SDS) was weighed and introduced into the reactor. It's necessary to have an inert atmosphere inside the reactor to avoid oxidation reactions due the presence of oxygen. Because of that, the nitrogen source was opened. At this time, the water for the condenser was also opened. After wait approximately half an hour, the water for the jacket was opened and the bath switched-on. The monomer, styrene, was weighed and introduced into the reactor, and into the tank for the pre-emulsion, only after the temperature reaches 70ºC. The initiator, potassium persulfate (KPS), was weighed in a glass bottle and dissolved in a little of water. Here, it was also introduced nitrogen for the same reasons. To start the reaction, the KPS was introduced into the reactor. The temperature and flow rate were controlled with some specific

computer programs. Whenever a sample is withdrawn from the reactor, it should be placed immediately on ice to stop the reaction.

2.3.2. Latex selection

In order to study the effect of size, solid content and size distribution on turbidity, five samples of polystyrene latexes were used (NB8, NB9, NB7, NB10 and NB13), which were not synthetized in this project. The latexes NB8, NB9, NB7 and NB10 were synthetized under a semi-batch process with the same quantity of water, KPS and monomer, but different quantities of SDS. The latex NB13 was produced under a batch process without surfactant. All the components used to produce these latexes, as well as the particle diameter (D_p) and solid content (SC), are listed in table below.

Table 2: Details of recipes for experiments, which results the samples NB8, NB9, NB7, NB10 and NB13, using SDS as surfactant.

Components	NB8	NB9	NB7	NB10	NB13
Water (g)	800				900
SDS (g/L $_{water}$)	10	1.5	1	0.5	-
Monomer (reactor+pré-emulsion) (g)	40+160				100+0
KPS (g/L $_{water}$)	1.6				4
D_p (nm)	53	86	276	479	654
SC (%w/w)	20			23	7

During the reactions, different samples (not available to use in this research work) were extracted and the respective diameters and solids content were measured. With these data, available in appendix II, the following graph was drawn:

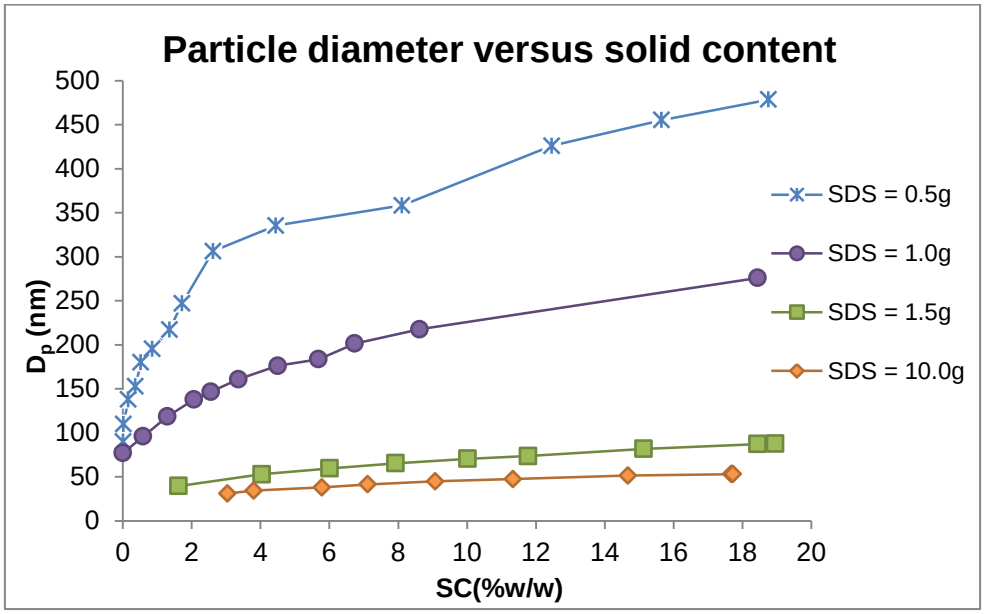

Figure 19: Evolution of particle diameter with solid content (%w/w) at different SDS concentrations.

Figure 19 is very useful to understand which reactions should be taken in account in order to use samples that can be comparable in coagulation studies. For example, to study the effect of SDS concentration on coagulation, only this parameter should vary between the samples to compare. Therefore, the chosen samples should have approximately the same particle size and solid content. Observing the figure 19, easily is concluded that it's possible to get samples with the same particle size and solid content (after appropriate dilution) with the reactions performed with SDS concentrations of 0.5 and 1 g/L_{water}, which correspond to samples NB10 and NB7, or with 1.5 and 10 g/L_{water}, which correspond to samples NB9 and NB10. It were performed two new semi-batch reactions with 1 g/L_{water} and 0.5 g/L_{water} of SDS concentrations, called MM1 and MM2, respectively, in order to have more latex quantities to use in coagulation studies. The components and their quantities used in these polymerizations are inserted in table 3. In tables 4 and 5 can be seen the time at which the samples were extracted from the reactor and respectives particle diameters and solids content.

Table 3: Details of recipes for experiments MM1 and MM2 using SDS as surfactant..

Reaction	MM1	MM2
Water (g)	800	
SDS (g/L_{water})	1	0.5
Monomer (reactor+pré-emulsion) (g/L_{water})	40+160	
KPS (g/L_{water})	1.6	

Table 4: Particle sizes and solid content of the different samples taken during the reaction MM1**.**

Sample	Time(min)	D_p(nm)	SC(%w/w)
1	10	45	2
2	30	100	3
3	60	140	5
4	90	197	7
5	128	200	10
6	150	230	13
7	180	207	9
8	210	215	9
9	240	236	12
10	270	245	14
11	300	270	17
Final	350	286	19

Table 5: Particle sizes and solid content of the different samples taken during the reaction MM2**.**

Sample	Time(min)	D_p(nm)	SC(%w/w)
1	60	138	1
2	120	157	2
3	150	158	2
4	180	204	4
5	210	264	10
6	240	352	16
7	270	412	23
Final	300	425	23

Almost all of the samples taken while the reaction MM1 was taking place continued to polymerize, although they have been placed on ice. Reason why the sizes and SC are not exactly proportional with time.

It was analyzed the coagulation in two more latex, called LP1 and LP2, which were not synthetized in this project and whose stabilization system was different. Here, instead of SDS was used a clay. The components and their quantities used in the polymerizations are inserted in table 6.

Table 6: Particle size and solid content for the two samples stabilized with a clay.

Components	LP1	LP2
Water (g)	800	
[clay] (g/L_{water})	1	2
Monomer (reactor+pré-emulsion) (g)	40+160	
KPS (g/L_{water})	1.6	
D_p(nm)	251	240
SC(%w/w)	18	18

2.3.3. Procedure- Turbiscan^{TM}Lab and Turbiscan^{TM}On Line

To get an optimal accuracy, is recommend to switch on both the Turbiscan^{TM} 30 minutes before measuring to let the electronic components become stabilized. The detailed explanation of how the Turbiscan^{TM} works can be seen in section 1.3.3.

The use of Turbiscan^{TM}Lab to measure the turbidity is very simple. A little portion (approximately 10 ml) of latex is introduced into an appropriate cell. Then, the cell is closed and introduced in the device. The cap of Turbiscan^{TM}Lab is closed and the measurement starts after choosing the mode of data acquisition. It was chosen the scan mode to acquire transmission and

backscattering data every minute for 10 minutes. With Turbiscan^{TM}Lab is possible to select the desired temperature to work. In all the studies the temperature was set to 25ºC.

The procedure developed for Turbiscan^{TM}Lab to coagulate samples is more complex than the one explained before. About 10 ml of latex are introduced in the cell (without close). This cell is placed into the Turbiscan^{TM}Lab, whose cap isn't closed to allow the introduction of an impeller inside the cell in order to mix well the latex during the studies (see figure 16). Before coagulation, the scan mode is used to acquire the backscattering and transmission profiles. In coagulation studies, the latex should not be saturated (otherwise it's not possible to see the effect of the parameter that we are varying) or transmit light (because the experiments were always done without transmission, so it's better to stay in the same domain). If these conditions are satisfied, it's possible to move for the next step. To make sure that the sample is well mixed, the stirrer is switched on and kept at 1600 rpm for a few seconds. To start the coagulation, the fixe mode was activated, in order to acquire data (backscattering) every 0.1 seconds, and the height of cell, in which is pretended to measure the signal, is chosen. If the sample is well mixed and stable, the signal should be stable. After a few seconds, the stirrer is switched on and kept for about 10 seconds at 1600 rpm to see the changes in backscattering. After the signal stabilizes, the stirrer is switched on again, the electrolyte is added when the 1600rpm are achieved and the stirrer is switched off after a few seconds (to warrant that the solution is mixed well). When the signal stabilizes again, the last procedure is repeated as many times as necessary. In the end, the measurement is interrupted, another scan is performed to check the changes before and after the coagulation and the impeller is removed from the cell and cleaned with acetone and water. In all the experiments, the electrolyte used was sodium chloride (NaCl). The PSD was measured with Mastersizer$^{®}$3000 before (in order to check if the sample wasn't coagulated) and after (to verify if the sample is actually coagulated) the coagulation. In coagulation studies, the temperature was also set to 25ºC. Here, is important to notice that the device is sensitive to temperature. It means that if the room temperature increases, the temperature of Turbiscan^{TM} will also increase. In spite of the existence of a fan to control the temperature, when it increases it takes a long time to decrease to the set value. Because of that is important to be attentive to temperature.

Before using the Turbiscan^{TM}On Line, and after wait the 30 minutes, the sensor should be cleaned with ethanol. Before staring a measurement, the transmission and backscattering values must respect the range of values recommend by the supplier. This can be done choosing "verification measures" in the Turbiscan^{TM}On Line software and waiting that the signal stabilizes. If the values are according to the range of values recommended, the device is ready to use; otherwise, the sensor should be cleaned with water, soap and ethanol and the values checked again. Finally, to start a measurement, approximately 250 g of latex are introduced in the glass tank (see figure 17). Then, the valve under the tank is opened at the same time that the acquisition of data and chronometer (to calculate the flow rate) are initiated. The latex circulates through the pipes and the sensor by the force of gravity. After getting out of the sensor, the latex is lead to a vessel. When there is no more latex in the tank, the measurement and the chronometer are stopped and the latex in the vessel is weighed.

After the measurements, the tank, pipes and sensor should be cleaned very well with a lot of water and soap, to eliminate any residue of latex. It's important to repeat the measurement 2 or 3 times to make sure that the values obtained are correct. In the end, the same procedure of checking the values of transmission and backscattering is performed. It was chosen the "PC data acquisition and processing" mode to acquire transmission and backscattering data every 0.1 seconds using the software 2.2.2.[29]

Chapter 3. Results and Discussion

In this chapter, divided in two parts, are inserted all the experimental data and respective treatment and discussion. The first part corresponds to the effect of size, solid content and particle size distribution on turbidity signal and the second part to the effect of amount of surfactant used, the solid content and the particle size on coagulation, determining the critical coagulation concentration (CCC) and Hamaker constant (A).

3.1. Effect of size, solid content and size distribution on turbidity

3.1.1. Effect of size- Turbiscan™Lab

The effect of mean size on the Turbiscan™Lab signal for the samples NB8, NB9, NB7, NB10 and NB13 was the first turbidity measure to be performed.

Before measure the turbidity, was important to measure the PSD, in order to see the dispersity of the samples or to check if the samples coagulated during the storage. For this propose, was used the Mastersizer®3000. The results can be seen in figures 20 to 24, where the volume density, in percentage, is a function of the particle diameter, in microns.

Before starting a measurement in Mastersizer®3000, it's possible to choose the number of measures for each sample. Due to this, in some figures more than one profile can be observed.

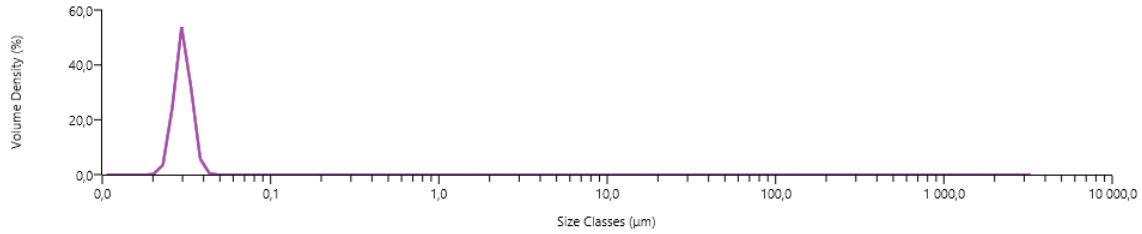

Figure 20: PSD of sample NB8 measured with Mastersizer®3000.

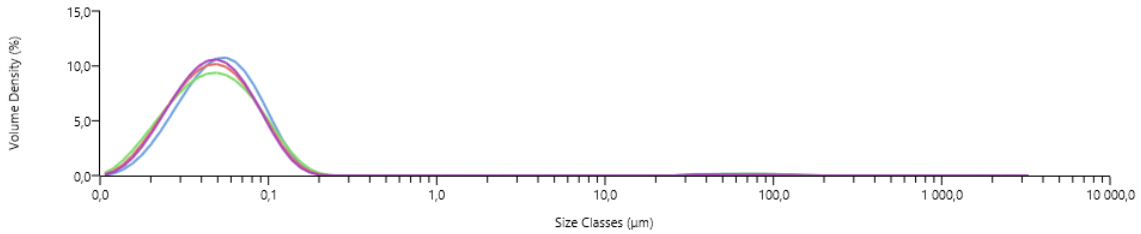

Figure 21: PSD of sample NB9 measured with Mastersizer®3000.

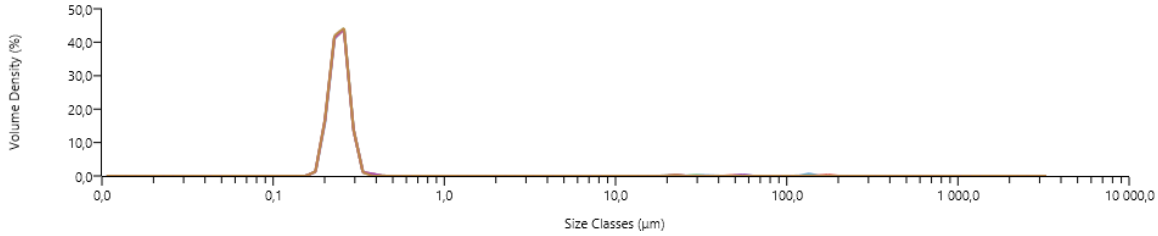

Figure 22: PSD of sample NB7 measured with Mastersizer®3000.

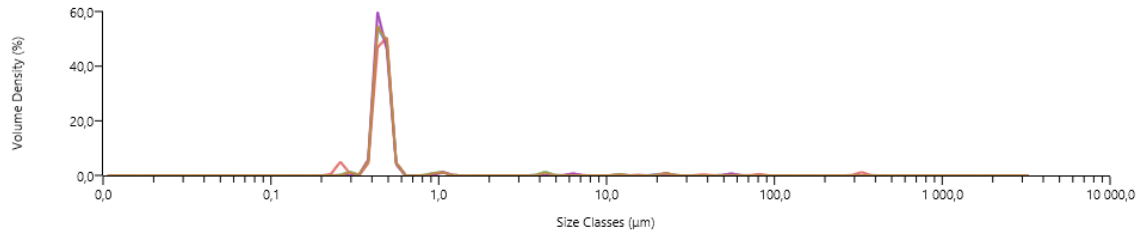

Figure 23: PSD of sample NB10 measured with Mastersizer®3000.

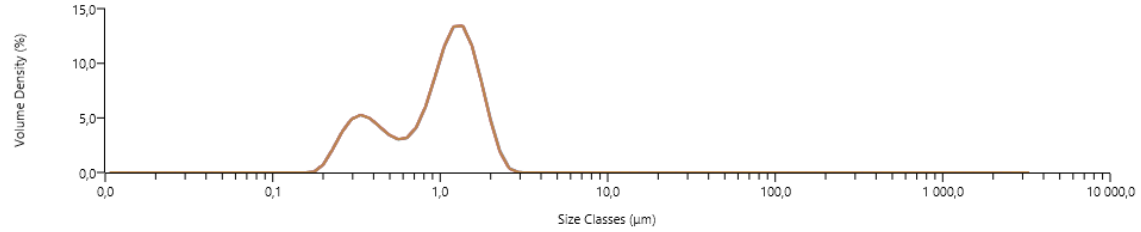

Figure 24: PSD of sample NB13 measured with Mastersizer®3000.

Observing the figures 20 to 22, it's possible to conclude that, since there is only one population, the samples are monodisperse, i.e., all the particles have the same size. The sample NB10 is reasonable monodisperse (see figure 23). On the other hand, the sample NB13 it's not totally monodisperse. This polydispersity is due to the absence of SDS, thus showing the importance of surfactant to produce stable and monodisperse latexes. None of the samples coagulated during the storage, because if that happened, the PSD should be located more to the right with a widest profile.

Since the objective was to compare the signal for different particle sizes, only one parameter at a time should vary, i.e., the samples to be compared should have the same solid content. So, the samples NB8, NB9 and NB7 were selected.

The results for sample NB8 are shown in figures 25 and 26, in which the abscissa axis corresponds to the cell height and the ordinate axis to the turbidity signal (percentage of transmission,

% T, or percentage of backscattering, %BS). The profiles of the other samples are inserted in appendix II.

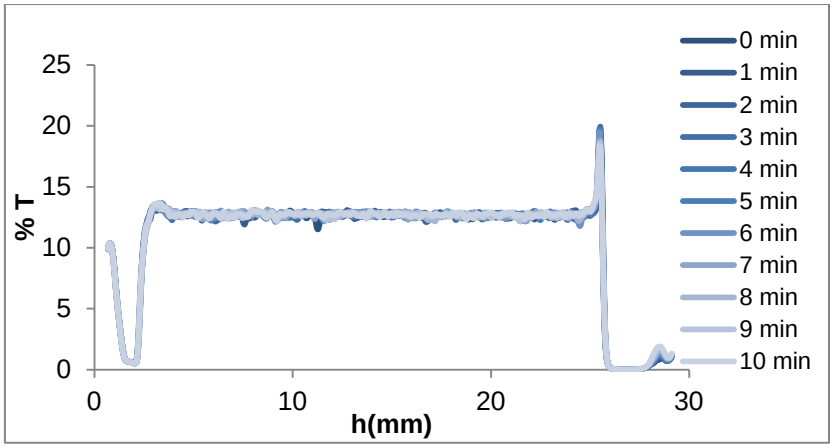

Figure 25: Transmission profiles of sample NB8, measured with Turbiscan^{TM}Lab..

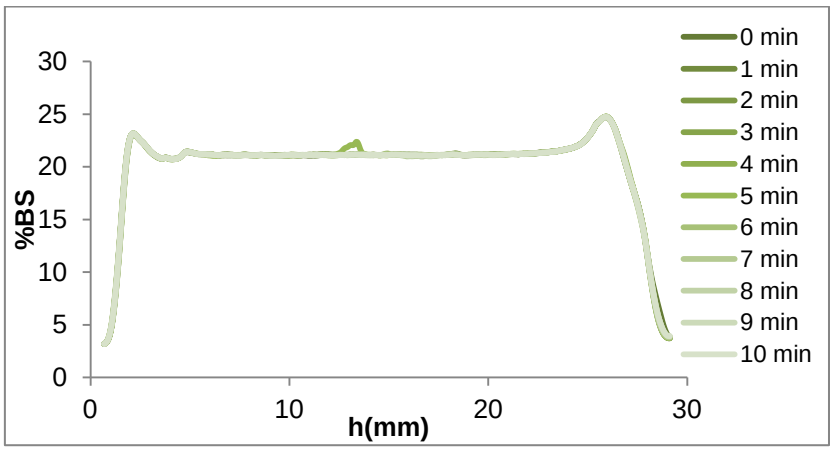

Figure 26: Backscattering profiles of sample NB8, measured with Turbiscan^{TM}Lab.

Observing the figures the first conclusion is that there is no flocculation or coalescence since the profiles of backscattering/transmission were constant during the 10 minutes. To understand better the effect of size on turbidity, were constructed not only the figures 27 and 28, but also the table 7. On these two figures, for each height of the cell, was made an average of the transmission and backscattering signal of the 10 profiles. The differences on the right hand side are simply due to slightly different quantities of latex in the cell. The transmission and backscattering values in table 7 are an average value between 5 and 23 mm, which is the only important zone since the signal is constant.

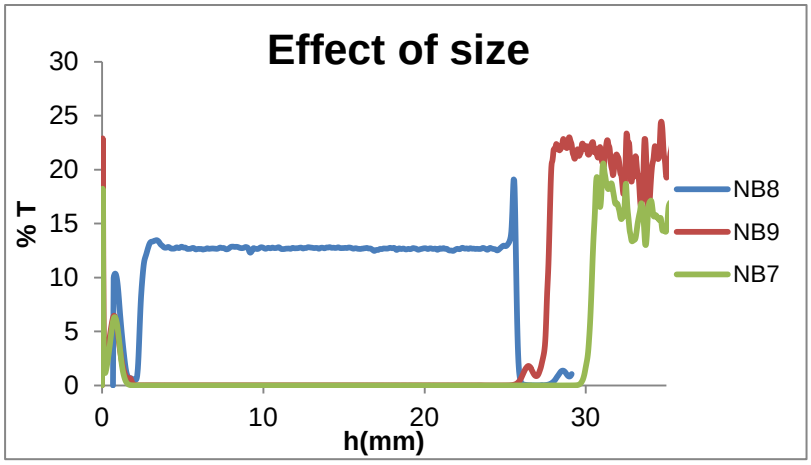

Figure 27: Transmission profiles of samples NB8 (53nm), NB9 (86nm) and NB7 (276nm) measured with Turbiscan^{TM}Lab.

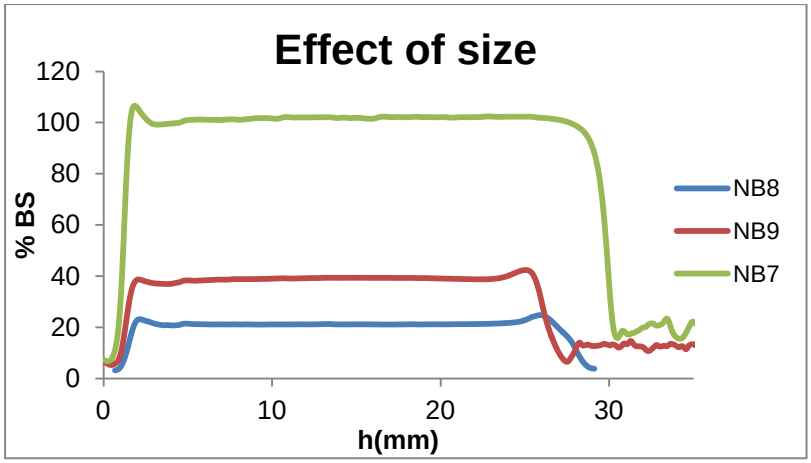

Figure 28: Backscattering profiles of samples NB8 (53nm), NB9 (86nm) and NB7 (276nm) measured with Turbiscan^{TM}Lab

Table 7: Transmission and Backscattering averages of samples NB8, NB7 and NB9.

	D_p(nm)	Transmission (%)	Backscattering(%)
NB8	53	13	21
NB9	86	0	39
NB7	276	0	102

The backscattering increases with the size, what was expected since the particles are smaller than the wavelength of the incident light (see section 1.3.3.). If the backscattering increases, it's obvious that the transmission decreases. It's important to notice that the only sample that transmits is the one with the smaller particles, NB8, and that NB7 is saturated (backscattering>100%).

Besides turbidity measurements, the Turbiscan^{TM}Lab software allows to determine the particle size according the equations (19) and (20). To do that, it's necessary to know the refractive indexes of the continuous (n_f) and dispersed (n_d) phases and the volume fraction of latex. The continuous phase and the dispersed phase correspond to water (n_f=1,33) and polystyrene (n_d=1,59), respectively. Since

the solid content is the same for the 3 samples, the volume fraction is also the same and very similar to the SC(%w/w). The explanation of how to calculate the SC(%v/v) is inserted in appendix III.

The Turbiscan^{TM}Lab software calculates the diameters in the form of graphs, what can be seen on figure 29. Table 8 represents the diameters measured by Zetasizer®, Mastersizer® and Turbiscan^{TM}Lab. It's is known that the diameter measured with Zetasizer®, D_z, can be compared with the diameter measured with Mastersizer®, $D_{v,50}$ (see section 2.2). There is no information if the diameter calculated using the calibration of the Turbiscan^{TM} can be compared to any of these. When a sample is saturated, in this case NB7, it is possible that the diameter calculated by Turbiscan ^{TM} is not the real, since we are working outside the range that this device works.

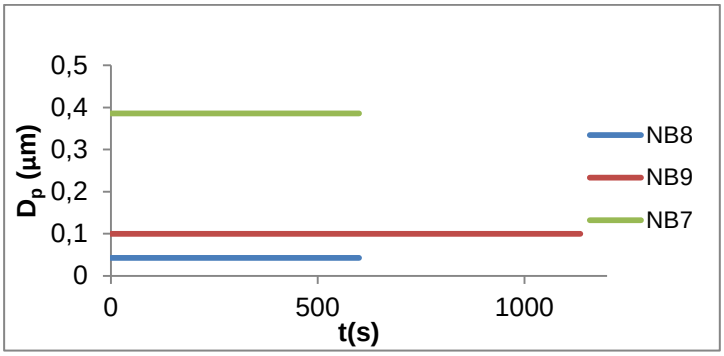

Figure 29: Particle diameter versus time of samples NB8, NB9 and NB7, measured with Turbiscan^{TM}Lab

Table 8: Particle diameter of samples NB8, NB9 and NB7 calculated with Zetasizer®, Mastersizer® and Turbiscan^{TM}Lab.

	D_p(nm)	$D_{v,50}$ Mastersizer(nm)	D_p Turbiscan(nm)
NB8	53	30	43
NB9	86	50	100
NB7	276	235	386

3.1.2. Effect of solid content- Turbiscan^{TM}Lab

In this section the effect of SC was studied on Turbiscan^{TM}Lab signal. The samples NB7 and NB10 were chosen and diluted to 15, 10 and 5%. The required equations, (28) and (29), to carry out the calculations of these dilutions are represented in appendix III.

For precaution, the PSD were measured for all the diluted samples in order to check if there was a change on the distribution. The two following figures are an example in which the PSD didn't change with the dilution, what was expected.[7]

[7] The comparison between the others SC for the samples NB7 and NB10 can be seen in appendix II.

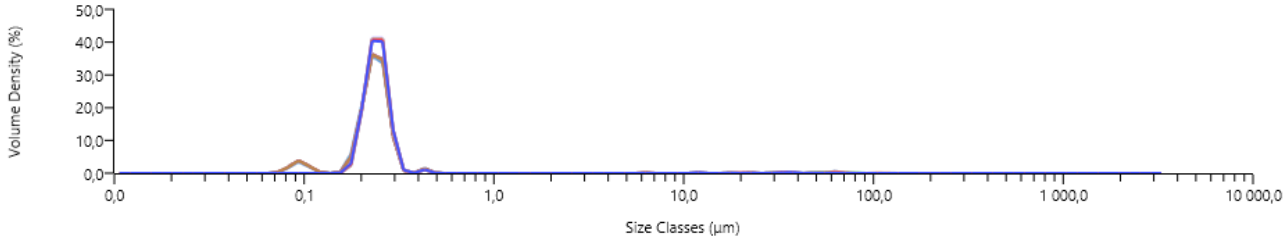

Figure 30: PSD of sample NB7 with SC=20%w/w (brown) and SC=15% w/w (blue), measured with Mastersizer®3000

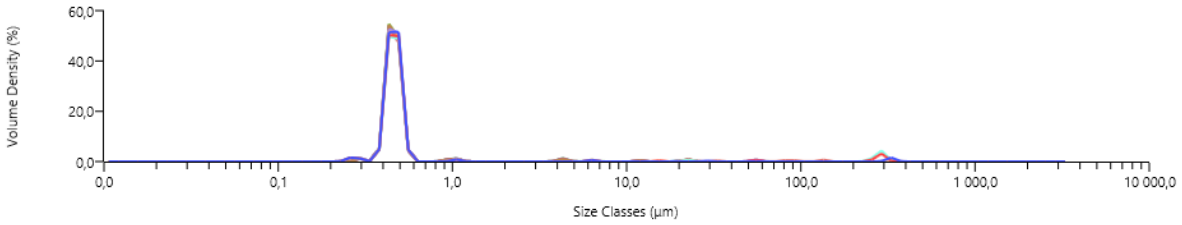

Figure 31: PSD of sample NB10 with SC=23% w/w (brown) and SC=15% w/w (blue), measured with Mastersizer®3000.

None of the diluted samples transmit light, reason why was decided to present in appendix II all the transmission profiles given by Turbiscan™Lab. In similarity to what was done in the study of the effect of particle size, to study the effect of solid content on turbidity two graphs were plotted and two tables were constructed. Once again, the differences on the right hand side are due to slightly different quantities of latex in the cell. The original backscattering profiles are inserted also in appendix II.

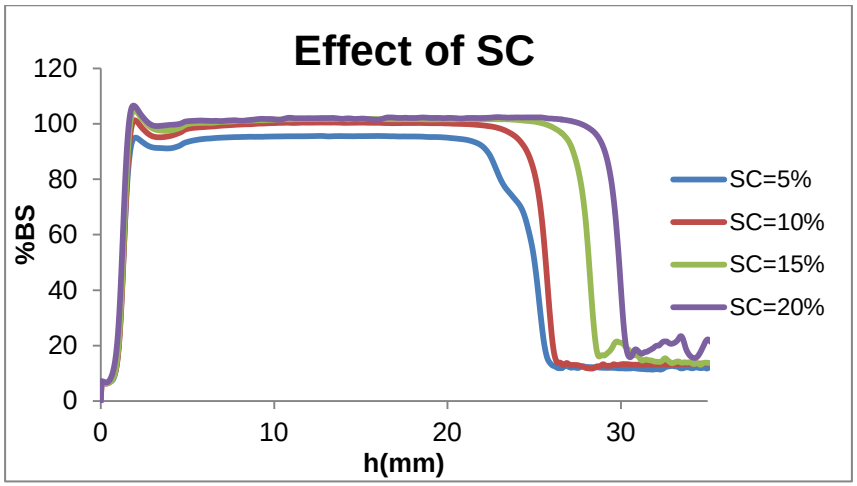

Figure 32: Backscattering profiles of sample NB7 at different solids content (%w/w), measured with Turbiscan™Lab.

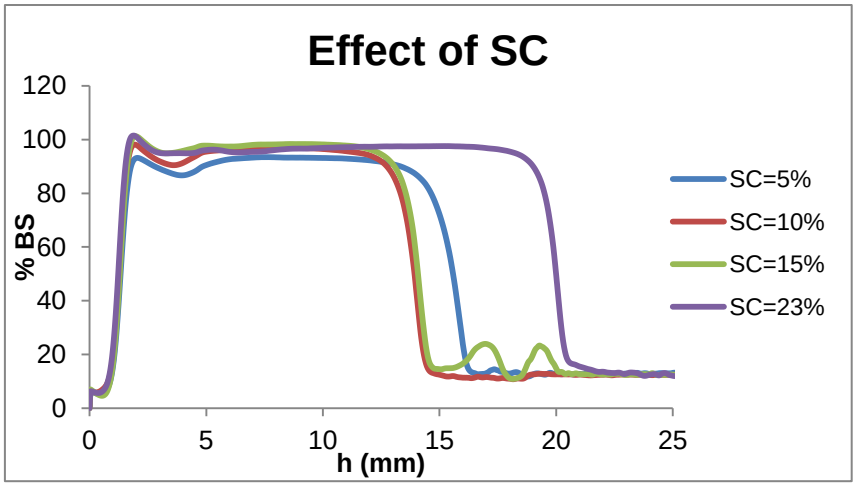

Figure 33: Backscattering profiles of sample NB10 at different solids content (%w/w), measured with Turbiscan^{TM}Lab

Table 9: Transmission and Backscattering averages of sample NB7 for different solids content (%w/w).

SC(%)	Transmission (%)	Backscattering(%)
5	0	96
10	0	101
15	0	102
20	0	102

Table 10: Transmission and Backscattering averages of sample NB10 for different solids content (%w/w).

SC(%)	Transmission (%)	Backscattering(%)
5	0	94
10	0	97
15	0	99
23	0	98

In section 1.3.3., it was affirmed that when the concentration is higher than the critical concentration (0.1%) there is no transmission signal and the backscattering level increases as the volume fraction increases. This statement is clearly confirmed with this study. It's important to notice that the sample NB7 becomes saturated over the 10%. The sample NB10 becomes almost saturated over the 15%. Therefore, the SC should be taken into account when working with Turbiscan^{TM}Lab.

3.1.3. Effect of size distribution-Turbiscan^{TM}Lab

In order to study the effect of size distribution on Turbiscan^{TM}Lab signal, the latex NB9 was mixed with NB10 in the proportions 7:3, 1:1 and 3:7. To perform correctly this study, both the latexes should have the same SC. So, before mixing, the latex NB10 was diluted until 20% of SC(%w/w), which is the SC of sample NB9.

Before studying the effect of mixing two latexes in turbidity, the PSD was analyzed after the mixture. Figures 33 to 38 show the PSD of the samples before and after the mixture.

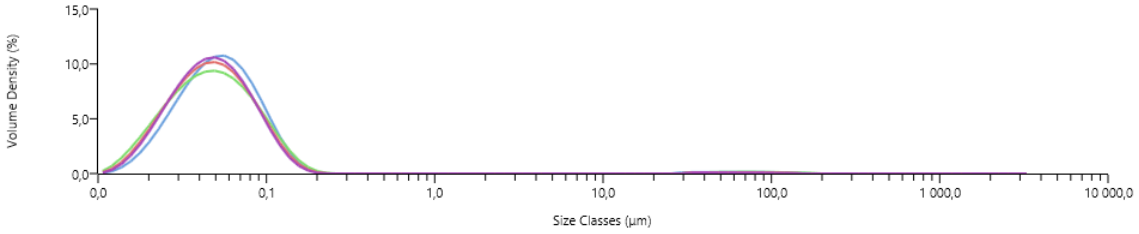

Figure 34: PSD of sample NB9 measured with Mastersizer®3000.

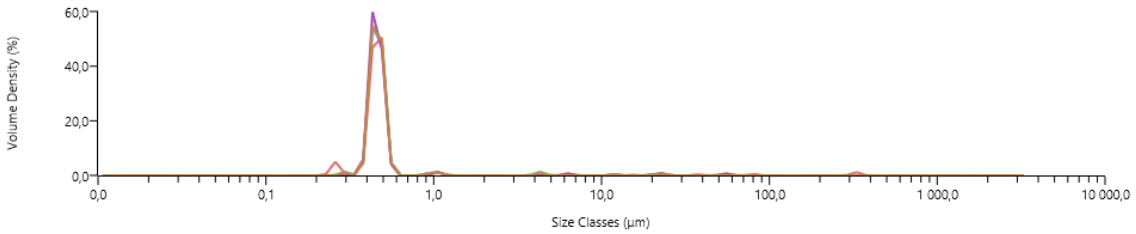

Figure 35: PSD of sample NB10 measured with Mastersizer®3000.

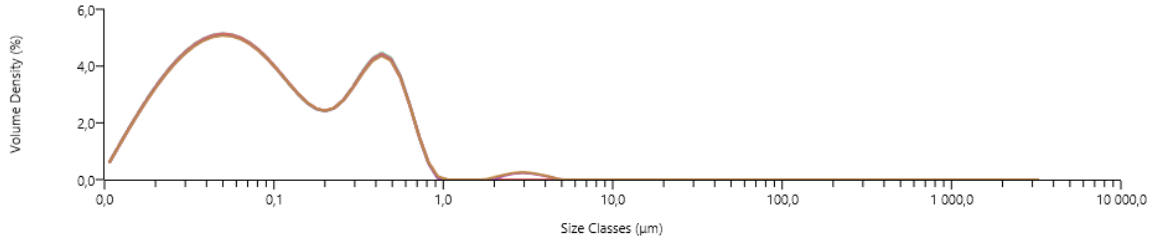

Figure 36: PSD of the mixture NB9+NB10 in proportion 7:3, measured with Mastersizer®3000.

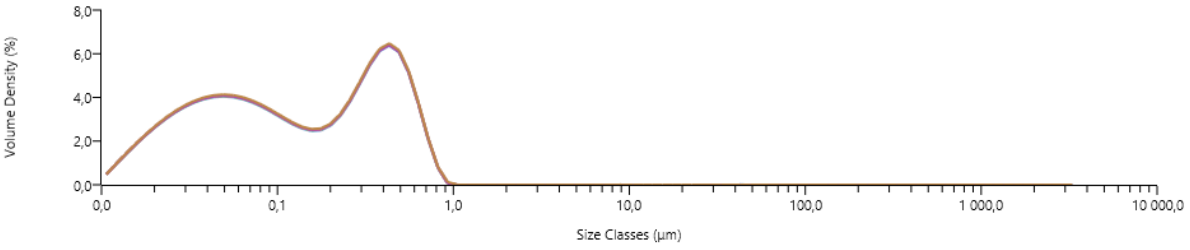

Figure 37: PSD of the mixture NB9+NB10 in proportion 1:1, measured with Mastersizer®3000.

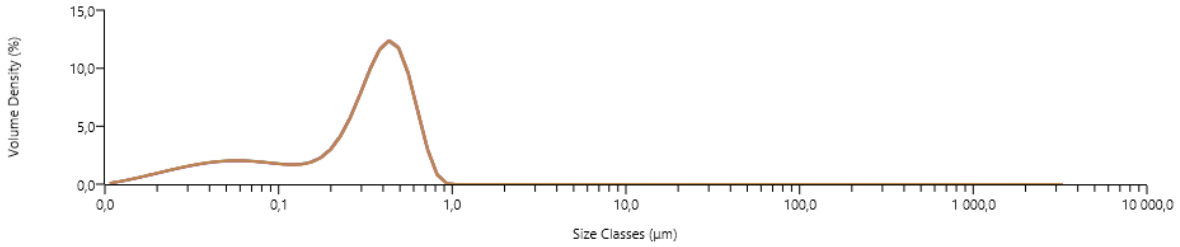

Figure 38: PSD of the mixture NB9+NB10 in proportion 3:7, measured with Mastersizer®3000.

After measuring the PSD, the effect of mixing the latex NB9 with the latex NB10 was study on turbidity signal. The procedure to perform this study and to treat the data was exactly the same that the one used in the previous studies. Again, the mixture of these two latexes doesn't transmit light. So, it was decided to present in appendix II the transmission profiles, as well as the original backscattering profiles. The results are presented in figure 39 and table 11.

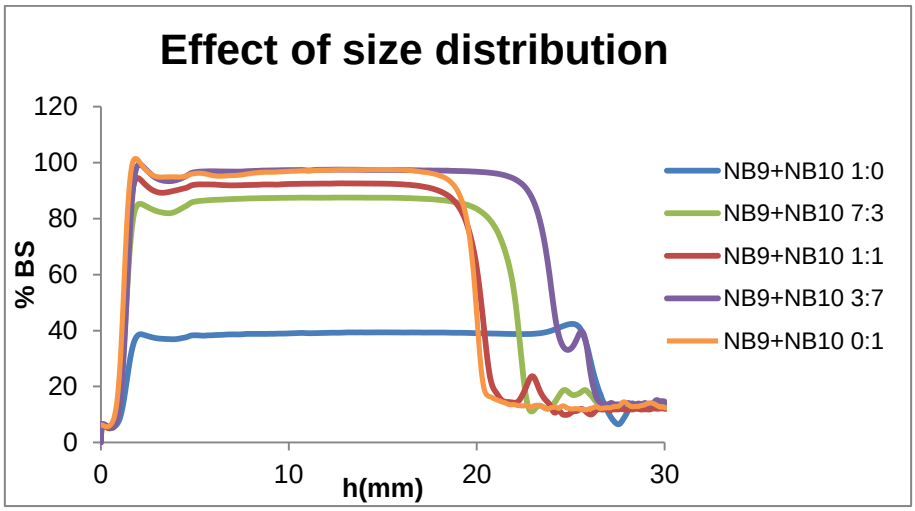

Figure 39: Backscattering profiles resulting from mixture NB9+NB10 at different proportions, measured with Turbiscan™Lab

Table 11: Transmission and Backscattering averages of the mixture NB9+NB10 at different proportions.

NB9+NB10	D_p (nm)	Transmission (%)	Backscattering (%)
1:0	86	0	39
7:3	140	0	87
1:1	168	0	92
3:7	310	0	98
0:1	479	0	98

Whatever the proportion, the backscattering is always closer to the backscattering of sample NB10 (proportion 0:1) what means that the backscattering is more affected by bigger particles.

In figure 40 is represented the diameter determined with Turbiscan™Lab for the different proportions. Table 12 represents the diameters measured by Zetasizer®, Mastersizer® and Turbiscan™Lab.

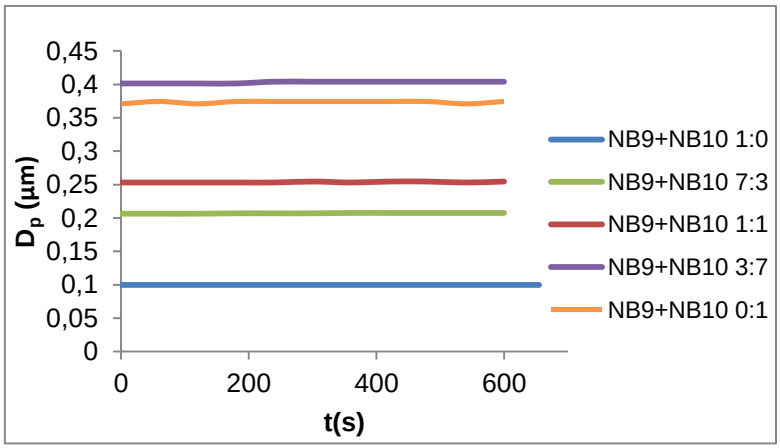

Figure 40: Particle diameter versus time for the mixture of NB9+NB10 at different proportions, measured with Turbiscan™Lab

Table 12: Particle diameter of the mixture NB9+NB10 at different proportions, determined with Zetasizer®, Mastersizer® and Turbiscan™Lab.

NB9+NB10	D_p(nm)	$D_{v,50\ Mastersizer}$(nm)	$D_{p\ Turbiscan}$(nm)
1:0	86	50	100
7:3	140	80	208
1:1	168	191	255
3:7	310	337	404
0:1	479	460	374

3.1.4. Effect of size and solid content- Turbiscan™On Line

It was decided to study also the effect of size and SC in Turbiscan™ On Line. Since the liquid circulating through pipes by the force of gravity, the study of SC is important to check if the more viscous latexes can be analyzed with this device.

Effect of size

As was said before, this apparatus measure the turbidity signal along the time, what can be seen in the following figures. It was made 2 or 3 tests for each sample, NB8, NB9 and NB7. The original profiles of samples NB9 and NB7 can be seen in appendix II. It's really important to make sure that there are no bubbles of air between the glass tank and the sensor to avoid the bad circulation of latex.

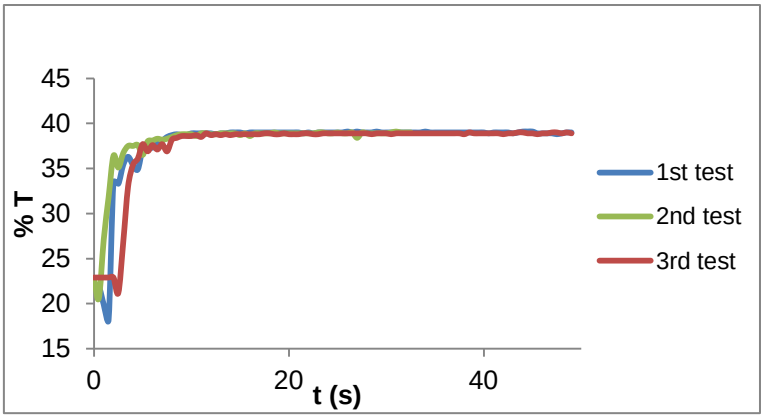

Figure 41: Transmission profiles of sample NB8, measured with Turbiscan^{TM}On Line.

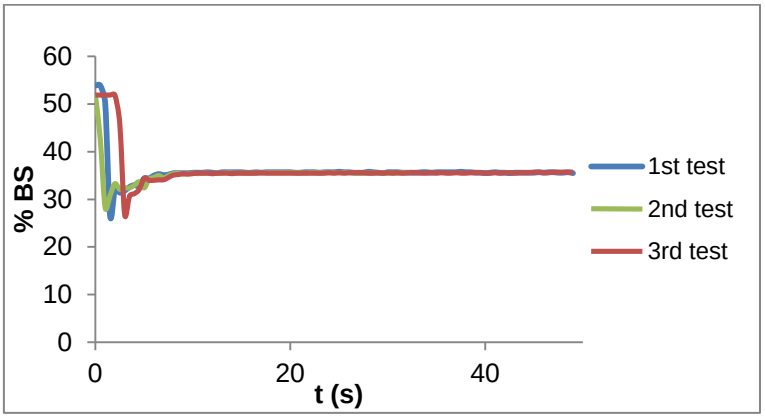

Figure 42: Backscattering profiles of sample NB8, measured with Turbiscan^{TM}On Line.

Similar to what was done with Turbiscan^{TM}Lab, it was made an average of the 3 tests for the same period of time, in order to visualize better the effect of the different particle sizes on transmission or backscattering signals. The figures resulting from that are shown below. Table 13 is a comparison between the both devices, where it's concluded that the values are very similar.

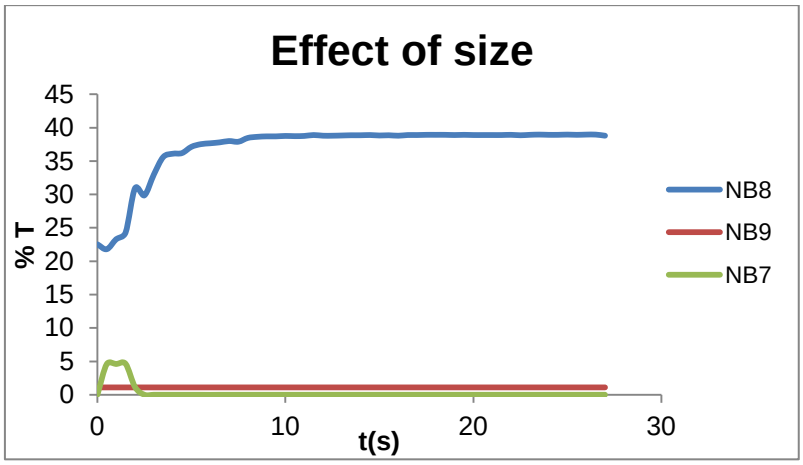

Figure 43: Transmission profiles of samples NB8(53nm), NB9 (86nm) and NB7 (276nm), measured with Turbiscan^{TM}On Line.

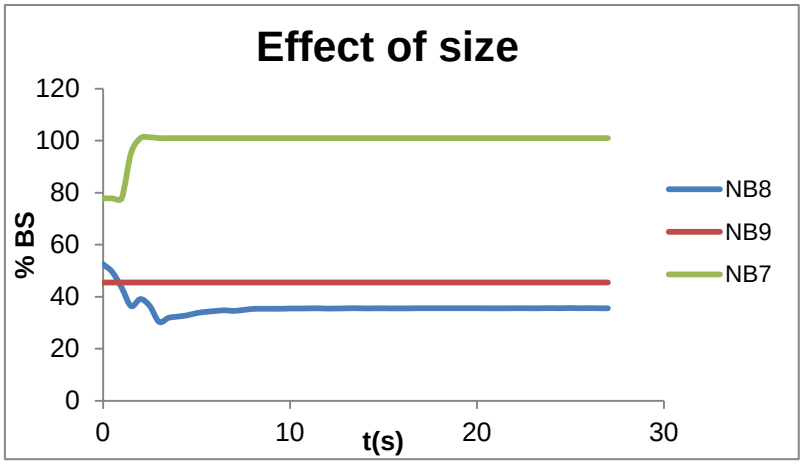

Figure 44: Backscattering profiles of sample NB8(53nm), NB9 (86nm) and NB7 (276nm), measured with Turbiscan^{TM}On Line.

Table 13: Comparison between the Turbiscan^{TM}Lab and the Turbiscan^{TM}On Line of transmission and backscattering of samples NB8, NB9 and NB7.

Sample	D_p(nm)	Transmission(%) Turbiscan^{TM}Lab	Transmission(%) Turbiscan^{TM}OnLine	Backscattering(%) Turbiscan^{TM}Lab	Backscattering(%) Turbiscan^{TM}OnLine
NB8	53	13	39	21	36
NB9	86	0	1	39	46
NB7	276	0	0	102	101

Turbiscan^{TM}On Line uses the same equations than Turbiscan^{TM}Lab to determine the diameter. The results are shown in figures 45 to 47. With the sample NB7, it was only possible to calculate the diameter with the data from the first test. For the other two tests, the following message appears: “No valid value for this calculation”. According to [29], this message appears when parameters keyed in can’t give any solutions. It is unknown why the diameter can be calculated with the data from the first test and not with others, being them very similar. The supplier, Formulaction, was contacted about this message, informing that if the transmission is higher than 0.2%, it should be used the transmission data obtained with the software 2.2.3. Otherwise, it should be used the backscattering data obtained with the software 2.2.2. Since the transmission is less than 0.2% it was used the second software and the backscattering data. However, the problem continued to not be solved. Due to this information from supplier, the diameter of NB9 was determined using the software 2.2.3.

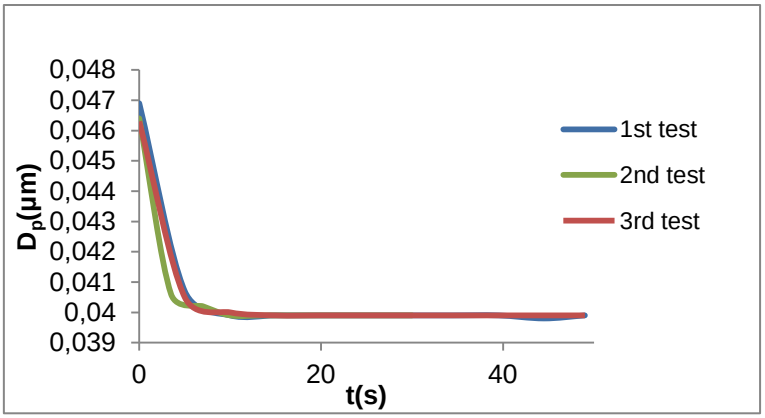

Figure 45: Diameter versus time of sample NB8, measured with Turbiscan^{TM}OnLine.

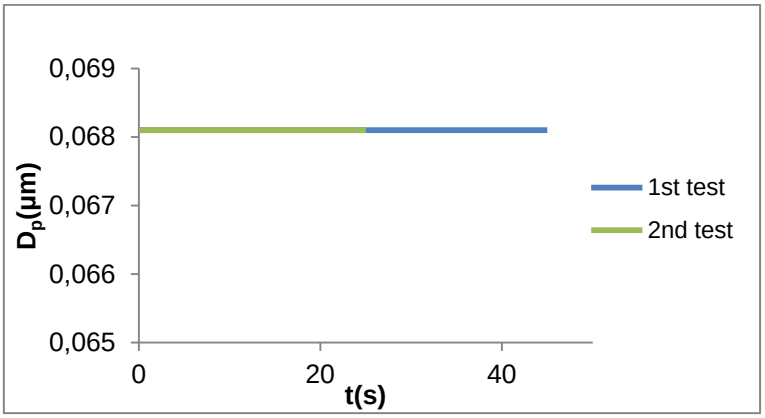

Figure 46: Diameter versus time of sample NB9, measured with Turbiscan^{TM}OnLine.

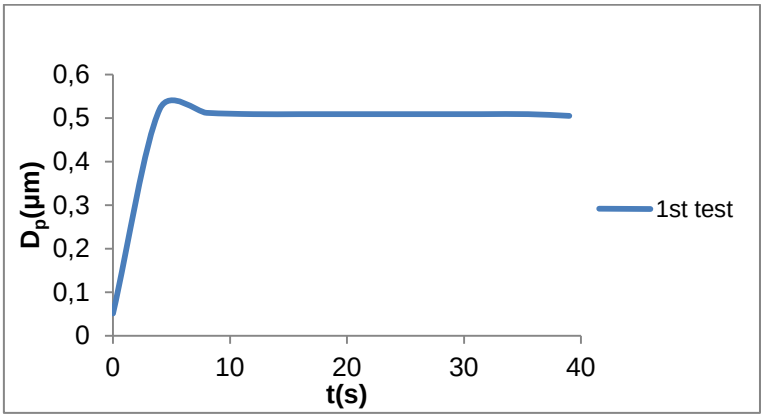

Figure 47: Diameter versus time of sample NB7, measured with Turbiscan^{TM}OnLine

In the table below, it's made a comparison between the samples diameter measured by different techniques.

Table 14: Particle diameter of samples NB8, NB9 and NB7 calculated with Zetasizer®, Mastersizer®, Turbiscan^{TM}Lab and Turbiscan^{TM}On Line.

	D_p(nm)	$D_{v,50\ Mastersizer}$(nm)	$D_{p\ Turbiscan^{TM}Lab}$ (nm)	$D_{p\ Turbiscan^{TM}\ OnLine}$ (nm)
NB8	53	30	43	40
NB9	86	50	100	68
NB7	276	235	386	509

As was said before, the diameter of NB7 measured with the Turbiscan^{TM}Lab could be a false diameter due the saturation of the sample. The same can be said to the diameter determined by Turbiscan^{TM}On Line.

The mass flow, Q_M, were calculated with the mass obtained in the end, M_{total}, and the time that the latex took to pass through the pipes, t. The mass flows for each sample are presented in table 15.

Table 15: Mass flow of samples NB8, NB9 and NB7.

Sample	Nº of tests	M_{total} (g)	t(s)	Q_M(g/s)
NB8	1st test	202	41	4.9
	2nd test	192	25	7.7
	3rd test	189	42	4.5
NB9	1st test	205	24	8.5
	2nd test	196	22	8,9
NB7	1st test	185	34	5.5
	2nd test	187	15	12.5
	3rd test	179	21	8.5

The mass flow of sample NB9 was consistent in both tests. The same didn't happen with the samples NB8 and NB7. A possible explanation is the fact that there were bubbles of air inside the pipes preventing the good circulation flow of latex. The mass flows show that the particle size not affects significantly the flow of latex.

Effect of solid content

In this section, the study of the effect of SC is important not only on the turbidity signal but also to see if the latexes with a higher SC can be analyzed with the Turbiscan^{TM}On Line without using a pump.

The NB7 diluted samples were chosen and the results are represented in figure 48. Since these samples don't transmit light, the transmission profiles are inserted in appendix II, as well as the original profiles of backscattering. The table 16 was constructed to compare the results obtained with both the Turbiscan^{TM}, from which is observed that the values are almost the same.

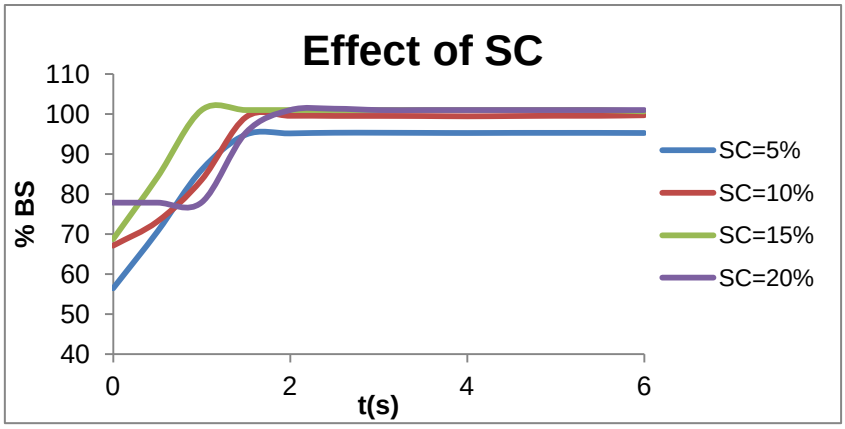

Figure 48: Backscattering profiles of sample NB7 at different SC, measured with Turbiscan^{TM}On Line.

Table 16: Comparison between the Turbiscan^{TM}Lab and the Turbiscan^{TM}OnLine of transmission and backscattering of sample NB7 at different SC (%w/w).

SC(%)	Transmission(%) Turbiscan^{TM}Lab	Transmission(%) Turbiscan^{TM}OnLine	Backscattering(%) Turbiscan^{TM}Lab	Backscattering(%) Turbiscan^{TM}OnLine
5	0	0	96	95
10	0	0	101	100
15	0	0	102	101
20	0	0	102	101

The mass flows are inserted in table 17. For the sample with 5% of SC, the mass flow obtained in the 2nd test is smaller than the mass flow of the 1st and 3rd tests, due the presence of air bubbles in the pipes. Excluding this point, and comparing all the mass flows of all the samples, it's concluded that the higher the SC more difficult it becomes to pass through the pipes and, consequently, more difficult is to analyze it with Turbiscan^{TM}On Line.

Table 17: Mass flow of sample NB7 at different SC (%w/w).

SC(%)	Nº of tests	M_{total} (g)	t(s)	Q_M(g/s)
5	1st test	244	7	34.8
	2nd test	209	46	4.5
	3rd test	239	6	39.8
10	1st test	248	10	24.8
	2nd test	247	6	41.1
	3rd test	215	7	30.6
15	1st test	221	8	27.7
	2nd test	219	8	27.3
	3rd test	217	10	21.7
20	1st test	202	41	4.9
	2nd test	192	25	7.7
	3rd test	189	42	4.5

To complete the study of the effect of SC in the mass flow, other latex, poly vinyl acetate with a particle size of 300 nm and a SC of 30%, was analyzed.[8] It was only performed one test for 5

[8] This latex wasn't synthetized in this project.

minutes. After opening the valve, the latex practically didn't flow. To increase the rate, the pipes were tightened manually. Then, the latex flow a little faster until reach the sensor.

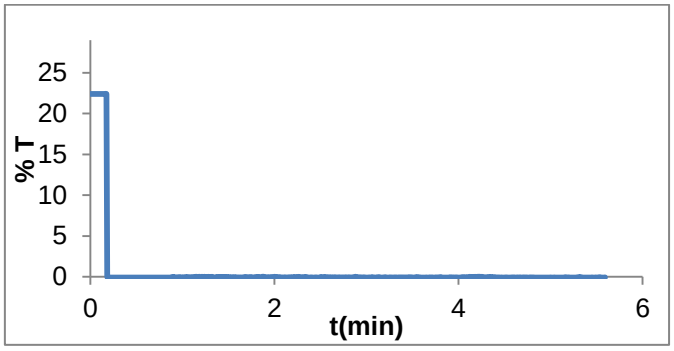

Figure 49: Transmission profile of poly vinyl acetate at 30%w/w.

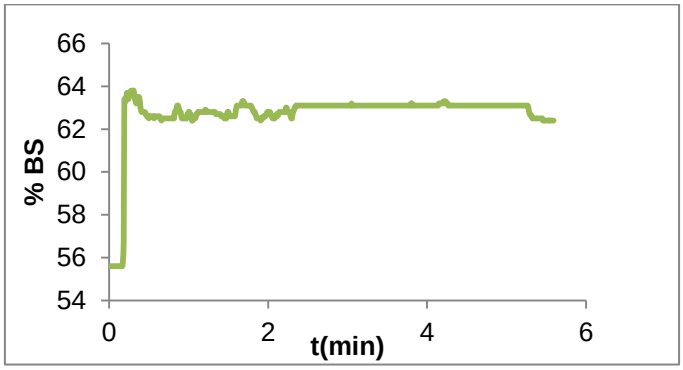

Figure 50: Backscattering profile of poly vinyl acetate at 30%w/w.

At the end of this study it is concluded that the way how the equipments were arranged is not the most correct for more viscous latexes because they do not flow with the simple force of gravity. One possible solution would be the use of a pump.

3.1.5. Conclusions

In this first part of the project the following conclusions are taken: the backscattering is proportional to the particle size and solid content (in both the devices Turbiscan^{TM}) and is much more sensitive to bigger particles when 2 latexes with different sizes, but same solid content, are mixed. The backscattering should not be saturated in order to have reliable results. The use of Turbiscan^{TM}On Line with the simple force of gravity to analyze latexes with a high solid content is not advisable since they do not flow properly.

3.2. Estimation of CCC and Hamaker constant

The estimation of CCC and Hamaker constant was made with experiments in which coagulation between polymer particles was provoked by electrolyte addition. All the experiments were performed in the Turbiscan^{TM}Lab.

3.2.1. Effect of SDS concentration on Hamaker constant

The effect of SDS concentration on coagulation was the first study to be performed. The aim is to get samples with the same particle size, the same SC but stabilized with different concentrations of SDS. For this purpose and take into account the data represented in figure 19, two reactions with SDS concentrations of 1 and 0.5 g/L_{water} (reactions MM1 and MM2, respectively), were carried out. To enrich this study, the sample obtained at the end of the reaction MM1 (called MM1 final from now on) was cleaned and also used for coagulation studies. The explanation of how the cleaning was done will be described later on.

The first sample to be analyzed was the MM1 final. The PSD was first measured and the results are shown in figure 51. It may be concluded that the sample wasn't coagulated. To check if the sample wasn't saturated and if wasn't transmitting light, a 5 ml sample was analyzed in Turbiscan^{TM}Lab with the scan mode for 4 minutes. The sample didn't transmit light. Since the backscattering was around 100%, the sample was diluted until 10% and 2% of SC(%w/w). The dilution until 10% wasn't enough, but for 2% the backscattering decreases until 80% (see figure 53). The transmission was zero (see figure 52) and backscattering was below the 100%, so it was possible to move on for coagulation.

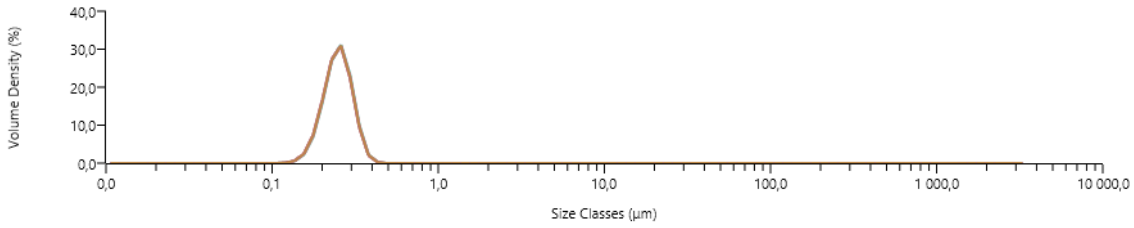

Figure 51: PSD of sample MM1 final, measured with Mastersizer®3000.

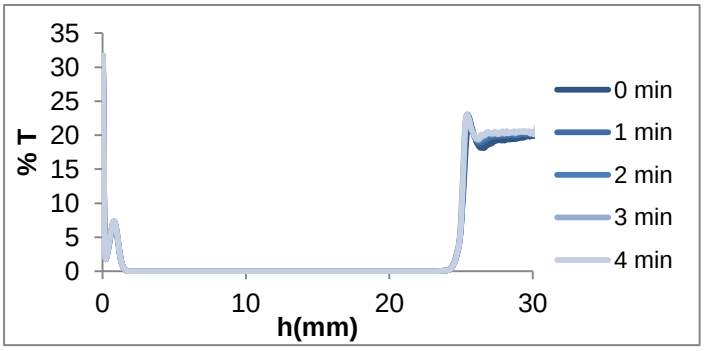

Figure 52: Transmission profiles before coagulation of sample MM1 final at 2%w/w, measured with Turbiscan^{TM}Lab.

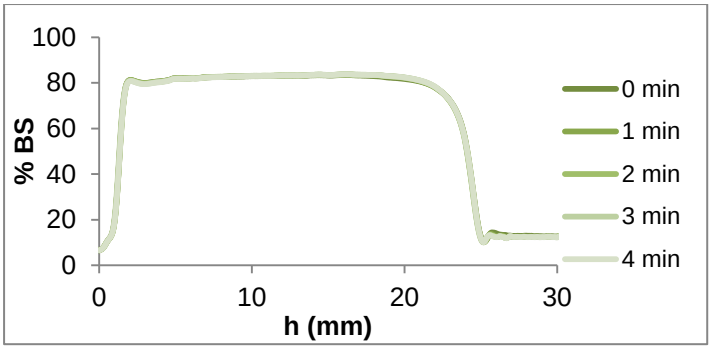

Figure 53: Backscattering profiles before coagulation of sample MM1 final at 2%w/w, measured with Turbiscan^{TM}Lab.

From now on, all the transmission profiles are inserted in the appendix II, since none of the samples transmit light.

About 10 ml of sample MM1 final were diluted until 2% and introduced into one of the appropriate cells for Turbiscan^{TM}Lab. Then, after insert the cell inside the device and the impeller inside the latex, the fixe mode was activated. After 1 minute, the agitation was switched on and kept for about 10 seconds. At 2.5, 5.5, 11.5, 16, 21 and 26.9 minutes, 40 µL of NaCl (with a concentration of 2M) were added. The resulting graph is represented in figure 54.

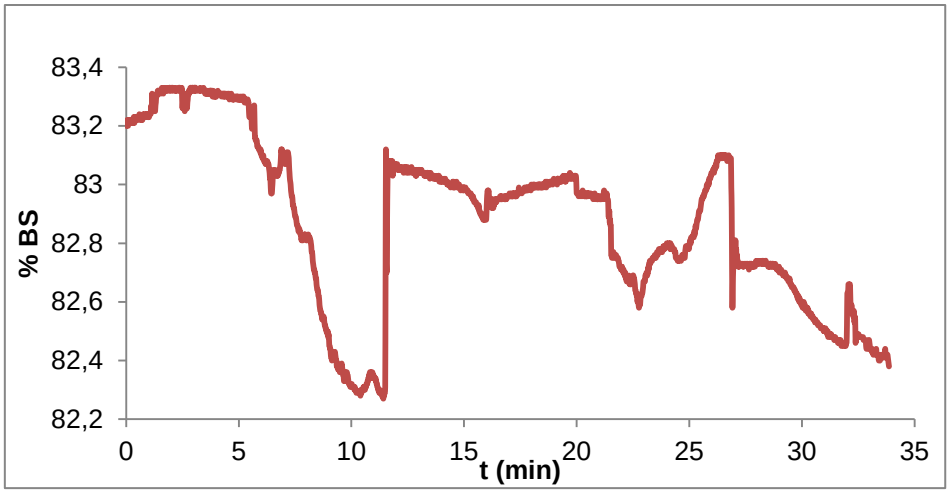

Figure 54: Evolution of backscattering during coagulation of sample MM1 final at 2%w/w, measured with Turbiscan^{TM}Lab. T=25ºC

Since the backscattering profile was always increasing and decreasing, it's very difficult to detect coagulation. So, It was decided to try to coagulate the same sample at different SC, namely 1% and 5%.

For 1% of SC the scan made before coagulation is represented in figure 55. The figure 56 corresponds to the backscattering profile during coagulation. At 1.5 minutes the agitation was switched on and at 3, 11, 21.5, 24, 31.8 and 36 were added 80 µL of NaCl (2M). It's oberved that the profile is similar to the one obtained before. So, the coagulation of this sample at this SC it's also difficult to evaluate.

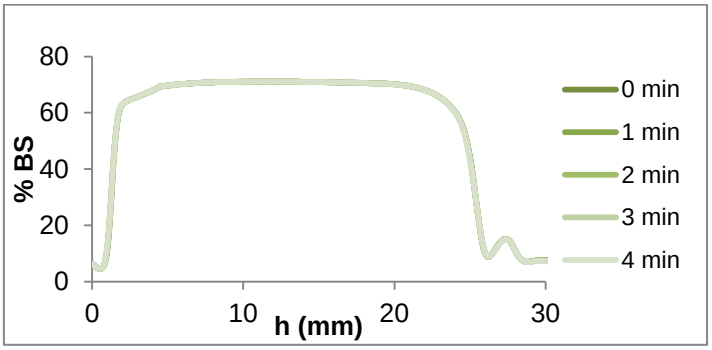

Figure 55: Backscattering profiles before coagulation of sample MM1 final at 1% w/w, measured with Turbiscan^{TM}Lab.

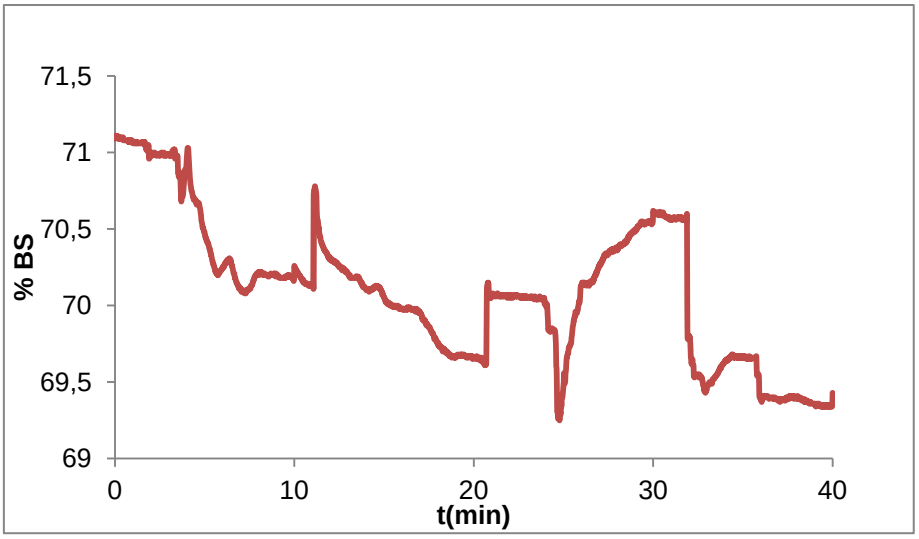

Figure 56: Evolution of backscattering during coagulation of sample MM1 final at 1%w/w, measured with Turbiscan^{TM}Lab. T=25ºC

For 5% of SC, the backsacttering before and during coagulation is represented in figures 57 and 58, respectively. For the coagulation process, the agitation was switched on at 1.2 minutes and at 2.8, 11.7, 17, 22, 24.5, 26.5 minutes were added 100 µL of NaCl (2M). After 6 shots of salt, the backscattering were not changing to much. So, it was decided to increase the amount of salt in the next shot. At 33.2, 35.4 and 38 minutes were, then, added 300 µL of NaCl (2M). The backscattering continued to decrease but the tendency was exactly the same, which lead to a new increase of the amount of salt. At 41.3, 43.5 and 45.6 were added 500 µL of NaCl (2M). The profile obtained was much more coherente and after 46 minutes adding salt, the backscattering decreased steeply. In order to check if the sample was coagulated, the PSD was measured. Comparing the figures 51 and 60, it's concluded that the sample is practically all coagulated. Therefore, the decrease of backscattering can be related to coagulation.

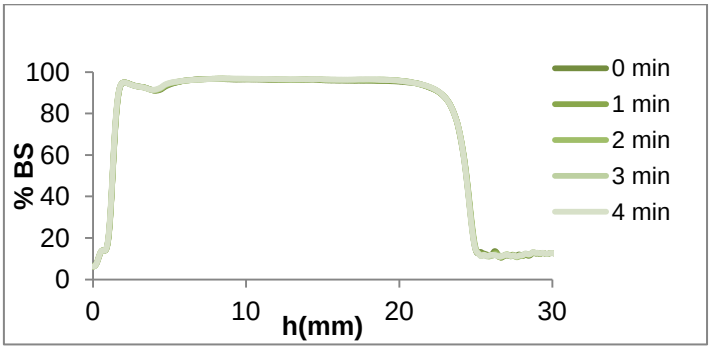

Figure 57: Backscattering profiles before coagulation of sample MM1 final at 5%w/w, measured with Turbiscan^{TM}Lab.

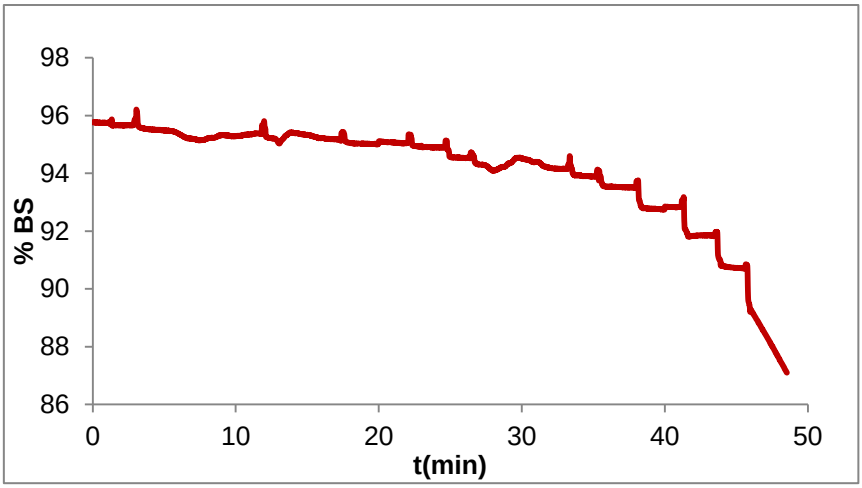

Figure 58: Evolution of backscattering during coagulation of MM1 final at 5%w/w, measured with Turbiscan^{TM}Lab. T=27ºC

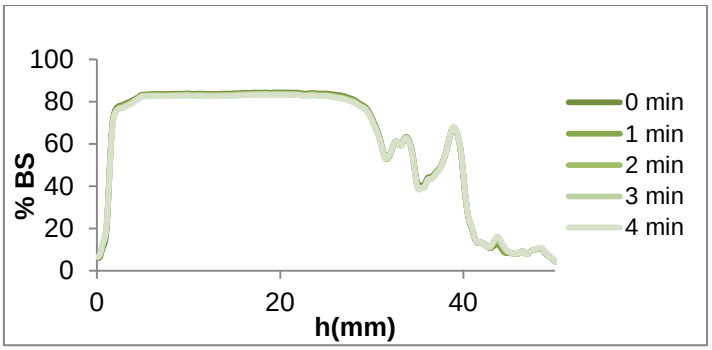

Figure 59: Backscattering profiles after coagulation of sample MM1 final at 5%w/w, measured with Turbiscan^{TM}Lab.

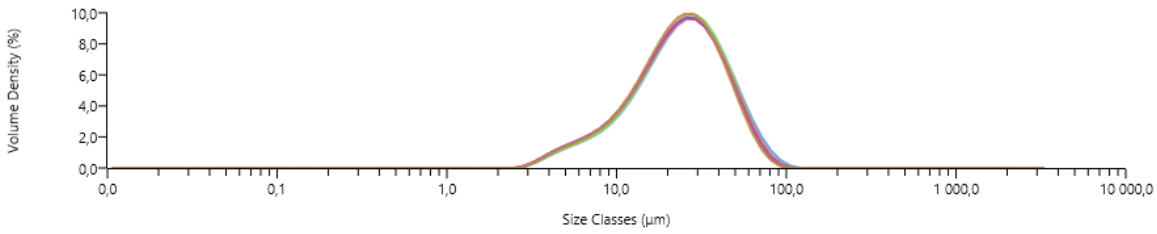

Figure 60: PSD of sample MM1 final at 5%w/w after coagulation, measured with Mastersizer$^{®}$3000.

To make sure that this method of coagulation is coherent, the 6th sample (called MM1(6)) extracted from the same reaction was diluted until 5% and coagulated exaclty the same way. The results can be seen in the figures below.

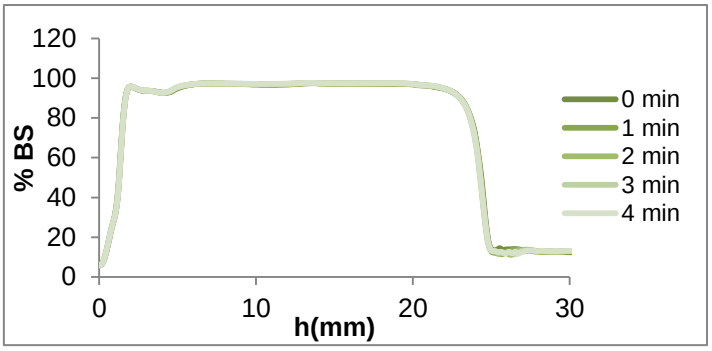

Figure 61: Backscattering profiles before coagulation of sample MM1 (6) at 5%w/w, measured with Turbiscan^{TM}Lab.

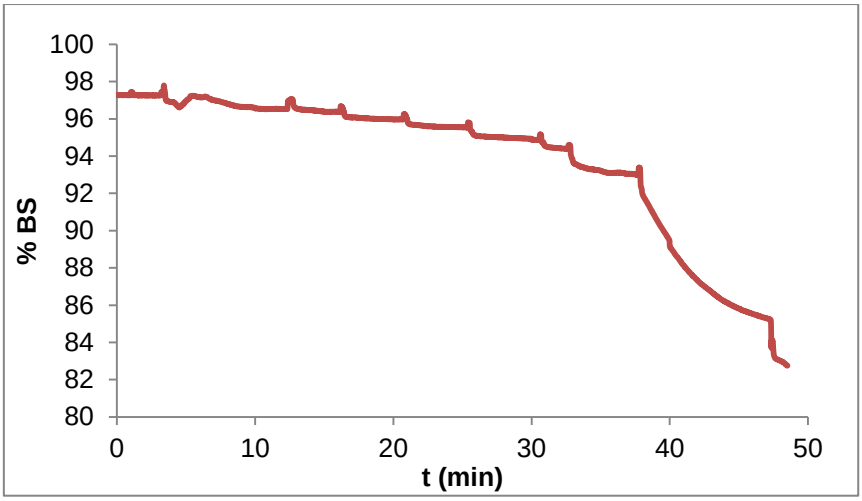

Figure 62: Evolution of backscattering during coagulation of sample MM1 (6) at 5%w/w, measured with Turbiscan^{TM}Lab. T=29ºC

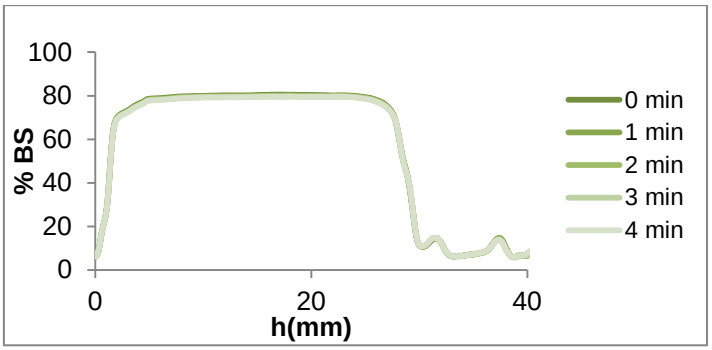

Figure 63: Backscattering profiles after coagulation of sample MM1 (6) at 5%w/w, measured with Turbiscan^{TM}Lab.

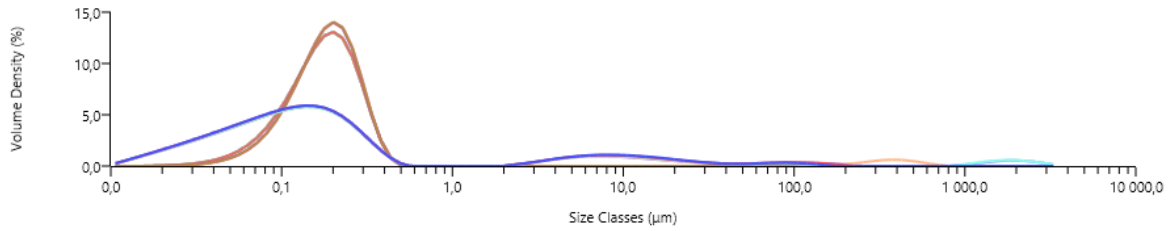

Figure 64: PSD of sample MM1(6) at 5%w/w, before (brown) and after coagulation (blue), measured with Mastersizer®3000.

It was observed that the method is coherent because the backscattering profile during coagulation has the same tendency along the time than those obtained previously and the sample coagulated, although not completely.

The next step was to study the effect of addition of water on coagulation. To do so, was used the sample MM1 final at 5% of SC. The procedure was exactly the same than those used to coagulate the previous latexes. The only diference was that instead of adding salt, was added water. In order to facilitate the data treatment, the amount of water added at each shot was the same than the amount of salt added to coagulate the same latex. The results are shown in figures 65 to 67.

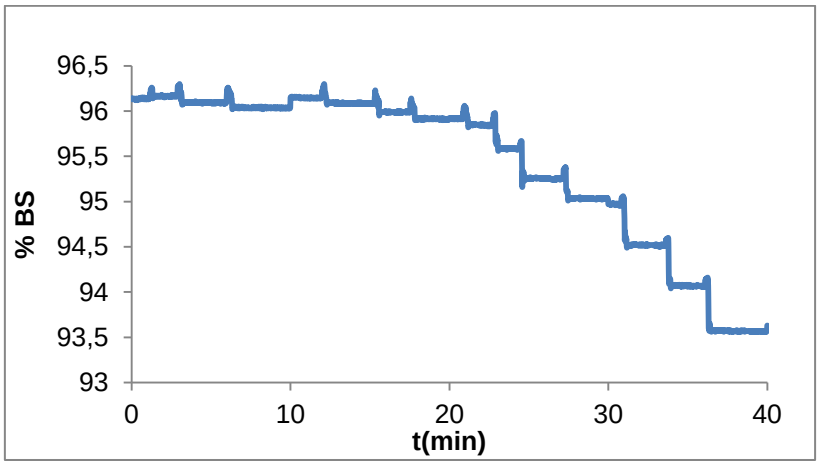

Figure 65: Evolution of backscattering during the addition of water of sample MM1 final at 5%w/w, measured with Turbiscan™Lab. T=27,5ºC

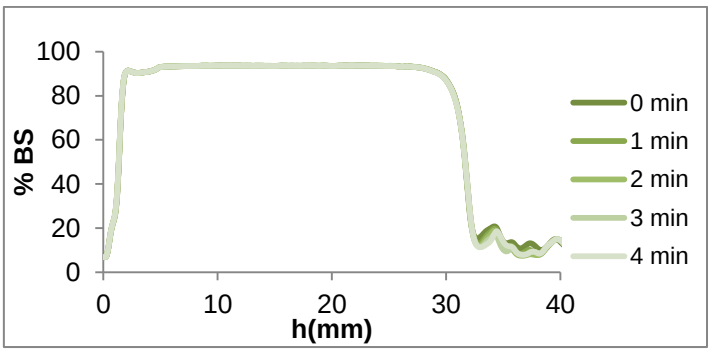

Figure 66: Backscattering profiles of sample MM1 final at 5%w/w after the addition of water, measured with Turbiscan™Lab.

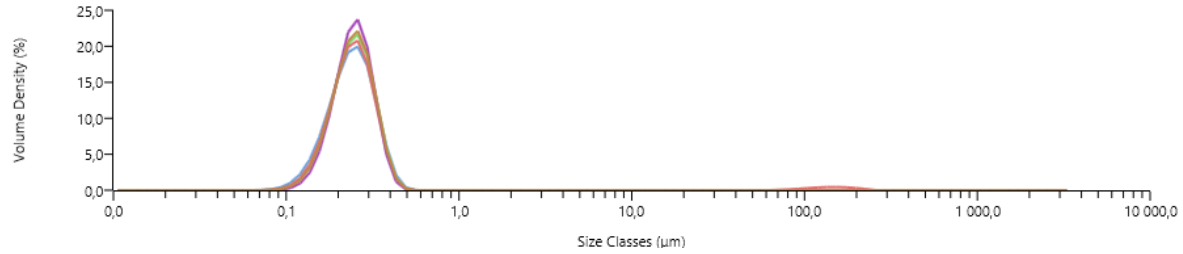

Figure 67: PSD of sample MM1 final at 5%w/w after the addition of water, measured with Mastersizer®3000.

The results show that the water doesn't have any effect on coagulation. However, as was demonstrate in previously studies about the effect of SC in backscattering, the water has an important effect on the decrease of backscattering, which can not be ignored, since when the salt is added, water is also added.

In order to perform data treatment with the aim to determine the CCC and Hamaker constant, the results from figures 58 and 65 were taken into account. The first step was to remove the effect of water during the coagulation. To this aim, the backscattering is normalized in order to obtain a graph with the profiles of salt and water starting at the same point. This graph is represented in figure 68, where the axis of ordenade is the % of backscattering and the axis of abscissae is the volume added (accumulative value) of salt or water, i.e., the volume of electrolyte in the solution after each addition. Since there were a lot of points at the same volume added, it was made an average of the backscattering for each volume (see figure 69). With the graph plotted in figure 68, it was possible to make the difference between the salt and water points (see figure 70).

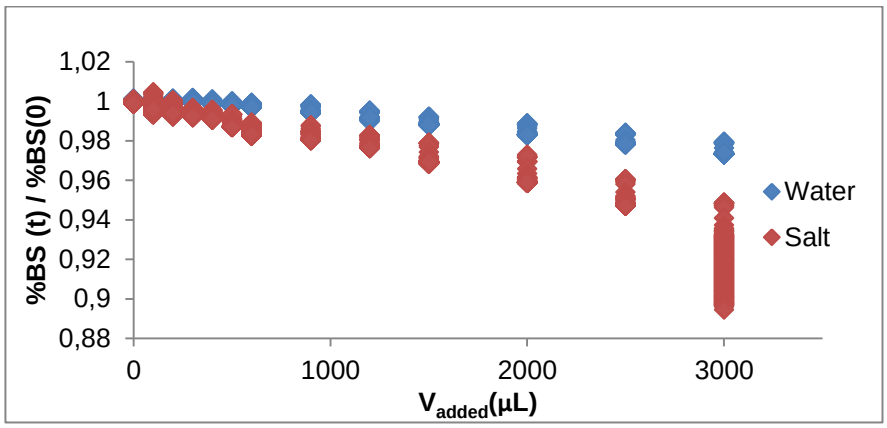

Figure 68: Evolution of backscattering normalized of sample MM1 final at 5%w/w during the addition of water and salt in function of V_{added}.

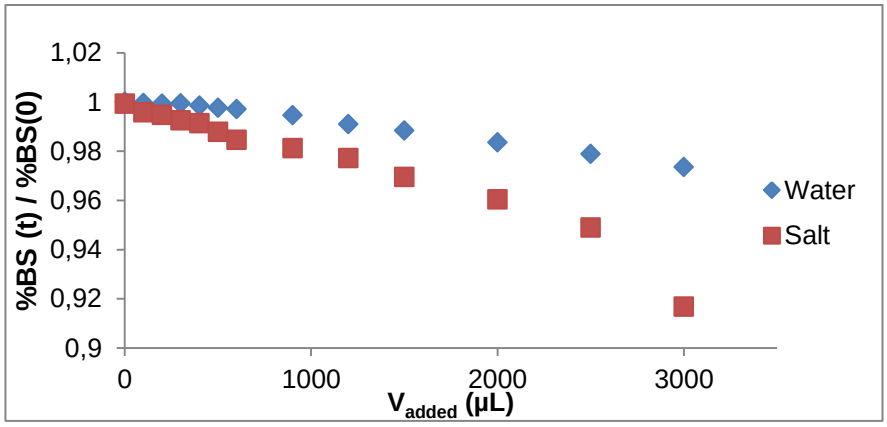

Figure 69: Evolution of backscattering normalized of sample MM1 final at 5%w/w during the addition of water and salt in function of V_{added} -Average.

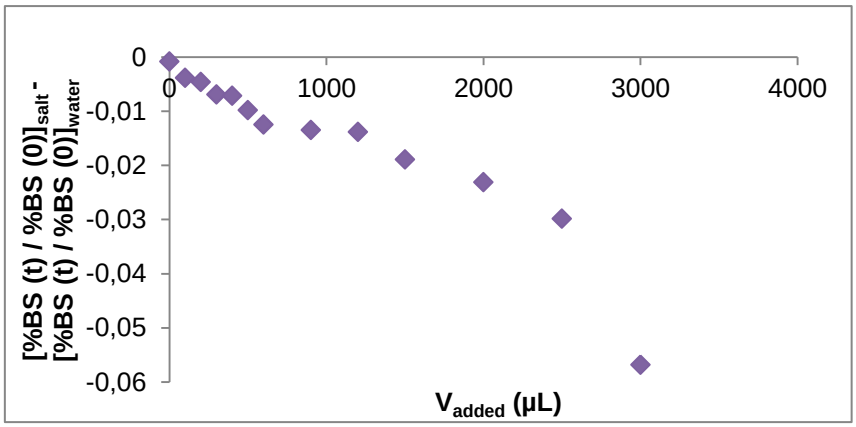

Figure 70: Evolution of backscattering with V_{added} of sample MM1 final at 5%w/w after removing the effect of water.

In the next step was applied the equation (21) to calculate the stability ratio, W. To do so, it was necessary to determine the electrolyte concentration in the solution after each addition, C_E, and estimate the CCC. The C_E, was calculated by the following equation:

$$C_E = \frac{V_{added} \times C_0}{V_{added} + V_0} \quad (23)$$

Where V_{added}, C_0 and V_0 correspond to the volume of electrolyte in the solution after each addition, the initial concentration of electrolyte and the initial volume of latex in the cell, respectively.

The CCC is estimated through the analysis of the graph of Figure 71 (which is similar to that represented in figure 70, where instead of the V_{added}, is the C_E that is in the axis of abcissae) and of a graph of logW versus logC_E. The CCC chosen should be the one that allows to obtain graphs similar to those of Figure 11. Generally, the CCC is located in the region where the backscattering signal begins to stabilize. In figure 71 no clear stabilization of the backscattering is oberved. Therefore, it was decided to repeat the experiment with an additional number of shots of salt.

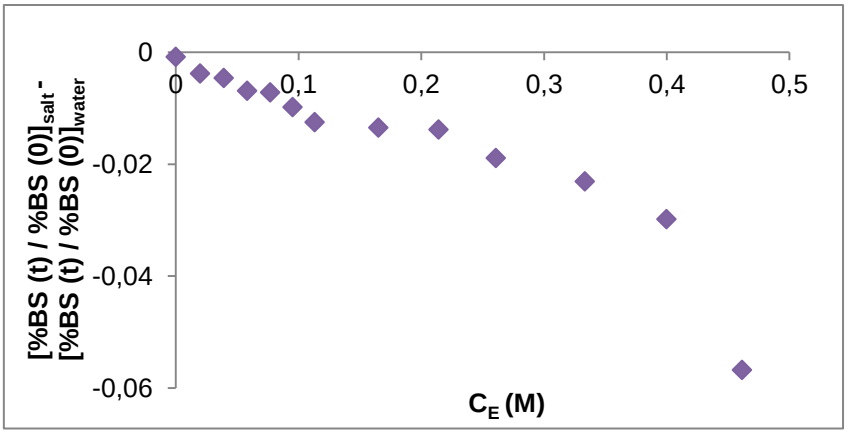

Figure 71: Evolution of backscattering with C_E after removing the effect of water of sample MM1 final at 5%w/w.

In figure 72 the new backsacttering profile during coagulation and upon addition of water is shown. The normalized backsacterring according to procedure previously described are represented in figures 73 and 74.

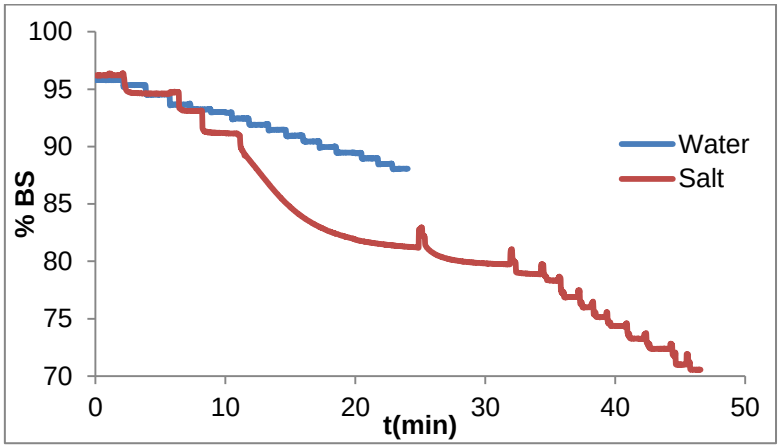

Figure 72: Evolution of backscattering of sample MM1final at 5%w/w, during coagulation (red) and addition of water (blue) measured with Turbiscan^{TM}Lab- 2nd test. T=25.5ºC

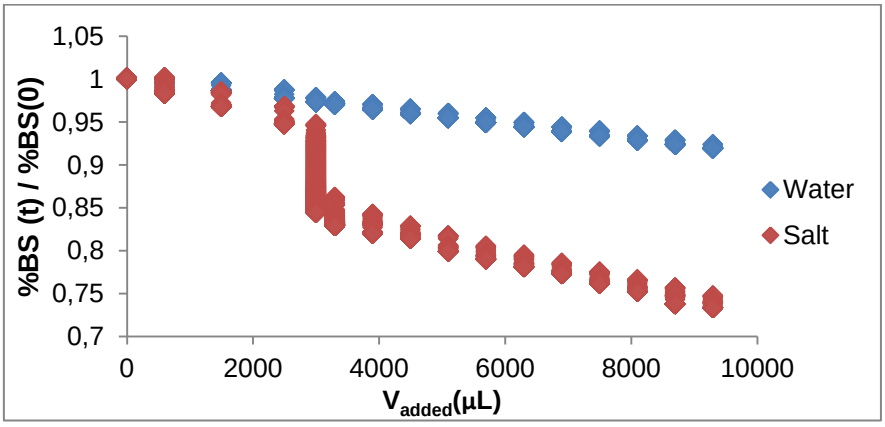

Figure 73: Backscattering normalized of sample MM1 final at 5%w/w during the addition of water and salt in function of volume added - 2nd test.

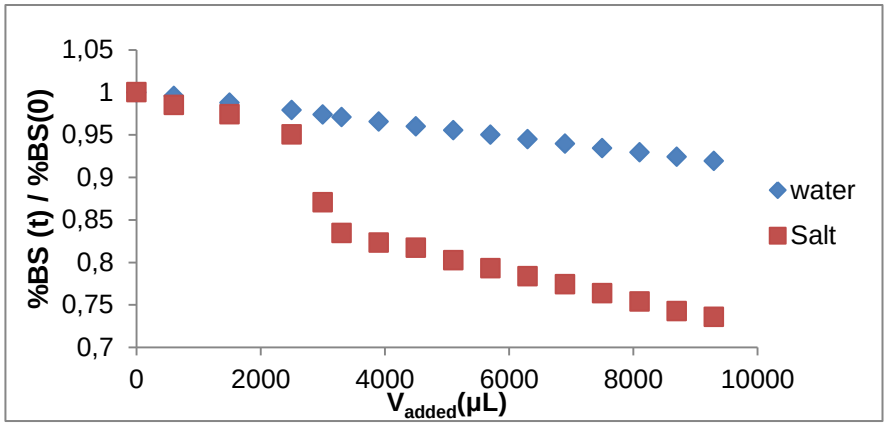

Figure 74: Backscattering normalized of sample MM1 final at 5%w/w during the addition of water and salt in function of volume added –Average- 2nd test.

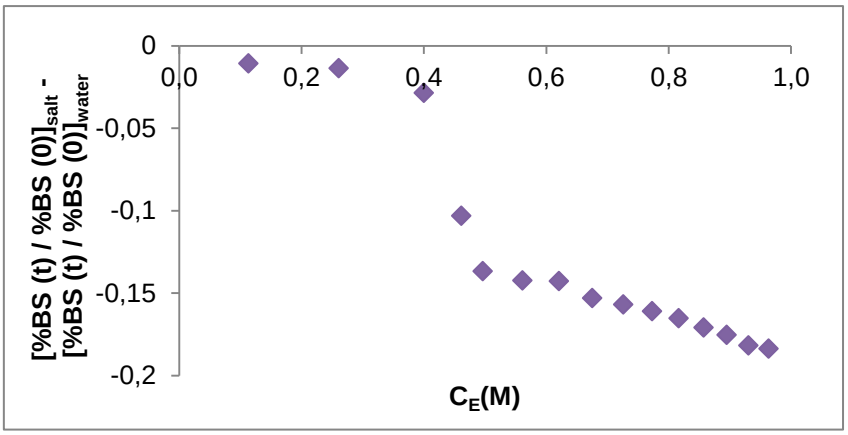

Figure 75: Evolution of backscattering with C_E of sample MM1 final at 5%w/w after removing the effect of water - 2nd test.

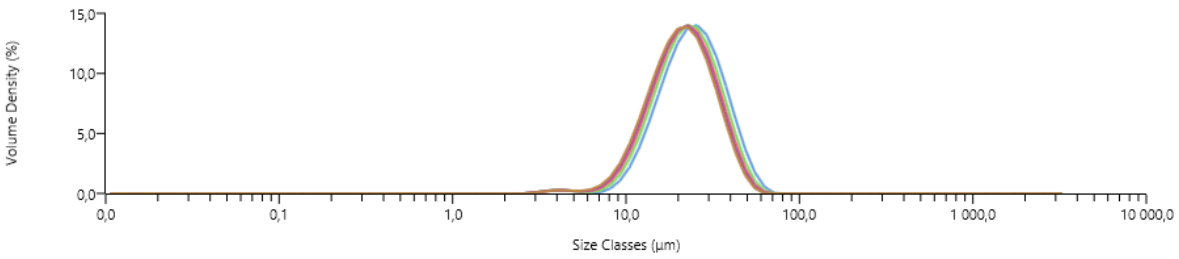

Figure 76: PSD of sample MM1 final at 5%w/w after coagulation, measured with Mastersizer®3000- 2nd test.

From figure 75 is now clear visible a fast decrease of backscattering followed by stabilization, which enables a more accurate determination of the CCC. The coagulation of the sample is confirmed by the PSD shown in figure 76.

The Hamaker constant was obtained from the slope of the graph of LogW vs $LogC_E$ [21], represented in figure 78, and using the equation (22). The 3 yellow points were used to determine this slope (see figure 79). The results are given in table 18.

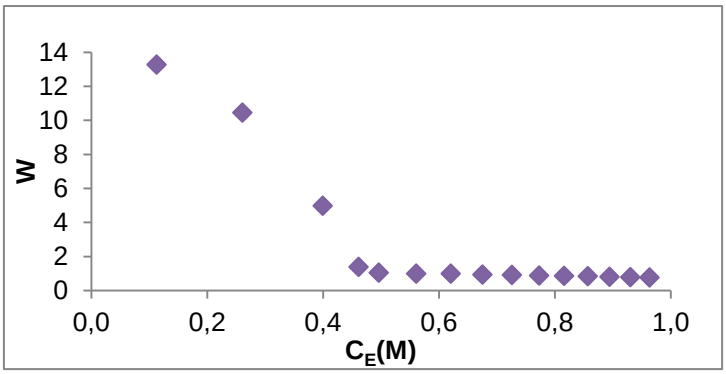

Figure 77: Experimental dependence of W on the C_E of sample MM1 final at 5%w/w- 2nd test.

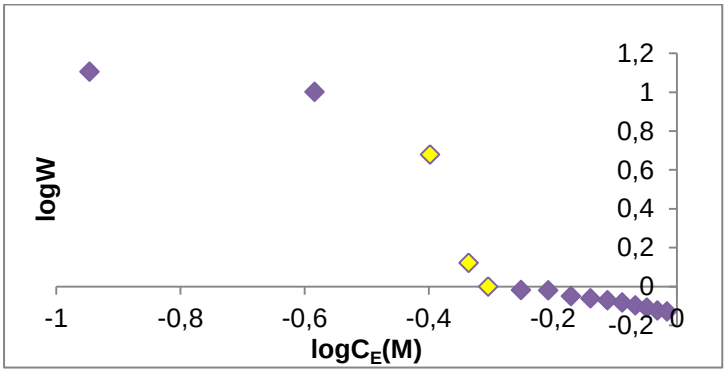

Figure 78: Experimental dependence of logW on the $\log C_E$ of sample MM1 final at 5%w/w- 2nd test.

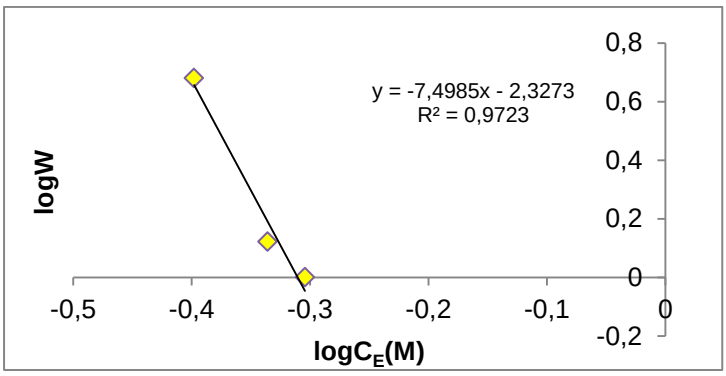

Figure 79: Slope of the stability curve of sample MM1 final at 5%w/w- 2nd test.

Table 18: Values of CCC and A determined by turbidity measurements of sample MM1 final at 5%w/w.

[SDS](g/L_{water})	**1**
r(nm)	143
$\frac{dlogW}{dLogC_E}$	7.50
CCC(M)	0.5
A(J)	3.1×10^{-21}

Since the slope was determined with only 3 points, the associate error may affect significantly the Hamaker constant. However, the order of magnitude is similar to those found in literature. [22]

In order to study the effect of SDS concentration, a sample with a similar diameter to MM1 final was selected from reaction MM2, which was stabilized with 0.5g/L_{water} of SDS. The chosen sample was the 5th sample taken from the reactor, called MM2 (5) from now on, and it was diluted until 5% of SC. The figures represented below are the most important to determine the CCC and A. All the other profiles are inserted in the appendix II.

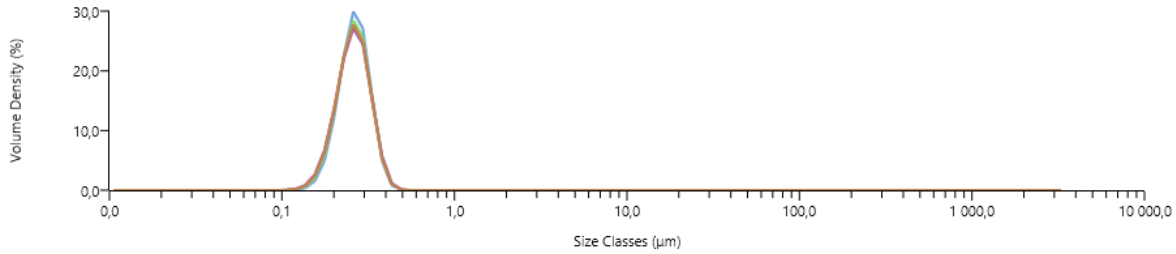

Figure 80: PSD of sample MM2 (5) at 5%w/w before coagulation, measured with Mastersizer®3000.

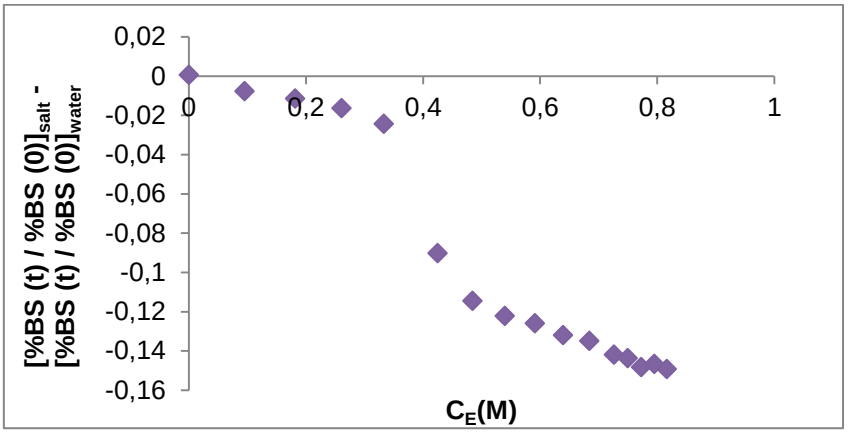

Figure 81: Evolution of backscattering with C_E of sample MM2 (5) at 5%w/w, after removing the effect of water.

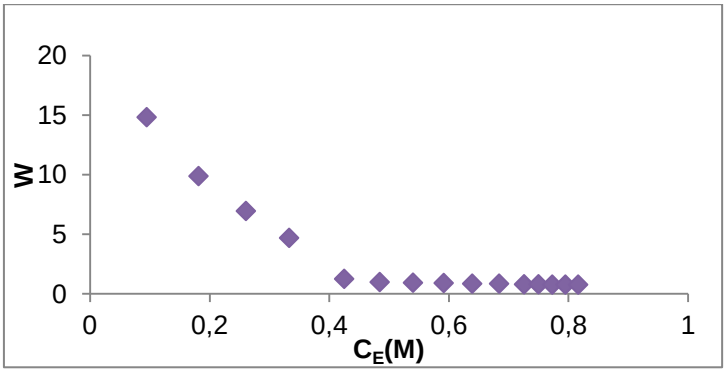

Figure 82: Experimental dependence of W on the C_E of sample MM2(5) at 5%w/w.

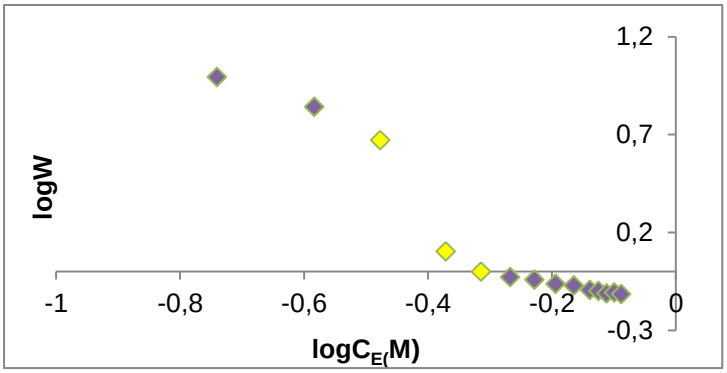

Figure 83: Experimental dependence of logW on the $logC_E$ of sample MM2(5) at 5%w/w.

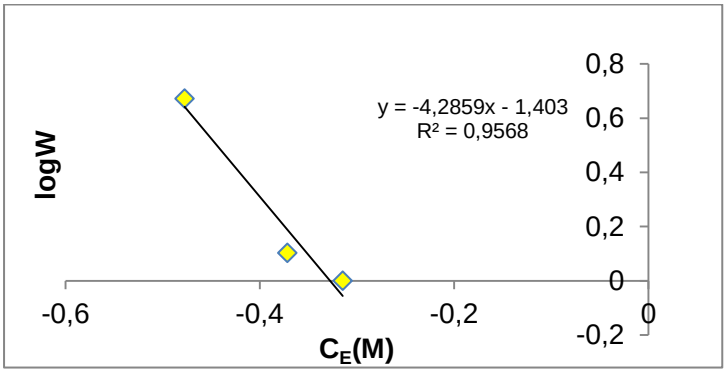

Figure 84: Slope of the stability curve of sample MM2(5) at 5%w/w.

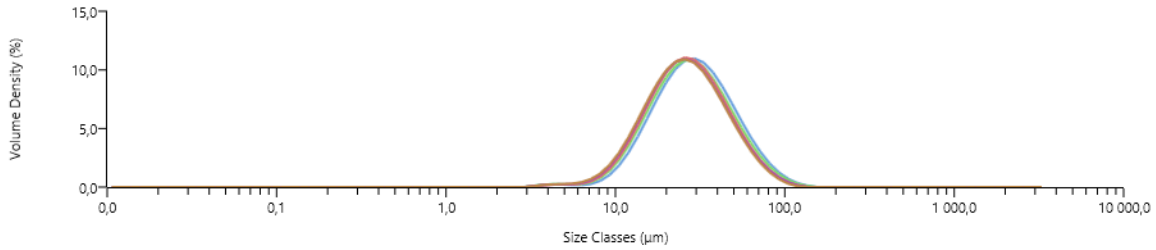

Figure 85: PSD of sample MM2 (5) at 5%w/w after coagulation, measured with Mastersizer®3000.

Table 19: Values of CCC and A determined by turbidity measurements of samples MM1 final and MM2 (5).

[SDS](g/L_{water})	**0.5**	**1**
r(nm)	132	143
$\frac{dlogW}{dLogC_E}$	4.3	7.5
CCC(M)	0.48	0.50
A(J)	1.9×10^{-21}	3.1×10^{-21}

The first thing to conclude is that the sample coagulated, what can be seen observing the figures 80 and 85.

The CCC is higher for a SDS concentration of 1g/L_{water}, what was expected because latexes with a higher SDS concentration are more stable, what makes more difficult the coagulation. If the coagulation is more difficult, the CCC will increase. The values of Hamaker constant are more difficult to explain. This constant characterizes the attraction between the polymer particles [15], [22]. Thus, low values of this constant correspond to a higher stability of latex due to the decrease of the attractive forces. However, the opposite trend was observed. The Hamaker constant increased with the increase of CCC and SDS concentration. One possible explanation is the high sensibility of this constant to the determined slope ($dlogW/dlogC_E$). In order to obtain the expected trend and since the Hamaker constant is directly proportional to the slope and inversely proportional to the CCC, it should have been observed a decrease in slope or at least it should remain constant when the concentration of SDS increase.

To investigate this problem, a new series of samples were studied. This series was obtained from sample MM1 final, which was diluted until 6%w/w and subjected to a cleaning procedure in order to remove the surfactant, residual initiator and remaining monomer. This cleaned sample was divided to 3 bottles in which was added 1, 2 and 3 g/L_{water} of SDS. The cleaning procedure consists in passing the sample over a mixture of anionic and cationic ion-exchange resins. The withdrawal of the ionic species is monitored by measuring the latex conductivity, and it is assumed that the washing step is complete when the conductivity no longer decreased with successive passes over the resin. At the end, the polymer content of the latex was around 5 %w/w. Figure 86 shows the conductivity of the sample after each passage by the resin.

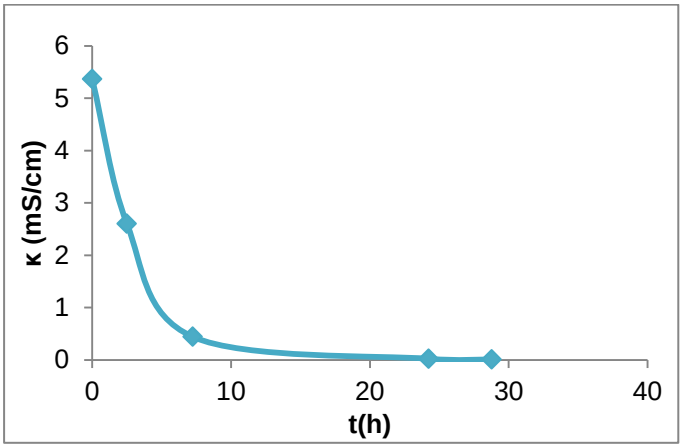

Figure 86: Conductivity of sample MM1 final.

The 3 new samples were coagulated and the results are represented in the next figures. In the appendix II, are inserted all the other figures obtained on the coagulation process. In table 20 are listed the slope, CCC and Hamaker constant for all the samples analyzed in this section.

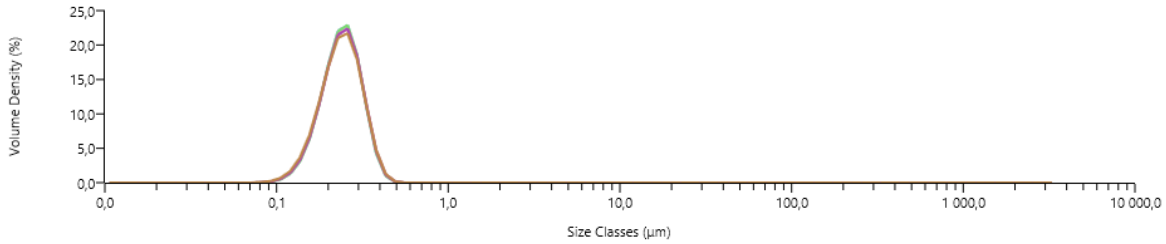

Figure 87: PSD of sample MM1 final cleaned at 5% w/w before coagulation, measured with Mastersizer®3000.

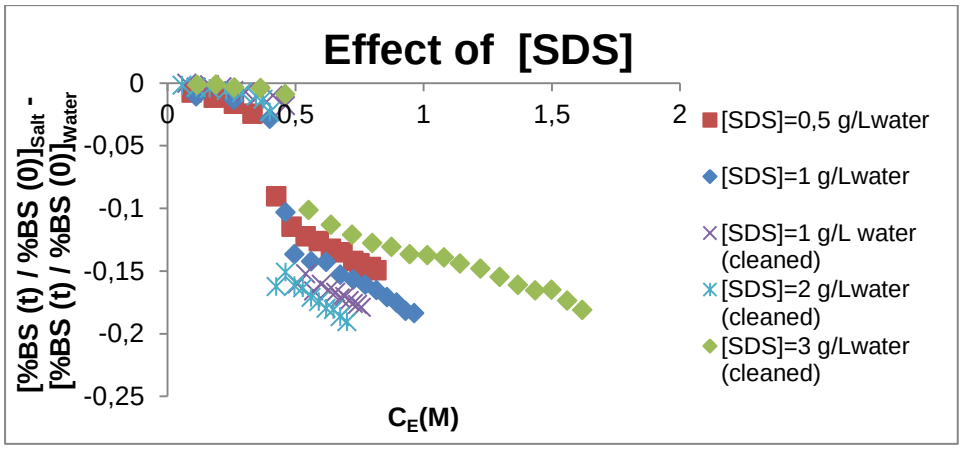

Figure 88: Evolution of backscattering with C_E of samples stabilized with different amounts of SDS and with a SC of 5% w/w, after removing the effect of water.

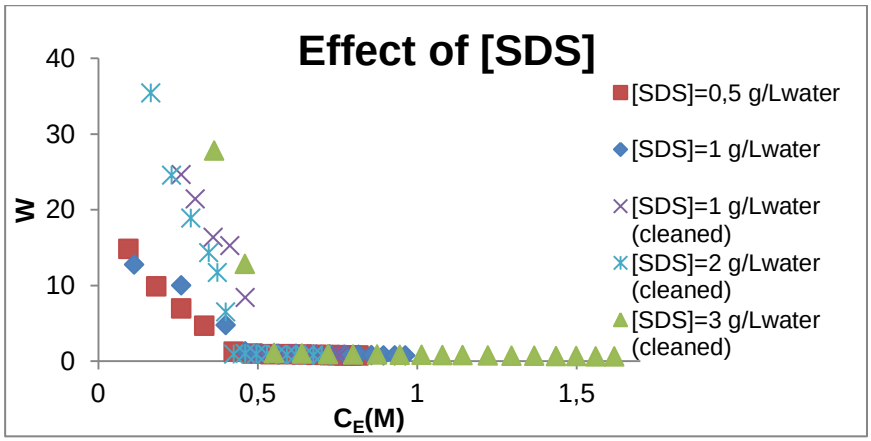

Figure 89: Experimental dependence of W on the C_E of samples stabilized with different amounts of SDS and with a SC of 5% w/w.

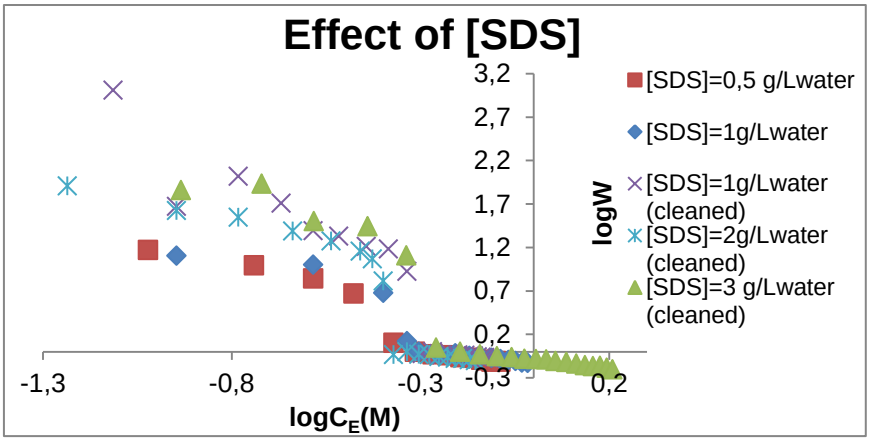

Figure 90: Experimental dependence of LogW on the $LogC_E$ of samples stabilized with different amounts of SDS and with a SC of 5% w/w.

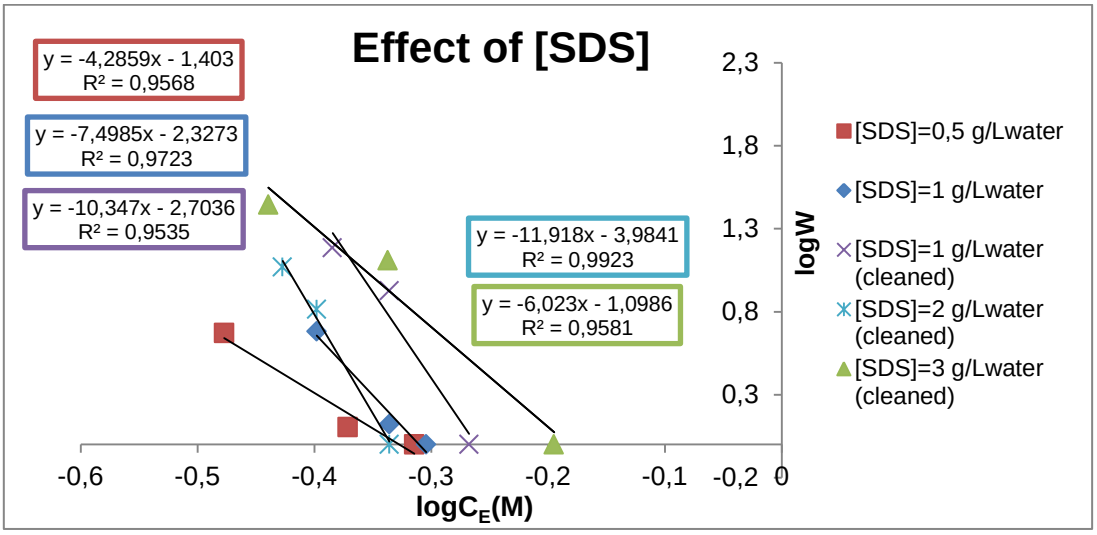

Figure 91: Slope of experimental dependence of logW on the $logC_E$ of samples stabilized with different amounts of SDS and with a SC of 5% w/w.

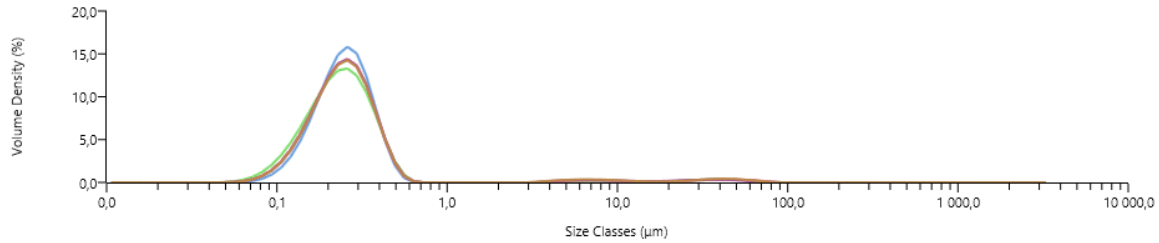

Figure 92: PSD of sample MM1 final cleaned with 5% w/w and stabilized with [SDS]= 1 g/L_{water} after coagulation measured with Mastersizer®3000.

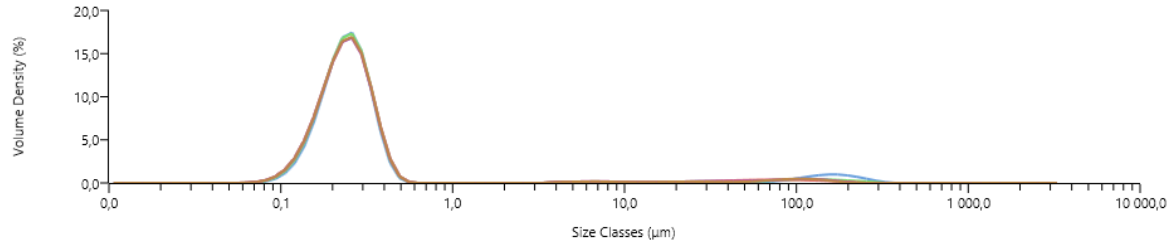

Figure 93: PSD of sample MM1 final cleaned with 5% w/w and stabilized with [SDS]= 2 g/L_{water} after coagulation, measured with Mastersizer®3000.

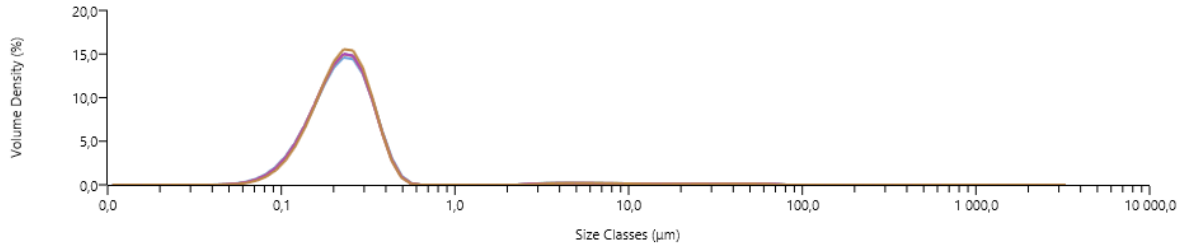

Figure 94: PSD of sample MM1 final cleaned with 5% w/w and stabilized with [SDS]= 3 g/L_{water} after coagulation, measured with Mastersizer®3000.

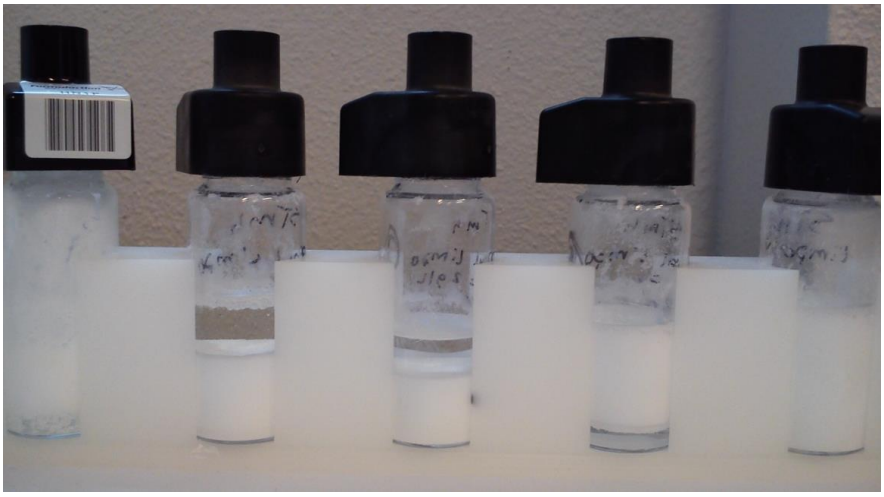

Figure 95: Samples MM1 final coagulated. From the left to the right: [SDS]= 1g/L_{water}, [SDS]= 1g/L_{water} (cleaned), [SDS]=2g/L_{water} (cleaned), [SDS]=3g/L_{water} (cleaned), [SDS]=3g/L_{water} (cleaned)-2nd test.

Observing figures 88 to 91 is quite clear that all the cleaned samples coagulated, since the tendency is similar to the others. Other evidence that they coagulated is given by figure 95. The first bottle corresponds to the MM1 final without cleaning, where it was possible to observe big particles. All the samples that were coagulated, but not cleaned before, had this aspect. However, after cleaning, adding salt and coagulate, the samples became much more unstable and the particles sedimented (2nd and 3rd bottles) or creamed (4th bottle) very quickly.

When a latex is cleaned, the charges are removed, some from the initiator and a lot from the surfactant. So, after washing a latex, there is very little surfactant and a little of initiator. Then, it is

added a control amount of surfactant to the surface. It's expected that the destabilization of the latex that was cleaned to be a little different from those not cleaned, depending on the surface coverage. This could be a reason why the cleaned samples had a different behavior after coagulated.

The more surfactant is added, the more different the surface will became and more difficult is to destabilize, and when destabilizes maybe the way that it happened is different. This could be an explanation for the creaming of the sample stabilized with 3g/L_{water} of SDS.

Another aspect that cannot be forgotten is that, according to Mastersizer® the cleaned samples didn't coagulate, since the PSD before and after the coagulation is practically the same, what can be seen in figures 87, 92, 93 and 94. The reason why it happened is completely unknown.

Due to all these unexpected results it was decided to repeat the experiments for the cleaned latexes with 2 and 3g/L_{water} of SDS. For the sample with 3g/$L_{water,}$ the results were quite the same: the CCC was the same, the A was similar (see table 20) and the PSD continued to show that the sample didn't coagulate. However, the particles didn't sediment or cream, what can be seen in the 5th bottle of figure 95. So, the samples destabilized in a different way. For the sample with 2g/L_{water}, the results are a little different: the CCC and A increased in this 2nd test. However the particles sedimented, as in the first test and according to the results given by Mastersizer®, the sample didn't coagulate.

Table 20: Values of CCC and A determined by turbidity measurements for the samples stabilized with different SDS concentrations.

[SDS] (g/L_{water})	**0.5**	**1**	**1 (cleaned)**	**2 (cleaned)**	**2 (cleaned)- 2nd test**	**3 (cleaned)**	**3 (cleaned)- 2nd test**
r(nm)	132	143	155				
$-\frac{dlogW}{dLogC_E}$	4.3	7.5	10.4	11.9	18.5	6.0	5.0
CCC(M)	0.48	0.50	0.54	0.46	0.51	0.64	0.64
A(J)	1.9 x 10^{-21}	3.1 x 10^{-21}	3.8 x 10^{-21}	4.7 x 10^{-21}	7.7 x 10^{-21}	2.0 x 10^{-21}	1.7 x 10^{-21}

Observing table 20, it's concluded that increasing the amount of SDS, the CCC also increases, except for the case of sample stabilized with 2g/L_{water}. According to reference [15] the CCC should increase with the SDS concentration.

Regarding the Hamaker constant is evident that it changes with different amounts of SDS. However, as was said previously, is difficult to explain how the SDS concentration affects this constant. In literature there are some theoretical values for polystyrene-water systems determined by different models. These values are comprised between 0.4x10^{-21} and 4.8 x10^{-21}. [22], [30] Except the Hamaker constant for 2g/L_{water}(2nd test), all the other values obtained in this work are within this range of values.

3.2.2. Effect of solid content on Hamaker constant

To study the effect of solid content, the samples to be analyzed must have the same size and, the amount of SDS with which were stabilized needs to be the same. So, it was chosen the sample MM2 (5) at 2, 5 and 10%w/w. The MM2 (5) at 5% was already analyzed. The results are shown in the following figures and table.

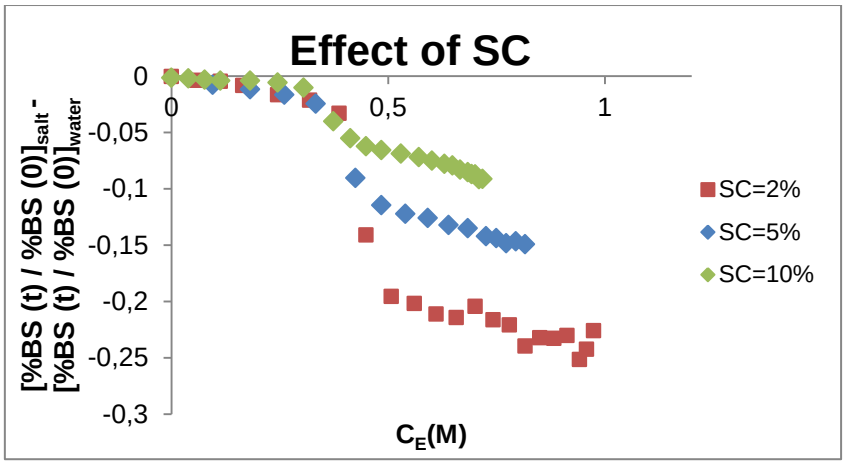

Figure 96: Evolution of backscattering with C_E of sample MM2 (5) at different SC, after removing the effect of water.

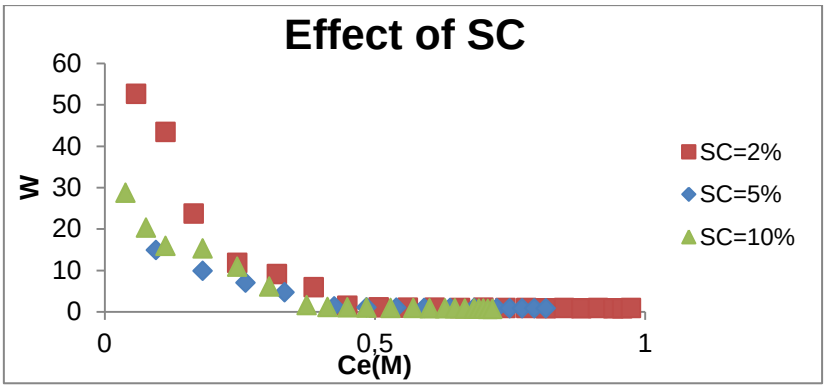

Figure 97: Experimental dependence of W on the C_E of sample MM2 (5) at different SC.

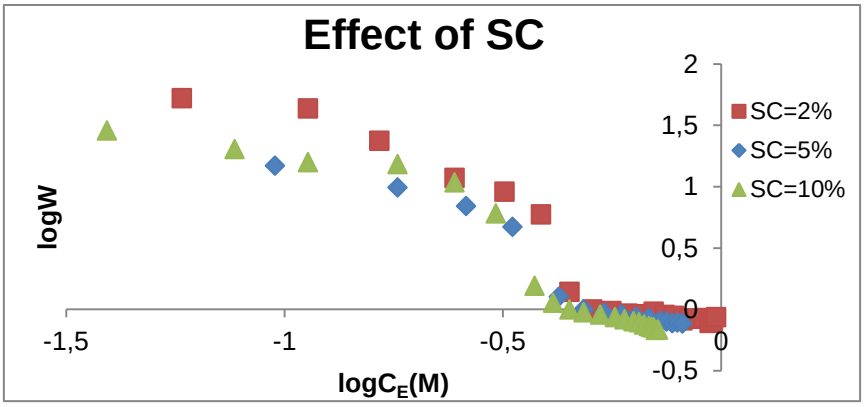

Figure 98: Experimental dependence of LogW on the $LogC_E$ of sample MM2 (5) at different SC.

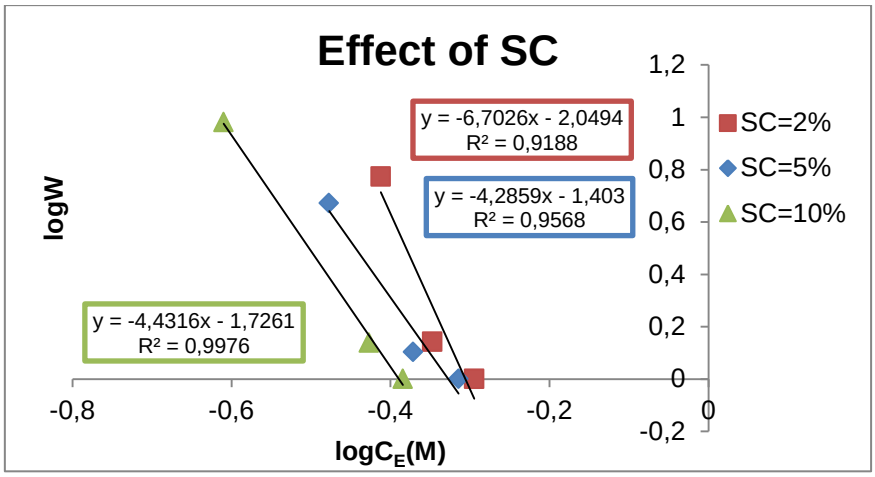

Figure 99: Slope of experimental dependence of LogW on the $LogC_E$ of sample MM2 (5) at different SC.

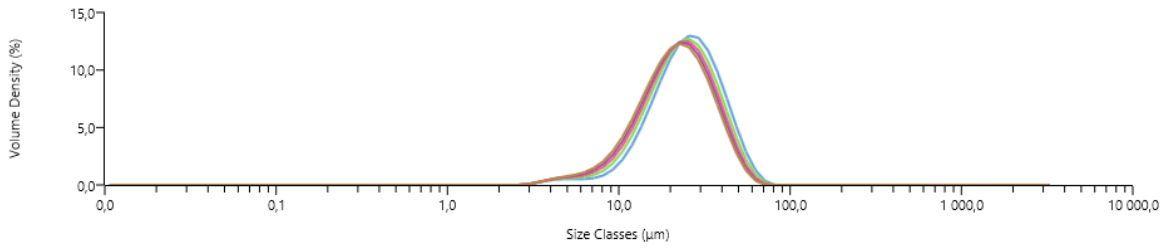

Figure 100: PSD of sample MM2 (5) at 2%w/w after coagulation, measured with Mastersizer®3000.

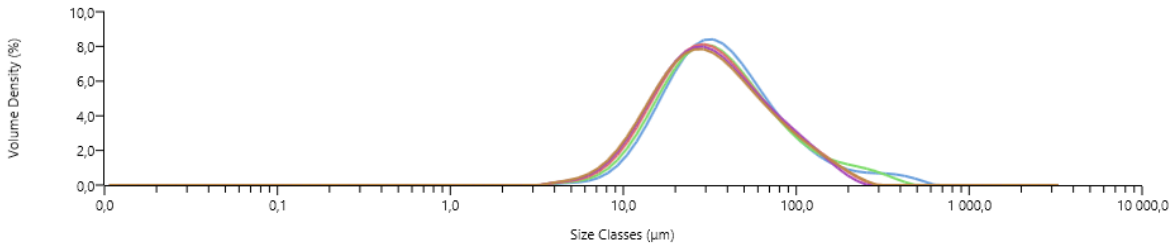

Figure 101: PSD of sample MM2 (5) at 10%w/w after coagulation, measured with Mastersizer®3000.

Table 21: Values of CCC and A determined by turbidity measurements for sample MM2 (5) at different SC.

SC(%w/w)	2	5	10
$-\frac{dlogW}{dLogC_E}$	6.7	4.3	4.4
CCC(M)	0.51	0.48	0.41
A(J)	3.0×10^{-21}	1.9×10^{-21}	2.2×10^{-21}

According with PSD (see figures 100 and 101), the sample MM2 (5) coagulated also at 2 and 10%.

Figure 96 shows that the backscattering is higher for samples with a higher solid content, what was already concluded with the previous studies (see sections 3.1.2 and 3.1.4).

Observing table 21, the CCC decreases with the increase of solid content, what was expected, since the increase of solid content means that there are more polymer particles so, the probability of coalescence and then coagulation is higher. Regarding the Hamaker constant, it should increase with the solid content, since this constant measure the attraction force between polymer particles. So, higher values of this constant correspond to a lower stability. This trend was observed when comparing the values obtained for 5 and 10%. Moreover, all the values for the Hamaker constant are within the range of theoretical values given in [22] and [30].

3.2.3. Effect of particle size on Hamaker constant

To study the effect of particle size on coagulation it were chosen the samples MM2 (5) and MM2(2) (2^{nd} sample taken from the reactor during the reaction MM2 which had a particle size of 157 nm) at 2%. The results are shown in figures 102 to 107 and in table 22.

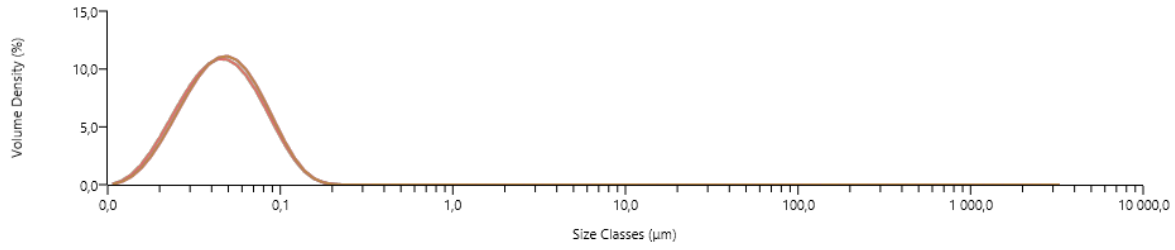

Figure 102: PSD of sample MM2 (final) before coagulation, measured with Mastersizer®3000

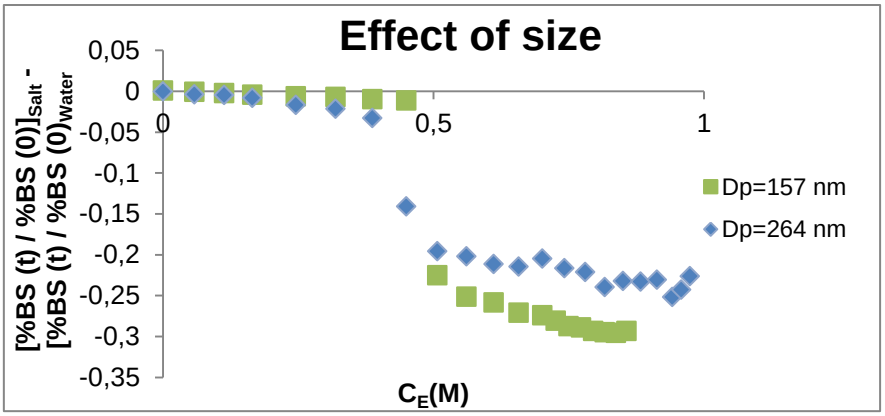

Figure 103: Evolution of backscattering with C_E of samples MM2 (2) (D_p=157 nm) and MM2 (5) (D_p=264 nm) at 2%w/w, after removing the effect of water.

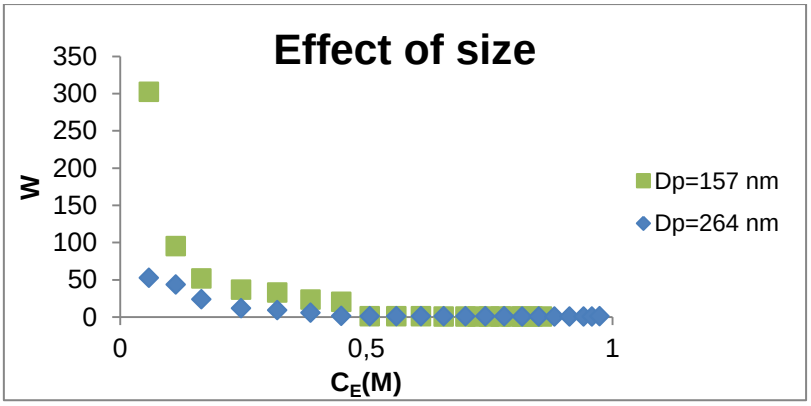

Figure 104: Experimental dependence of W on the C_E of samples MM2 (2) (D_p=157 nm) and MM2 (5) (D_p=264 nm) at 2%w/w.

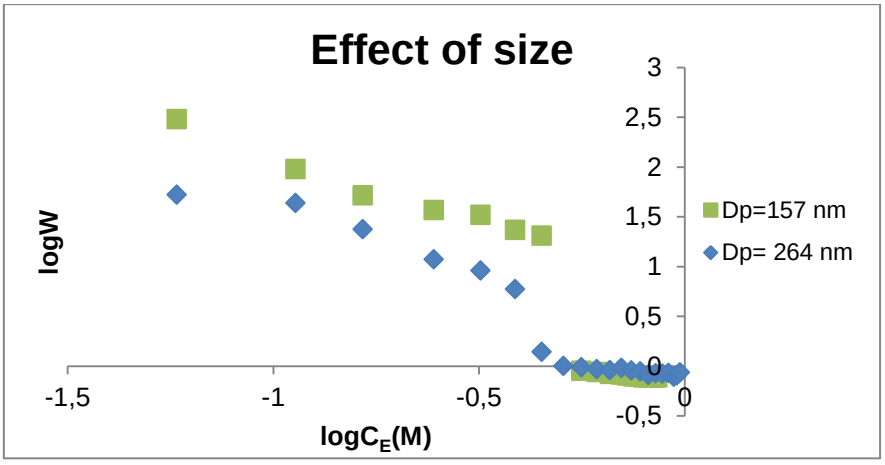

Figure 105: Experimental dependence of LogW on the LogC_E of samples MM2 (2) (D_p=157 nm) and MM2 (5) (D_p=264 nm) at 2%w/w.

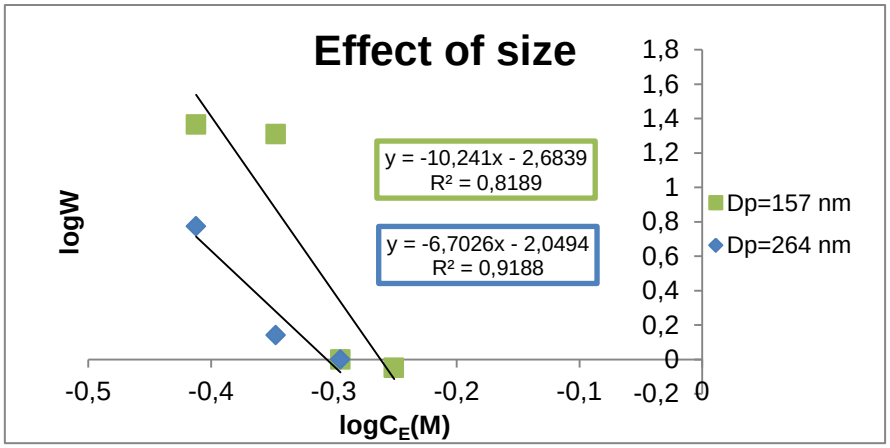

Figure 106: Slope of experimental dependence of LogW on the $LogC_E$ of samples MM2 (2) (D_p=157 nm) and MM2 (5) (D_p=264 nm) at 2%w/w.

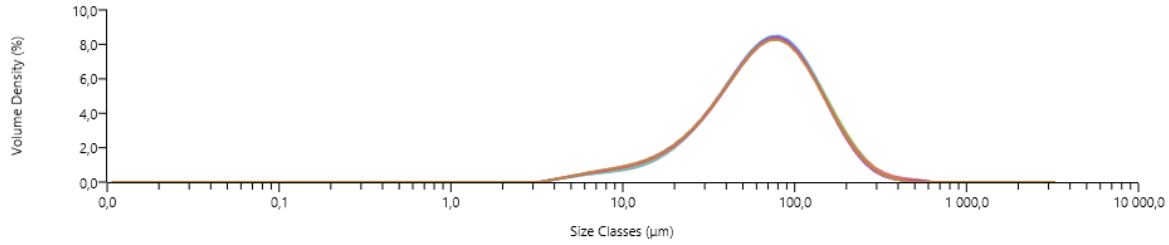

Figure 107:PSD of sample MM2 (final) at 2%w/w after coagulation, measured with Mastersizer®3000

Table 22: Values of CCC and A determined by turbidity measurements for samples MM2 (2) (D_p=157 nm) and MM2 (5) (D_p=264 nm) at 2%w/w.

D_p(nm)	**157**	**264**
$-\frac{dlogW}{dLogC_E}$	10.2	6.7
CCC(M)	0.56	0.51
A(J)	7.2×10^{-21}	3.0×10^{-21}

According to [31], the DLVO approach and the concept of stability ratio, W, predict that the small particles are more easily coagulated than the larger particles. However, the application of the theory in its kinetics forms (i.e., W criterion) to specific particle size effects has not been successful, since there are evidences in literature that the stability appears to decrease with increasing particle size[31], [32], [33]. In this project, the application of the theory in its kinetics forms wasn't also successful since the stability decreases with the increase of particle size, what can be seen in figure 104. Table 22 shows that the CCC is higher for small particles, what means that the bigger particles coagulate more easily.

Reerink and Overbeek[34] predicted that the slope of the curves logW against $LogC_E$ should increase with particle size. However, this wasn't observed. In fact, the slope decrease with increasing

particle size (see figure 106 and table 22). In [30], the theory predictions wasn't also observed. The polystyrene particles are spherical and monodisperse so neither the polydispersity or non-spherical shape can be invoked to explain this disagreement, as Reerink and Overbeek did to explain some results.

Ottewill and Shaw[30] concluded that there is a variation, a decrease, of Hamaker constant with particle size. The same was noticed in this work, what can be seen in table 22.

In literature there are some values of experimental Hamaker constant for systems polystyrene-water. These values are inserted in table 23. The Hamaker constants found in this work are within this range.

Table 23: Experimental Hamaker constant of polystyrene determined by different authors.

A ($x10^{-21}$J)	References
1,03-11	30
2-11	35
5-15	33
1.3-6.1	36
13	37
3-8	38
3.5	39
0.5-5	40
20-50	41
3.1-8.1	42
0.96-4.45	43

It weren't analyzed only this two particle sizes. A sample with a particle size of 425 nm (final sample of reaction MM2) were coagulated 2 times, being the evolution of backscattering represented in figure 108. Until 0.3 M the backscattering is always increasing, decreasing after this point. A possible explanation for this behavior can be found in figure 12. When the coagulation is being provoked, the particle size is increasing. Maybe, the 0.3 M corresponds to the peak of the graph represented in figure 12, reason why the backscattering increases and then decreases. With this profile was impossible to calculate the CCC.

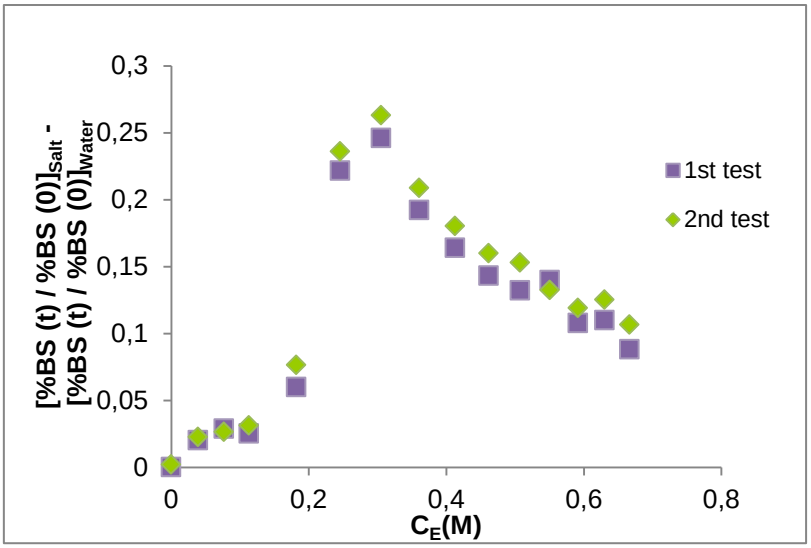

Figure 108: Evolution of backscattering with C_E of sample MM2 final ([SDS]=0.5 g/L_{water}, SC=2%w/w and D_p=425nm). T=26ºC.

3.2.4. Other studies

In order to enrich this work and to confirm if the method used to coagulate a latex is effective, it was induced the coagulation in other 2 polystyrene samples, with similar particle sizes and stabilized with different amount of a clay, named LP1 and LP2. Both of these latexes were diluted until 5%. The results are shown in figure 109 to 116 and summarized in table 24.

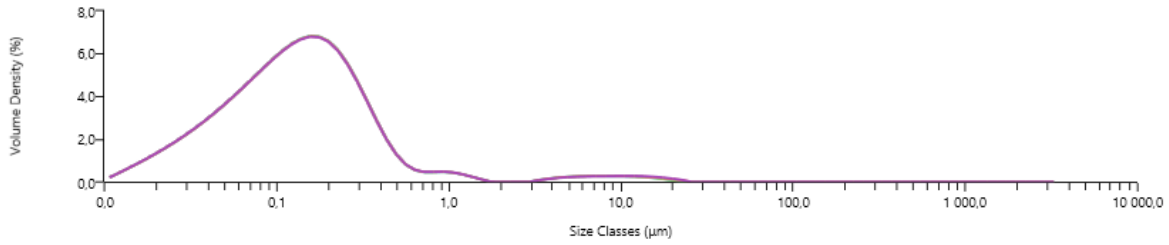

Figure 109:PSD of sample LP1 at 5%w/w before coagulation, measured with Mastersizer®3000

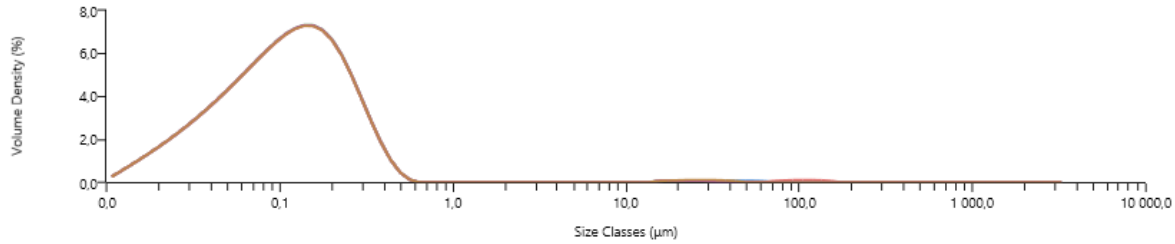

Figure 110: PSD of sample LP2 at 5%w/w before coagulation, measured with Mastersizer®3000.

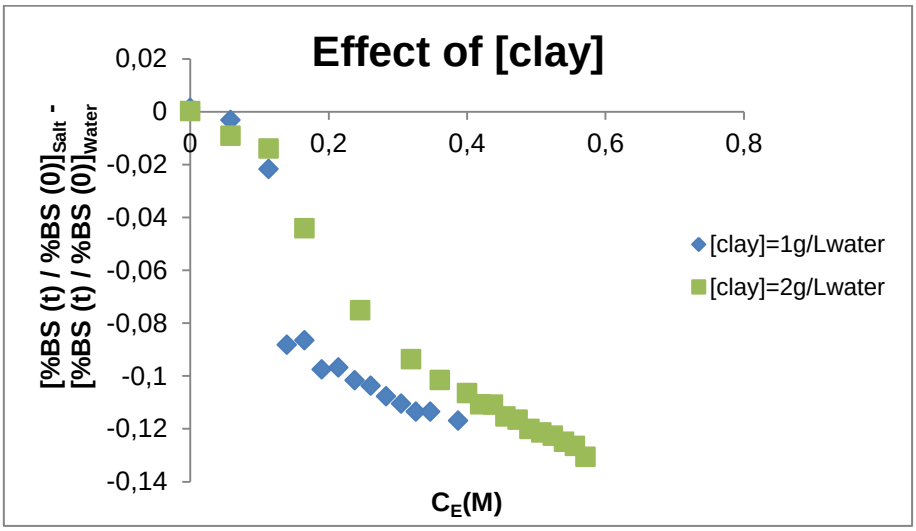

Figure 111: Evolution of backscattering with C_E of samples LP1 and LP2 at 5%w/w, which were stabilized with 1 and 2 g/L_{water} of clay, respectively, after removing the effect of water. T=25.5ºC

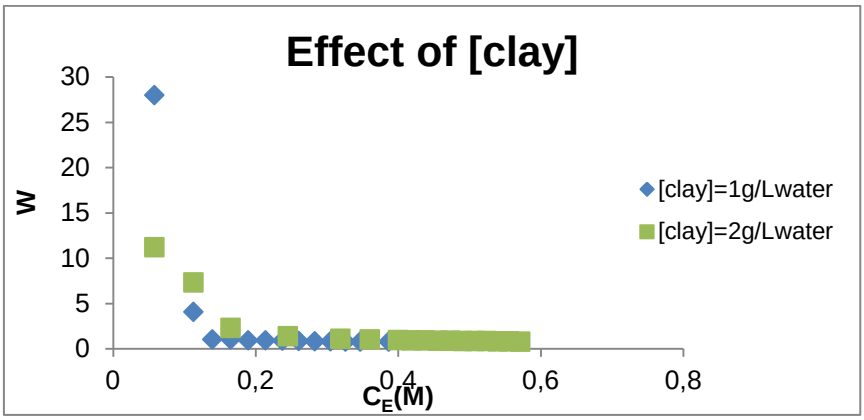

Figure 112: Experimental dependence of W on the C_E of samples LP1 and LP2 at 5%w/w, which were stabilized with 1 and 2 g/L_{water} of clay, respectively.

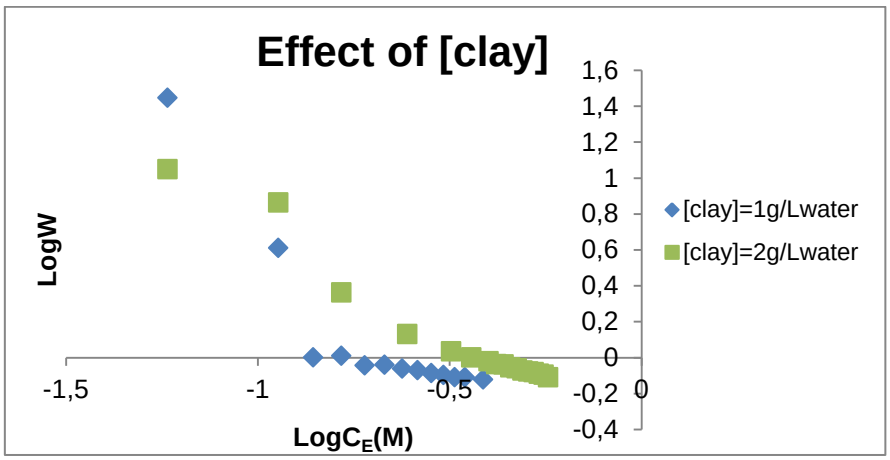

Figure 113: Experimental dependence of LogW on the $LogC_E$ of samples LP1 and LP2 at 5%w/w, which were stabilized with 1 and 2 g/L_{water} of clay, respectively.

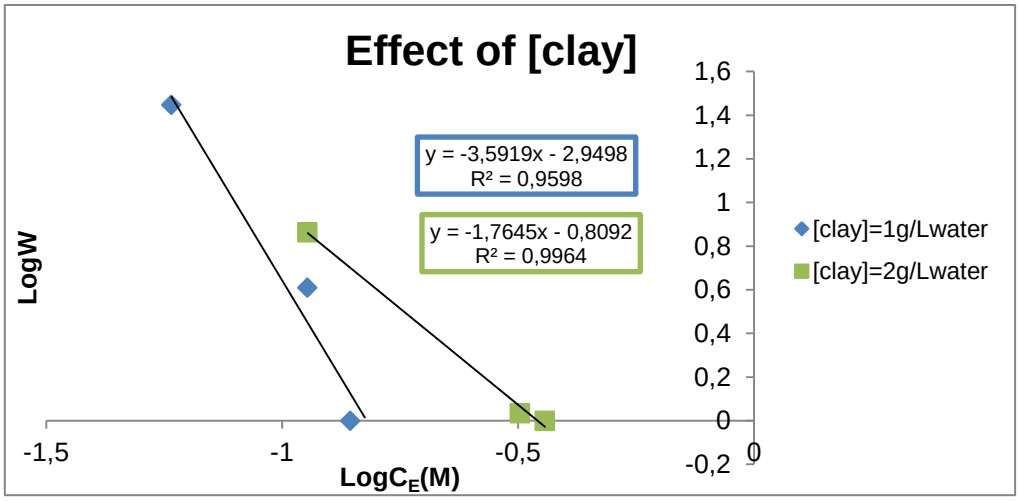

Figure 114: Slope of experimental dependence of LogW on the $LogC_E$ of samples LP1 and LP2 at 5%w/w, which were stabilized with 1 and 2 g/L_{water} of clay, respectively.

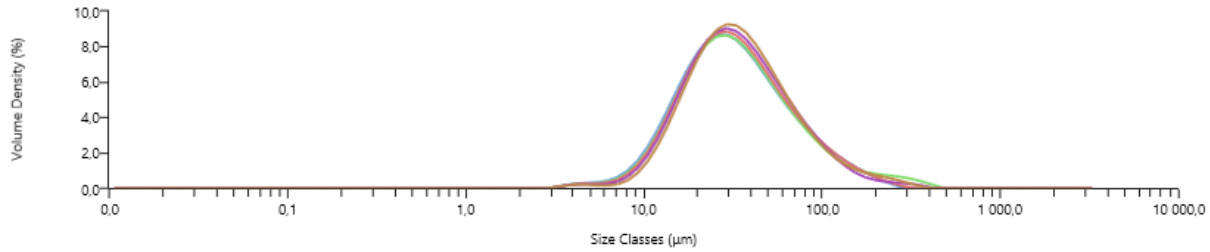

Figure 115: PSD of sample LP1 at 5%w/w after coagulation, measured with Mastersizer®3000.

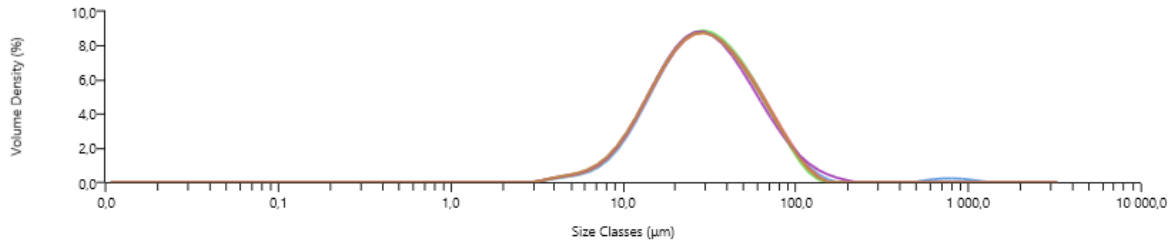

Figure 116: PSD of sample LP2 at 5%w/w after coagulation, measured with Mastersizer®3000.

Table 24: Values of CCC and A determined by turbidity measurements of samples LP1 and LP2 at 5%w/w, which were stabilized with 1 and 2 g/L_{water} of clay, respectively.

[clay] (g/L_{water})	**1**	**2**
r(nm)	126	120
$-\frac{dlogW}{dLogC_E}$	3.6	1.8
CCC(M)	0.1	0.4
A(J)	3.2×10^{-21}	9.7×10^{-22}

The results show that the CCC is higher for the sample stabilized with a higher amount of clay, what was expected. The Hamaker constant is in agreement with theory that affirms that this constant should decrease with the increase of surfactant, in this case a clay[9]. It was also observed a variation in the slope of the curves logW vs $LogC_E$. It wasn't found literature about Hamaker constant with this stabilization system. However, the values obtained are similar to those obtained with SDS as surfactant.

The results of sample MM1 final can be compared to those of sample LP1, since both were stabilized with a concentration of 1g/L_{water} and have similar diameters. Figure 117 shows experimental curves logW vs $logC_E$ for these samples and in table 25 are inserted the results obtained, which show that the polystyrene latex is more stable with the use of SDS, since the CCC is bigger, and that the values of Hamaker constant are practically the same.

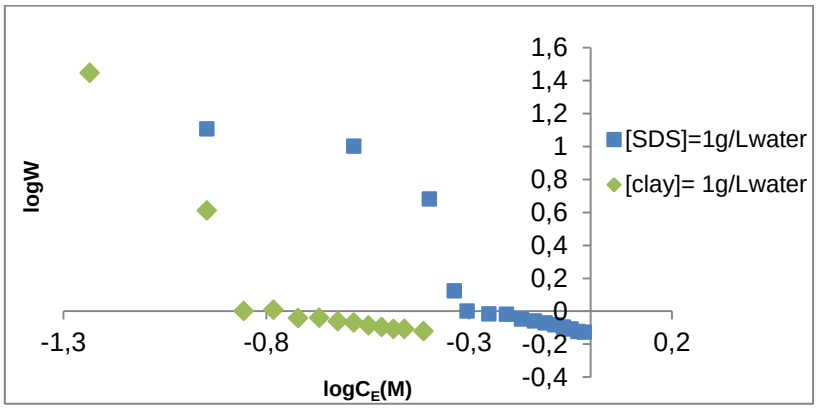

Figure 117: SDS concentration versus clay concentration at 1g/Lwater.

Table 25: Values of CCC and A determined by turbidity measurements of samples MM1 final and LP1, both stabilized with 1g/L_{water} of SDS and clay, respectively.

Stabilization system	**SDS**	**Clay**
r(nm)	143	126
$-\frac{dlogW}{dLogC_E}$	7.5	3.6
CCC(M)	0.50	0.1
A(J)	3.1×10^{-21}	3.2×10^{-21}

[9] Notice that the clay is not a surfactant but performs the same function of stabilize the latex.

Conclusions and perspectives

The purpose of this research project was to develop experimental protocols with the Turbiscan^{TM} devices to study the latex stability under different conditions and to indentify key parameters influencing the results. This work was divided in two parts.

In the first part, were used four latexes, produced by emulsion polymerization and not synthesized in this project, with the aim of studying the effect of particle size, solid content and particle size distribution of the latex in turbidy. For this study, two different equipments were used, the Turbiscan^{TM}Lab and Turbiscan^{TM}On Line. Results have shown that the backscattering is proportional to the particle size and solid content and is much more sensitive to bigger particles when 2 latexes with different sizes, but same solid content, are mixed. The use of Turbiscan^{TM}On Line with the simple force of gravity to analyze latexes with a high solid content is not advisable since they do not flow properly. Additional work with this device clearly deserves to be done. To improve the flux of the fluid, a pump can be tested. However, this must be done very carefully, since it's known that pumping latexes can provoke coagulation.

In the second part, were performed two styrene polymerizations using different amounts of surfactant. It was studied the effect of SDS concentration, of solid content and of particle size on coagulation. The main objectives were to determine the CCC and the Hamaker constant, an important parameter in coagulation models. To do so, the coagulation was provoked by addition of an electrolyte, in this case NaCl. In order to clarify the effect of SDS on the Hamaker constant the final polystyrene latex of one of these polymerizations was cleaned and used for coagulation studies upon addition of different concentrations of SDS. To acquire the backscattering profile was used the Turbiscan^{TM}Lab.

Latexes stabilized with a higher amount of surfactant should have a higher CCC, what was confirmed. Regarding the Hamaker constant, it changes with the amount of SDS used. However is complicated to explain how the SDS concentration affects this constant, because no clear trend was observed. The uncertainly associated to the calculation of the slope of curves logW vs logC_E can be an explanation for this. Although it's not possible to conclude how the surfactant affects the Hamaker constant, the order of magnitude of the values obtained is within the range of values found in the literature. Another interesting point was how the cleaned samples destabilized in a different way than the non cleaned ones when coagulation was induced.

Concerning the effect of the solid content on coagulation, a decrease of CCC value with the increase of the latex concentration, was observed. This behavior was the expected since the existence of more polymer particles in the latex leads to a higher probability of coagulation between them. Similarly to what happened with the Hamaker constants determined from the previous study, the values determined here do not follow a clear trend when increasing the solid content but are in the some order of magnitude of the ones found in literature.

In what concerns the effect of particle size on coagulation it could be expected that the particles with smaller sizes will tend to be more easily coagulated then the bigger ones. So, the CCC should be higher for bigger particles. However, this didn't happen. In fact, some authors predict an increase of the slope of the curves logW against C_E with particle size and others show the opposite. In this work, it was observed that the slope is lower for the small particles. About the Hamaker constant, the values found are within the range reported in literature, and decrease with particle size, as already observed by other authors. The ideal will be to have more particle sizes to compare. Thus, a sample with a bigger particle size was coagulated. The results are interesting since during coagulation the backscattering profile increases until a certain electrolyte concentration, but after this point, it starts to decrease, what makes impossible the calculation of CCC and Hamaker constant.

Finally, it was tested other stabilization system, using a clay instead the well known SDS. In this case, the CCC is proportional to the clay concentration and the Hamaker constant inversely proportional.

Future researches should focus on understanding if there are other factors that can be affect the Hamaker constant and how they affect it, in order to get more accurate values that will allow the development of a mathematical model for coagulation of emulsion polymers.

References:

[1] Asua, J.M., Polymer Reaction Engineering, Blackwell Publishing Ltd, 2007.

[2] Moad, G., Solomon, D.H., The Chemistry of Radical Polymerization, 2nd Edition, 2005.

[3] Meyer, Th., Keurentjes, J., Handbook of Polymer Reaction Engineering, 2005.

[4] Hiemenz, P.C., Lodge, T.P., Polymer Chemistry, 2nd edition, 2007.

[5] Anderson, C.D., Daniels, E.S., Emulsion Polymerization and Latex Applications, Vol. 14, Number 4, 2003.

[6] Vale, H., Population Balance Modeling of Emulsion Polymerization Reactors: Applications of Vinyl Chloride Polymerization, 2007.

[7] Vieira, C.R., Novas Dispersões Aquosas com Morfologia Controlada para Revestimentos, 2013.

[8] http://commons.wikimedia.org/wiki/File:Sodium_dodecyl_sulfate.svg, visited at August.

[9] http://swiftcraftymonkey.blogspot.pt/2010/06/question-differences-between.html, visited at August.

[10] Harkins, W.D., "Theory of the mechanism of emulsion polymerization," Journal of the American Chemical Society, vol. 69, pp. 1428– 1444, 1947.

[11] http://www.substech.com/dokuwiki/doku.php?id=surfactants, visited at August.

[12] Khaddazh, M., Gritskova, I.A., Litvinenko, G.I., An Advanced Approach on the Study of Emulsion Polymerization: Effect of the Initial Dispersion State of the System on the Reaction Mechanism, Polymerization Rate, and Size Distribution of Polymer-Monomer Particles, 2012.

[13] Mengual, O., Meunier, G., Cayré, I., Puech, K., Snabre, P., Turbiscan MA 2000: multiple light scattering measurement for concentrated emulsion and suspension instability analysis, 1999.

[14] Mengual, O., Meunier, G., Cayré, I., Puech, K., Snabre, P., Characterization of instability of concentrated dispersions by a new optical analyser : the Turbiscan MA 1000, 1999.

[15] Heredia, M.F., Graillat, C., McKenna, T., Coagulation of Anionically stabilized Polymer Particles, 2004.

[16] Heredia, M.F., Modélisation de Procédés pour la synthèse de latex multipopulés, 1992.

[17] Stability of Pigment Inkjet Inks, Formulaction, 2009.

[18] Turbiscan Lab, Guide d'utilisation, Formulaction.

[19] Abismail, B., Canselier, J.P., Wilhelm, A.M., Delmas, H., Gourdon, C., Emulsification processes: on-line study by multiple light scattering measurements, 2000.

[20] Santos, A., Santos, A.F., Sayer, C., Araújo, P.H. H., Heredia, M. F., Coagulation of Carboxylic Acid-Functionalized Latexes, 2008.

[21] Verwey, E. J. W., Overbeek, J.Th.G ; Theory of Stability of Lyophobic Colloids, The Interaction of Sol Particles having an Electric Double Layer; 1948.

[22] Romero-Cano, M.S., Martín-Rodríguez, A., Chauveteau, G., de las Nieves, F.J., Colloidal Stabilization of Polystyrene Particles by Adsorption of Nonionic Surfactant, II. Electrosteric Stability Studies; 1997.

[23] On-Line Emulsification Process Monitoring and Control.

[24] Dyab, A.K.F., Al-Lohedan, H.A., Essawy, H.A., El-Mageed, A.I.A.A., Taha, F., Fabrication of core/shell hybrid organic–inorganic polymer microspheres via Pickering emulsion polymerization using laponite nanoparticles, 2011.

[25] BYK Additives & Instruments, Technical Information B-RI 21, Laponite, Performance Additives

[26] Horiba, Z-Aberage Particle Size: An Explanation.

[27] http://www.malvern.com, visited at September.

[28] http://www.malvern.com, visited ate September.

[29] Turbisoft On Line 2.1 user guide, formulaction.

[30] Ottewill, R.H., Shaw, J.N., Stability of Monodisperse Polystyrene Latex Dispersions of Various Sizes, 1966.

[31] Wiese, G.R., Healy, T.W., Effect of Particle Size on Colloid Stability, 1969.

[32] Mathews, B.A., Rhodes, C.T., J. Colloid Interface Sci., 1968, 28, 71.

[33] Watillon, A., Joseph-Petit, A.M., Disc. Faraday Soc., 1966, 42, 143.

[34] Reerink and Overbeek, Disc. Faraday Soc., 1954, 18, 74.

[35] Watillon, A., Joseph-Petit, A.M., A. C. S. Symposium or Coagulation Coagulant Aids, 1963, p.61. Abstract

[36] Curtis, A.S.G., Hocking, L., Trans. Faraday Soc, 1968, 66, 138.

[37] Kotera, A., Furusawa, K., Kudo, K., Kolloid Z. Z. Polym., 1970, 240, 837.

[38] Goldstein, B., Zimm, B.H., J. Chem. Phys., 1971, 54, 4408.

[39] Krapp, H., and Walter, G.J., Colloidl Interface Sci., 1972, 39, 421.

[40] Schild, R.L., El-Aasser, M.S., Pehlein, G.W., Vanderhoff, J.W., “Emulsion lateses and Dispersions”, 1978, p.99.

[41] Bijsterbosch, G.H., Colloid Poly. Sci., 1978, 256, 343.

[42] Ono, H., Jidai, E., Shibayama, K., Colloid Olym. Sci., 1975, 253, 114.

[43] Tsaur, S-L., Fitch, R.M., Preparation and properties of Polystyrene Model Colloids, II. Effect of Surface Charge Density on Coagulation Behavior, 1986.

Appendixes

I. Free radical polymerization

Free radical polymerization is the process used to manufacture almost all commercial emulsion polymers. In this mechanism, there is three steps: initiation, propagation and termination. These steps can be seen in figure 118.

In the first step, the water-soluble initiators form radicals in the aqueous phase by thermal decomposition (described by an Arrhenius-type equation). The reaction starts when these radicals react with the monomer dissolved in the aqueous phase. Due to the constantly initiator decomposition, new polymer chains are also constantly formed. During propagation the initiated monomeric molecules, which contains an active free radical end group, come into contact with the uninitiated ones and react to form dimers with active end groups. These dimmers react with monomers to become oligomers. The oligomeric chain growth by propagation and continue to develop in molecular weight. The rate of growth depends on the temperature and the propagation rate constant. The final step, termination, occurs when the chain stops growing due to the deactivation of the free radical end group on a growing polymer chain. [1], [5]

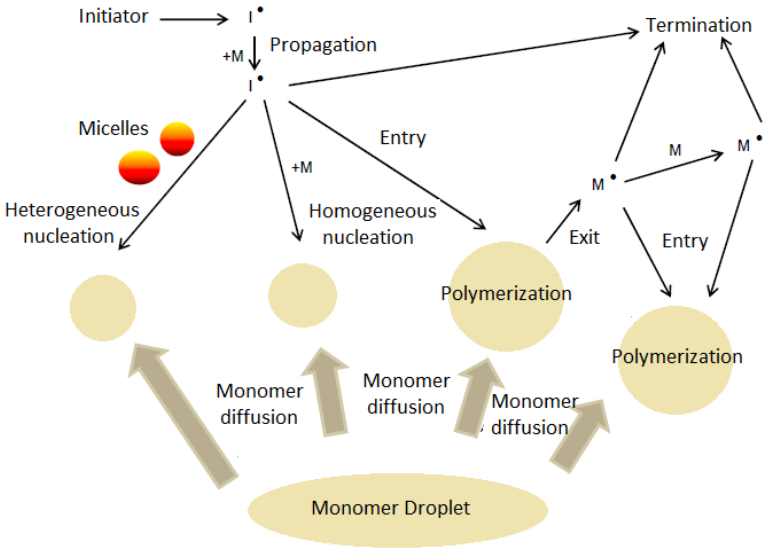

Figure 118: Mechanisms involved in emulsion polymerization [Adapted from [7]]

Although free radical polymerization is most common, other types of polymerization have been carried out, such as reversible addition-fragmentation transfer (RAFT), atom transfer radical polymerization (ATRP) and stable free radical polymerization (SFRP). [1], [5]

II. Experimental data

❖ Polymerization reactions

Table 26: Particle size and solid content of the different samples taken during the reactions for different SDS concentration.

	[SDS]=0.5 g/l		[SDS]=1.0 g/l		[SDS]=1.5 g/l		[SDS]=10 g/l	
	D_p(nm)	SC(%w/w)	D_p(nm)	SC(%w/w)	D_p(nm)	SC(%w/w)	D_p(nm)	SC(%w/w)
1	90	0.01	77	0.002	40	1.6	31	3.1
2	110	0.02	96	0.6	53	4	35	3.8
3	138	0.2	119	1.3	60	6	38	5.8
4	153	0.4	138	2.1	66	7.9	42	7.1
5	180	0.5	147	2.6	71	10.1	45	9.1
6	195	0.9	161	3.4	74	11.8	48	11.3
7	217	1.4	176	4.5	82	15.1	52	14.7
8	247	1.7	184	5.7	87	18.4	53	17.7
9	307	2.6	202	6.7	88	19	-	-
10	336	4.5	218	8.6	-	-	-	-
11	358	8.1	276	18.4	-	-	-	-
12	426	12.5	-	-	-	-	-	-
13	455	15.7	-	-	-	-	-	-
14	479	18.8	-	-	-	-	-	-

❖ **PSD profiles**

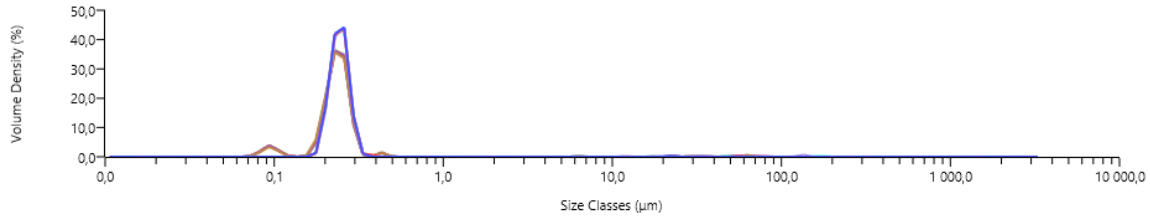

Figure 119: PSD of sample NB7 with SC=20%w/w (brown) and SC=5% w/w (blue), measured with Mastersizer®3000

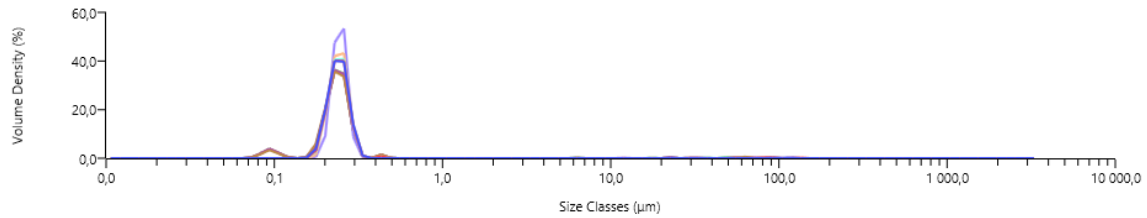

Figure 120: PSD of sample NB7 with SC=20% w/w (brown) and SC=10% w/w (other colors), measured with Mastersizer®3000

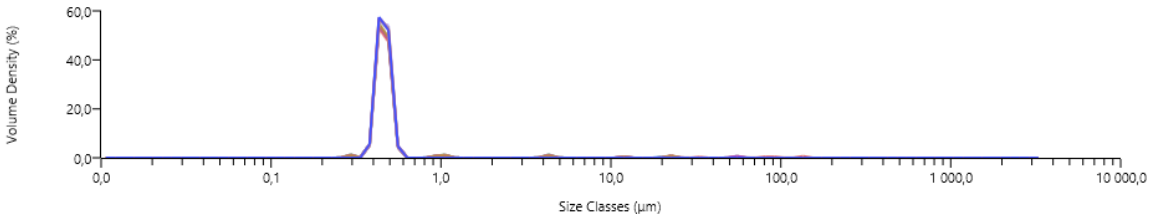

Figure 121: PSD of sample NB10 with SC=23% w/w (brown) and SC=5% w/w (other colors), measured with Mastersizer®3000

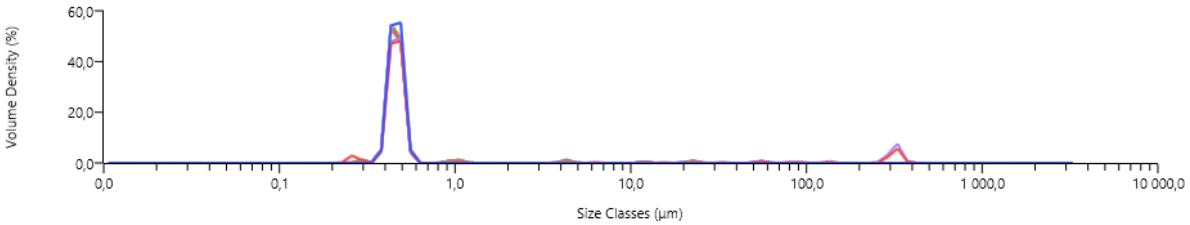

Figure 122: PSD of sample NB10 with SC=23% w/w (brown) and SC=10% w/w (other colors), measured with Mastersizer®3000

❖ **Transmission/backscattering profiles**

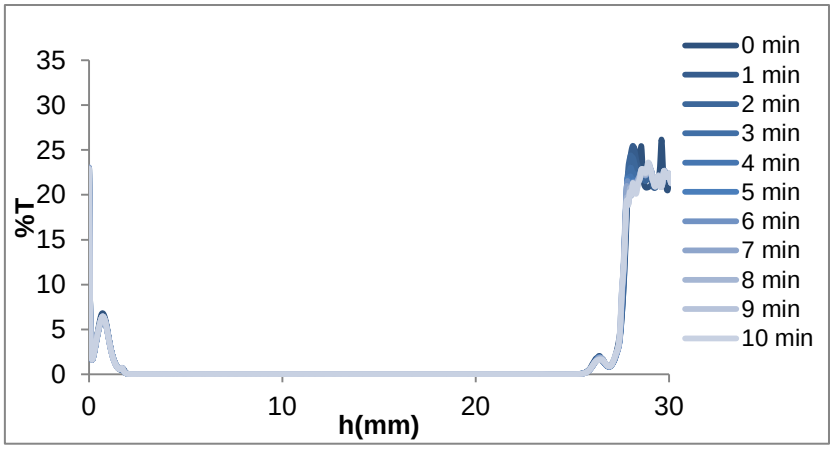

Figure 123: Transmission profiles of sample NB9, measured with Turbiscan™Lab.

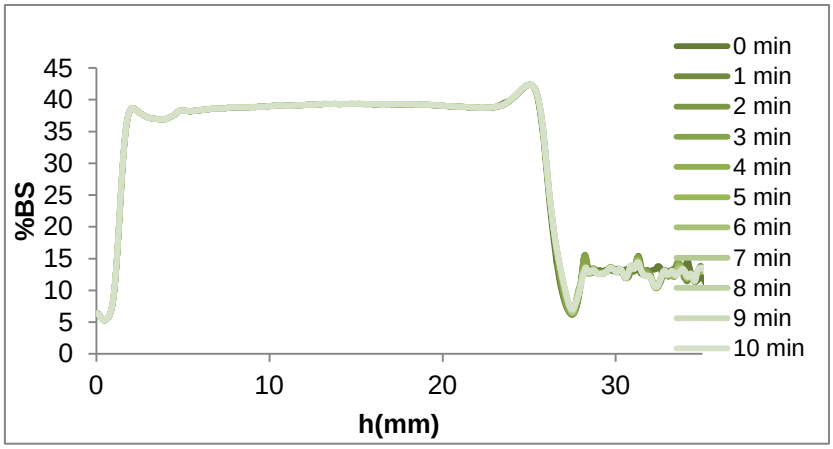

Figure 124: Backscattering profiles of sample NB9, measured with Turbiscan^{TM}Lab.

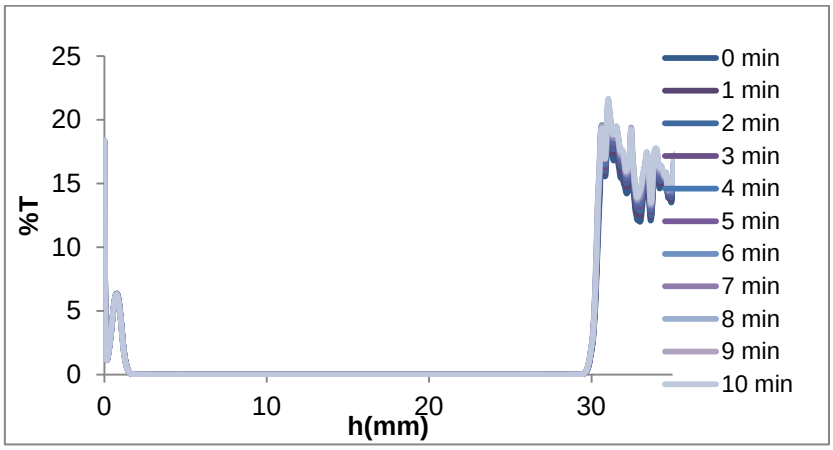

Figure 125: Transmission profiles of sample NB7, measured with Turbiscan^{TM}Lab.

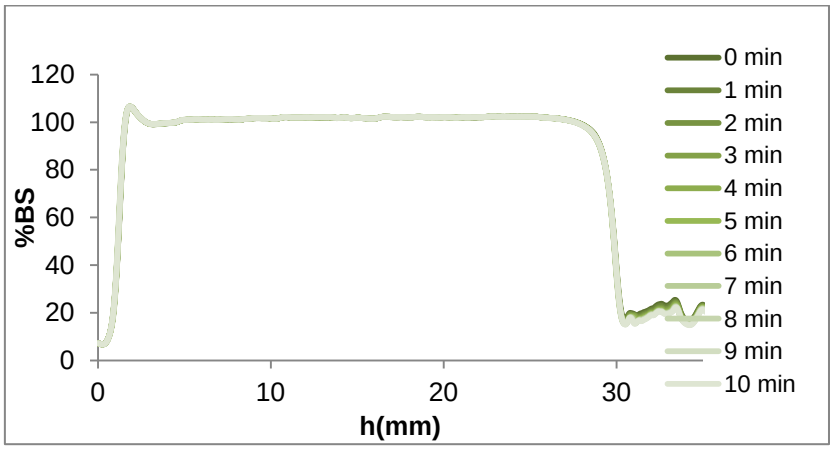

Figure 126: Backscattering profiles of sample NB7, measured with Turbiscan^{TM}Lab.

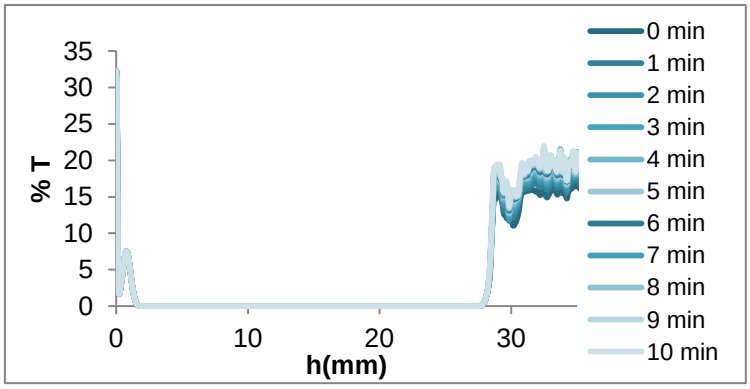

Figure 127: Transmission profiles of sample NB7 at 15%w/w, measured with Turbiscan^{TM}Lab.

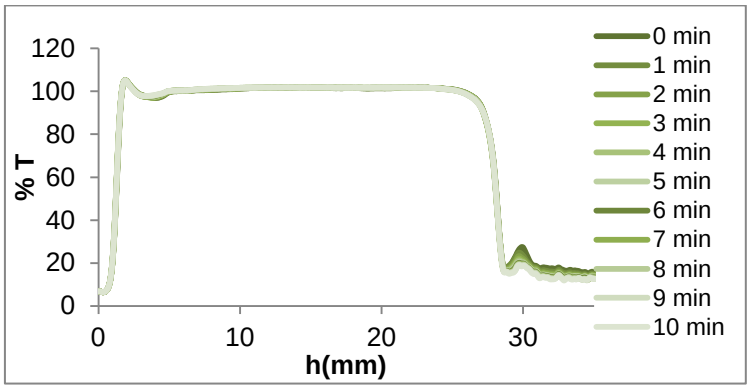

Figure 128: Backscattering profile of sample NB7 at 15**%**w/w, measured with Turbiscan^{TM}Lab.

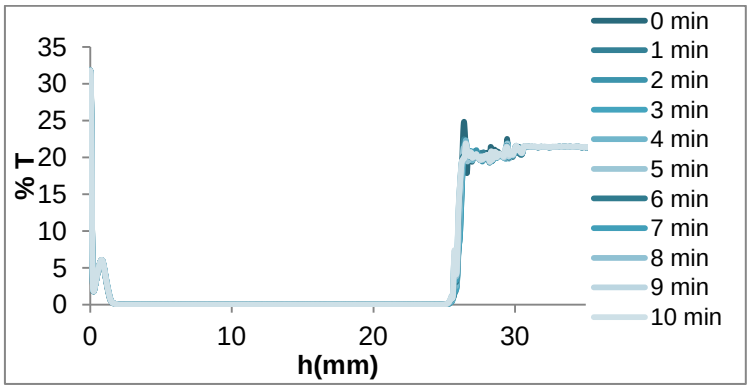

Figure 129: Transmission profile of sample NB7 at 10% w/w, measured with Turbiscan^{TM}Lab.

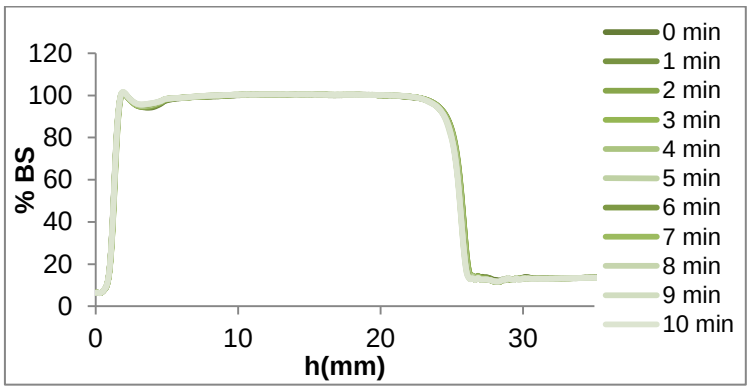

Figure 130: Backscattering profile of sample NB7 at 10% w/w, measured with Turbiscan^{TM}Lab.

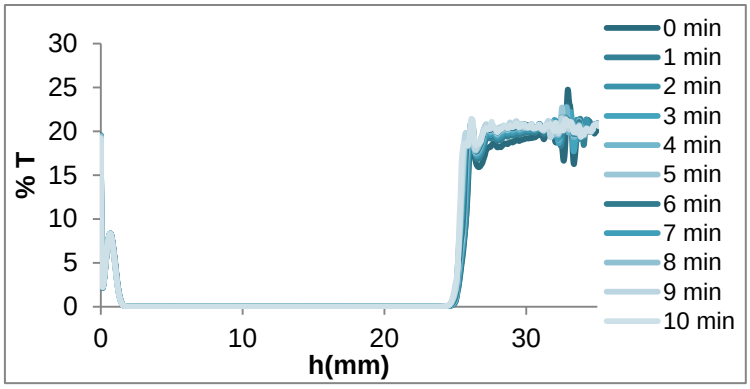

Figure 131: Transmission profiles of sample NB7 at 5% w/w, measured with Turbiscan^{TM}Lab.

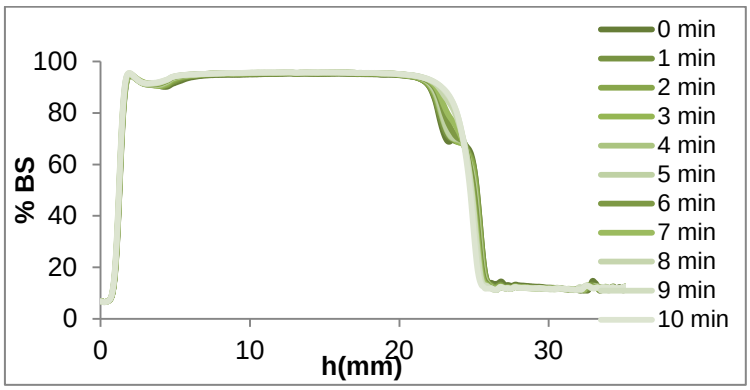

Figure 132: Backscattering profiles of sample NB7 at 5% w/w, measured with Turbiscan^{TM}Lab.

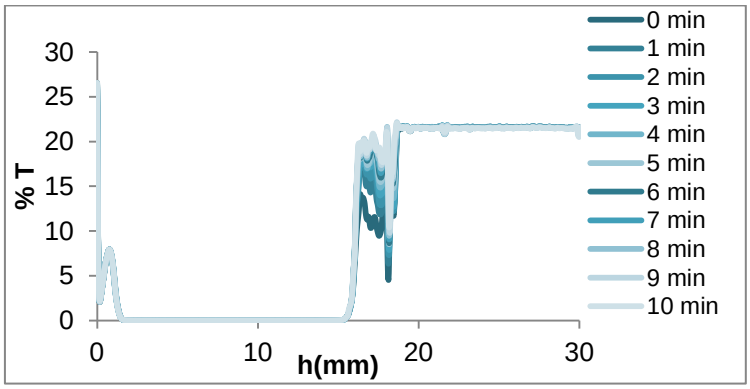

Figure 133: Transmission profiles of sample NB10 at 5% w/w, measured with Turbiscan^{TM}Lab.

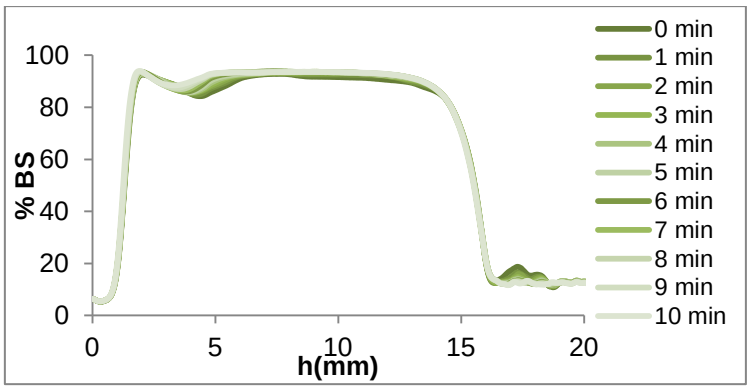

Figure 134: Backscattering profiles of sample NB10 at 5% w/w, measured with Turbiscan^{TM}Lab.

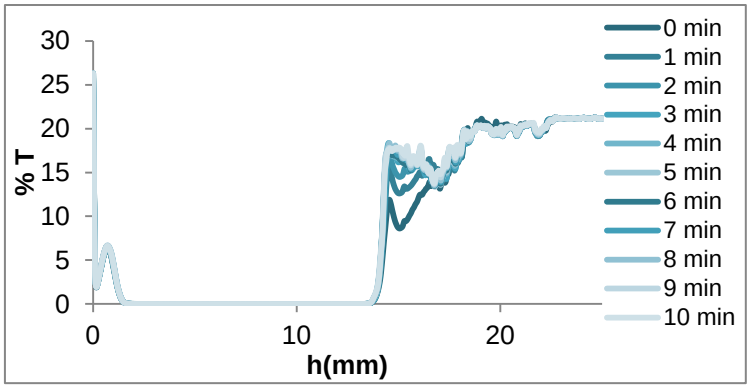

Figure 135: Transmission profiles of sample NB10 at 10% w/w, measured with Turbiscan^{TM}Lab.

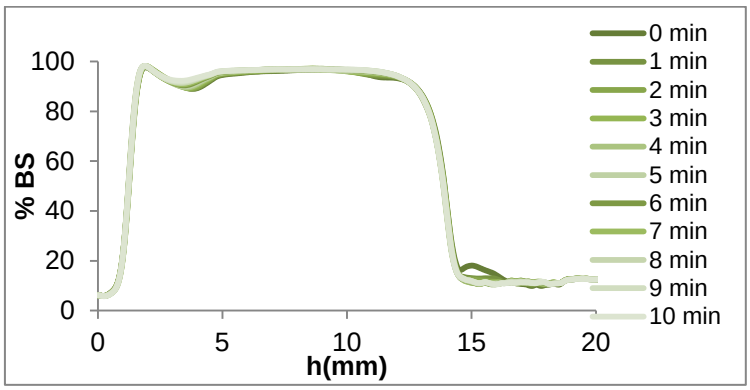

Figure 136: Backscattering profiles of sample NB10 at 10% w/w, measured with Turbiscan^{TM}Lab.

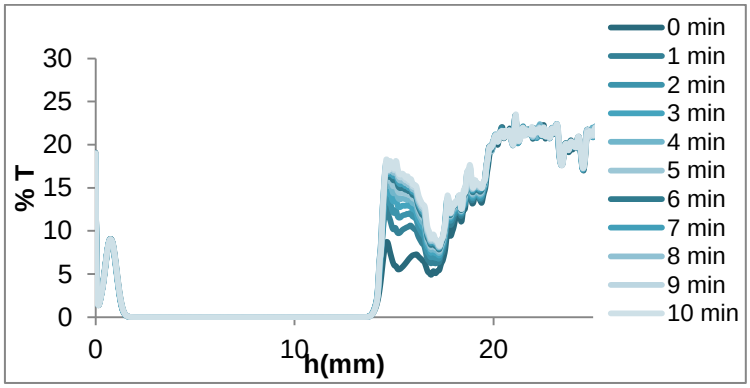

Figure 137: Transmission profiles of sample NB10 at 15% w/w, measured with Turbiscan^{TM}Lab.

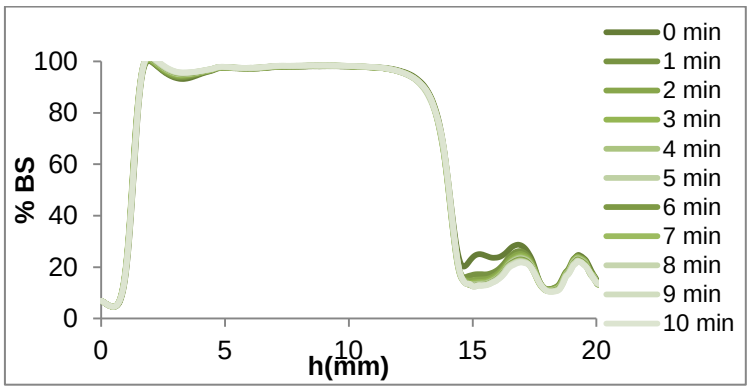

Figure 138: Backscattering profiles of sample NB10 at 15% w/w, measured with Turbiscan^{TM}Lab.

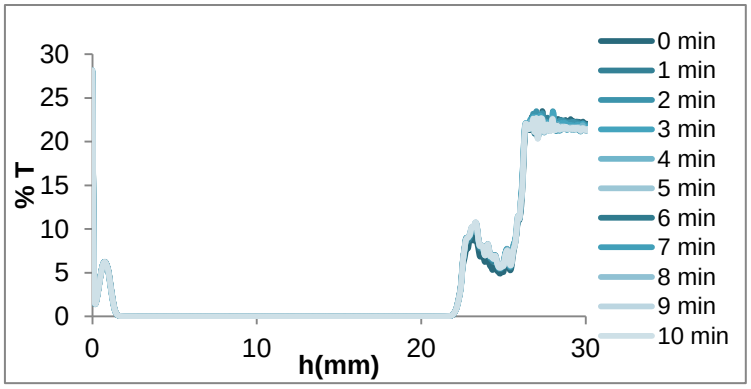

Figure 139: Transmission profiles of the mixture NB9+NB10 at proportion 7:3, measured with Turbiscan^{TM}Lab.

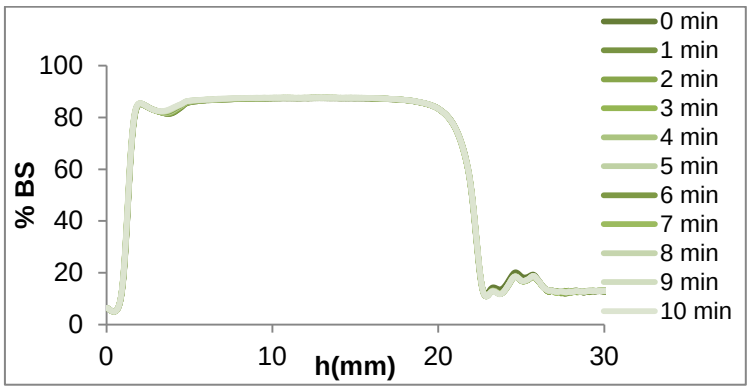

Figure 140: Backscattering profiles of the mixture NB9+NB10 ate proportion 7:3, measured with Turbiscan^{TM}Lab.

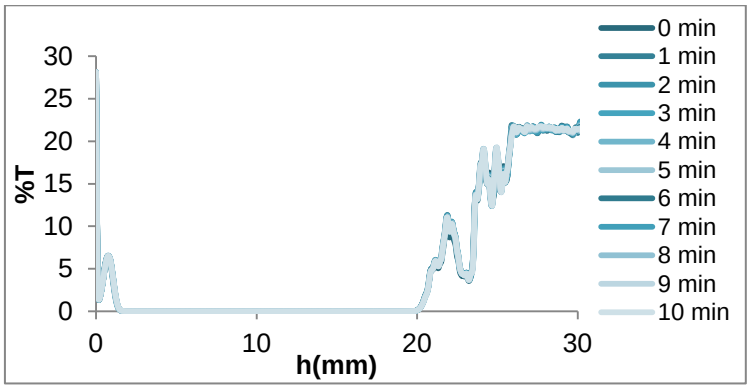

Figure 141: Transmission profiles of the mixture NB9+NB10 at proportion 1:1, measured with TurbiscanTMLab.

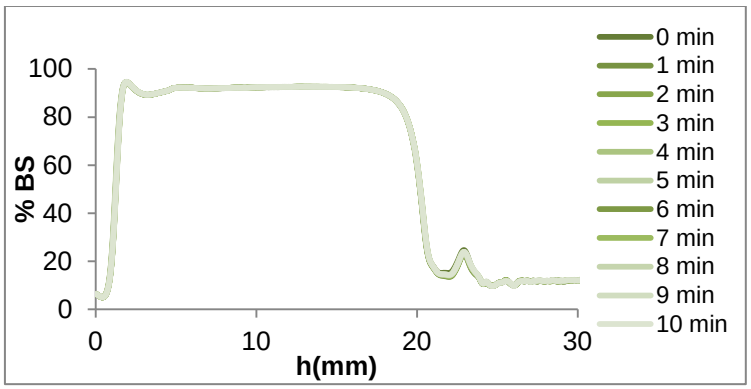

Figure 142: Backscattering profiles of the mixture NB9+NB10 at proportion 1:1, measured with Turbiscan^{TM}Lab.

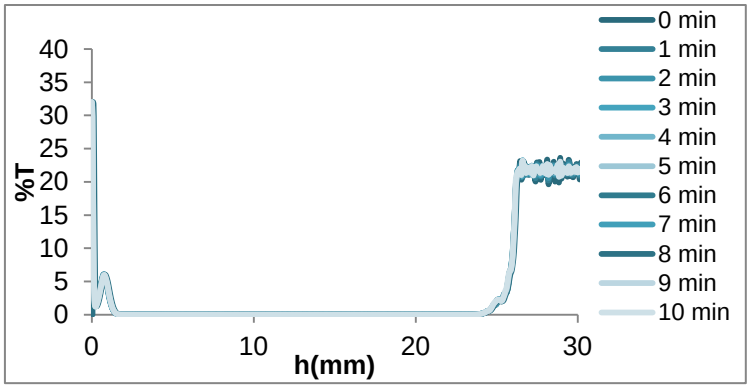

Figure 143: Transmission profiles of the mixture NB9+NB10 at proportion 3:7, measured with Turbiscan^{TM}Lab.

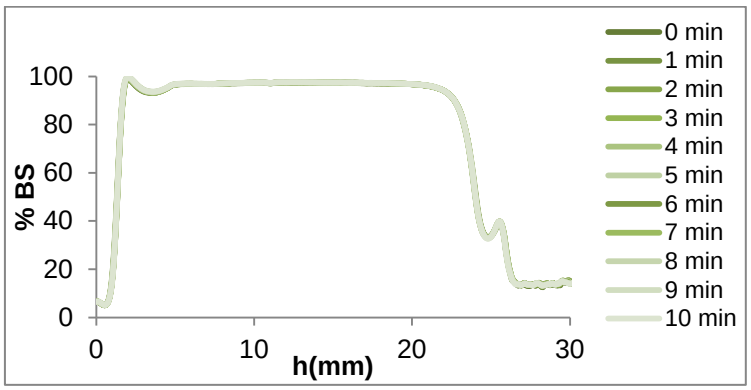

Figure 144: Backscattering profiles of the mixture NB9+NB10 at proportion 3:7, measured with Turbiscan^{TM}Lab.

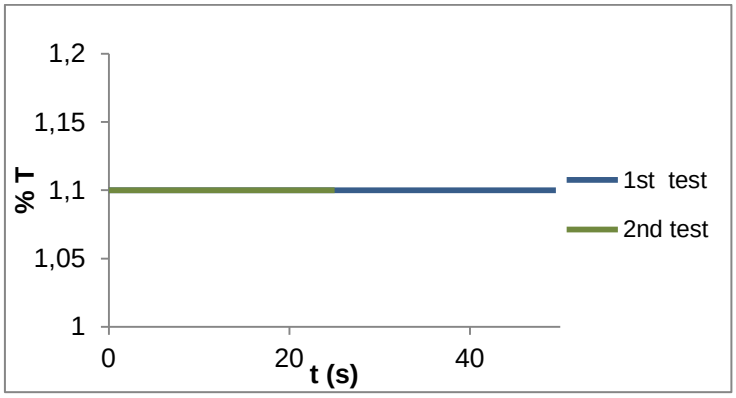

Figure 145: Transmission profiles of sample NB9, measured with Turbiscan^{TM}On Line.

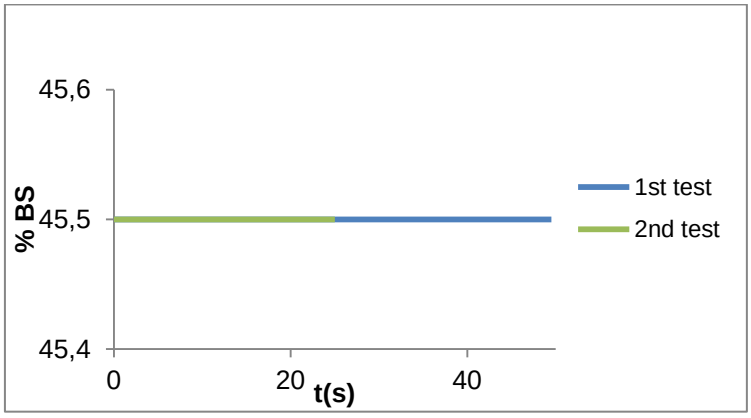

Figure 146: Backscattering profiles of sample NB9, measured with Turbiscan^{TM}On Line.

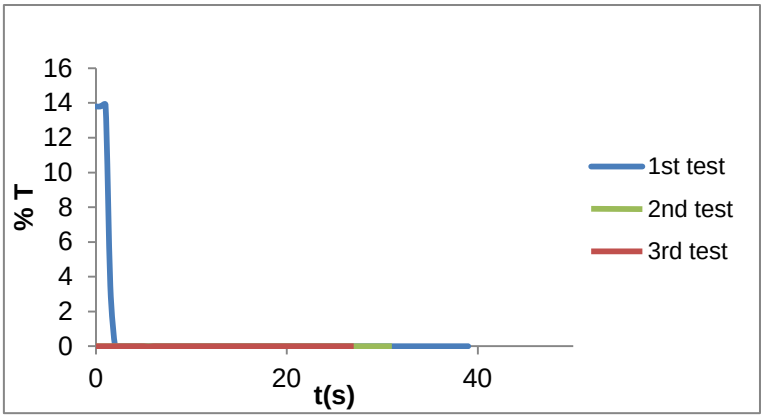

Figure 147: Transmission profiles of sample NB7, measured with Turbiscan^{TM}On Line.

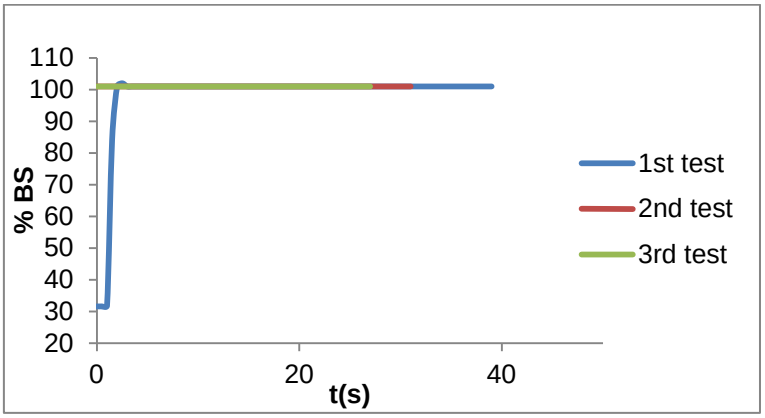

Figure 148: Backscattering profiles of sample NB7, measured with Turbiscan^{TM}On Line.

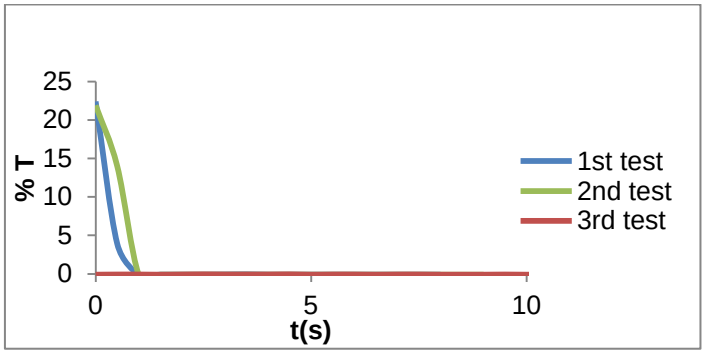

Figure 149: Transmission profiles of sample NB7 at 15% w/w, measured with Turbiscan^{TM}On Line.

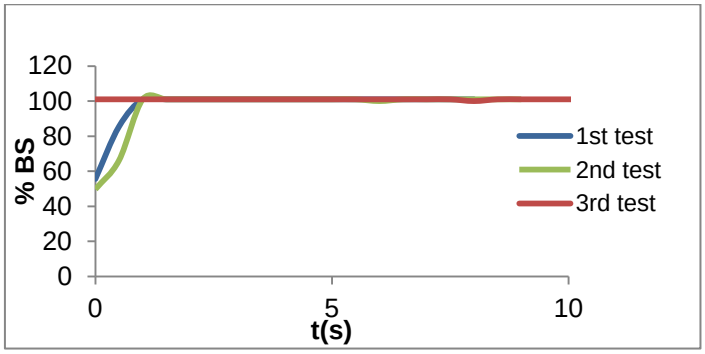

Figure 150: Backscattering profiles of sample NB7 at 15% w/w, measured with Turbiscan^{TM}On Line.

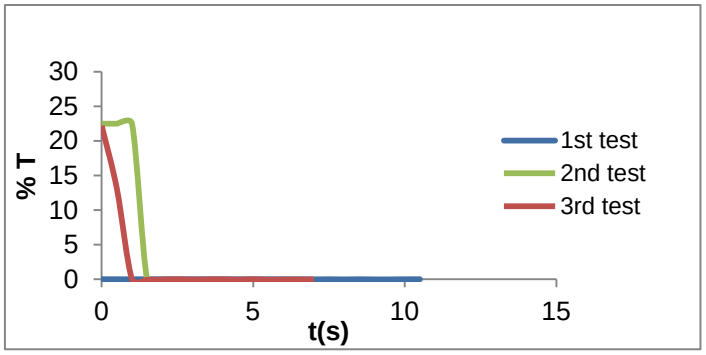

Figure 151: Transmission profiles of sample NB7 at 10% w/w, measured with Turbiscan™On Line.

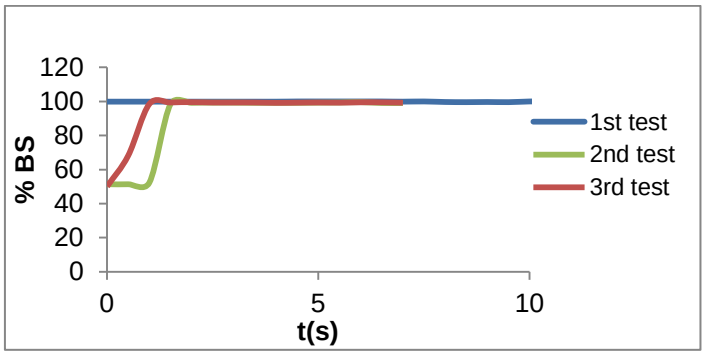

Figure 152: Backscattering profiles of sample NB7 at 10% w/w, measured with Turbiscan™On Line.

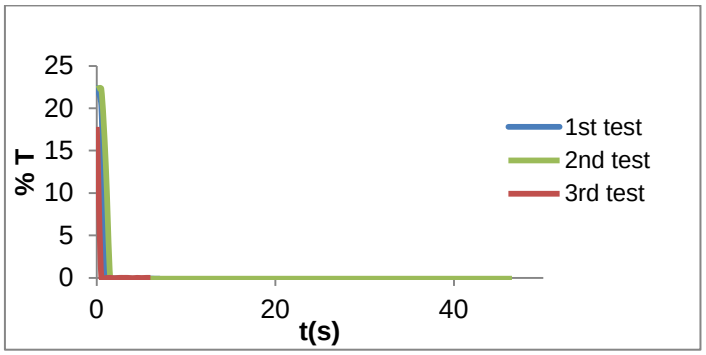

Figure 153: Transmission profiles of sample NB7 at 5% w/w, measured with Turbiscan™On Line.

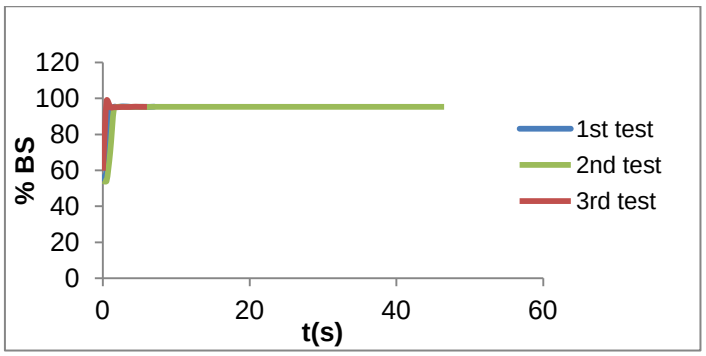

Figure 154: Backscattering profiles of sample NB7 at 5% w/w, measured with Turbiscan™On Line.

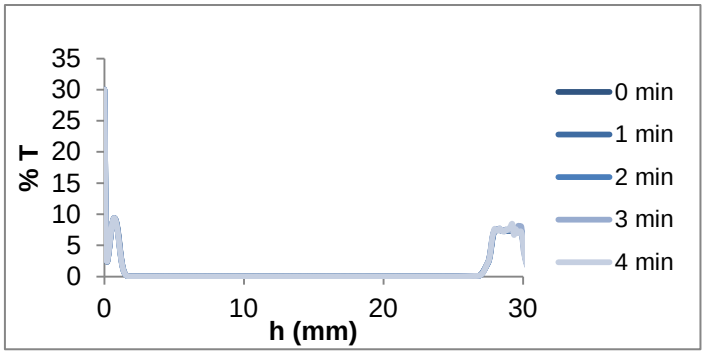

Figure 155: Transmission profiles before coagulation of sample MM1 final at 1%w/w, measured with Turbiscan^{TM}Lab.

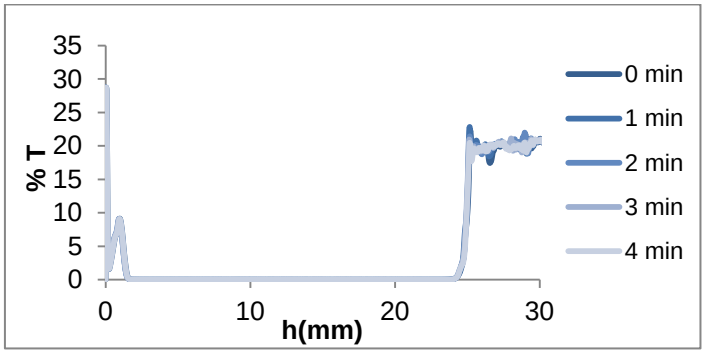

Figure 156: Transmission profiles before coagulation of sample MM1 final at 5%w/w, measured with Turbiscan^{TM}Lab.

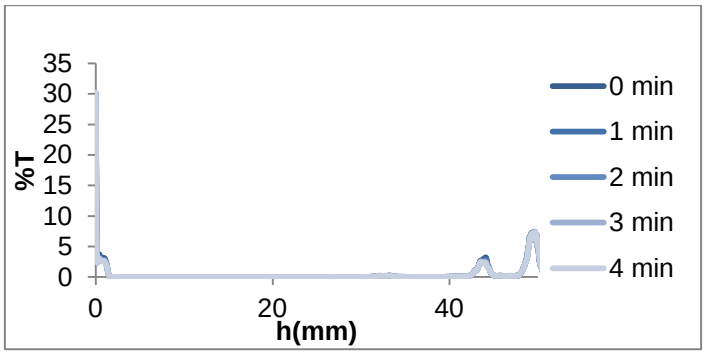

Figure 157: Transmission profiles after coagulation of sample MM1 final at 5%w/w, measured with Turbiscan^{TM}Lab.

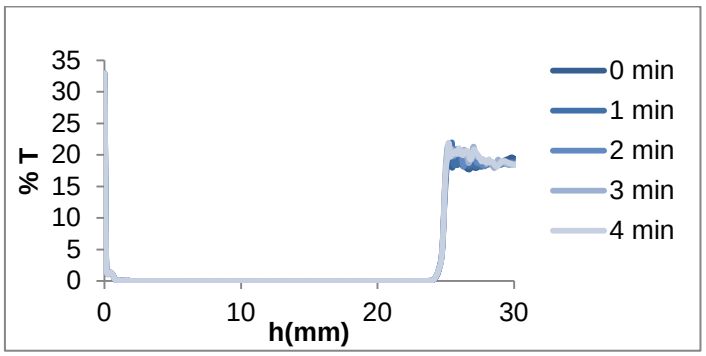

Figure 158: Transmission profiles before coagulation of sample MM1 (6) at 5%w/w, measured with Turbiscan^{TM}Lab.

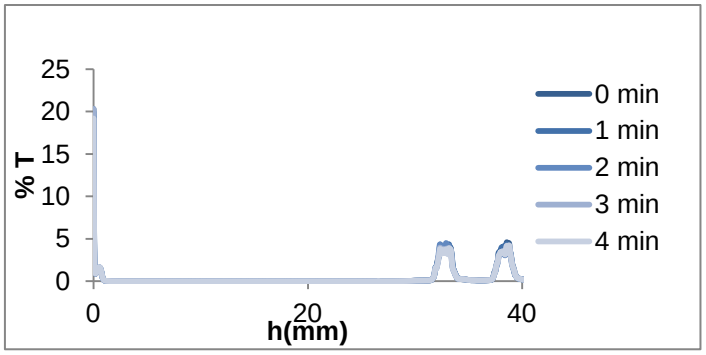

Figure 159: Transmission profiles after coagulation of sample MM1 (6) at 5%w/w, measured with Turbiscan^{TM}Lab.

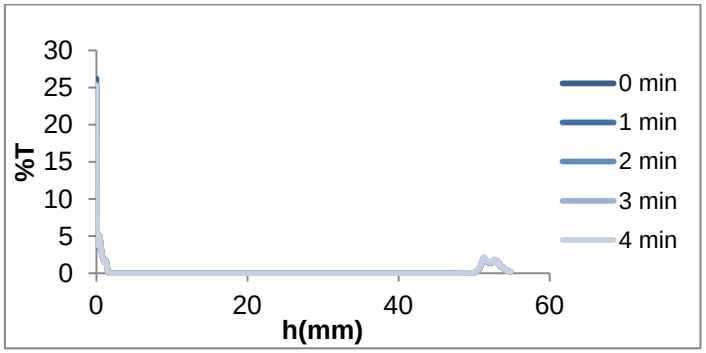

Figure 160: Transmission profiles after coagulation of sample MM1 final at 5%w/w, measured with Turbiscan^{TM}Lab-2nd test.

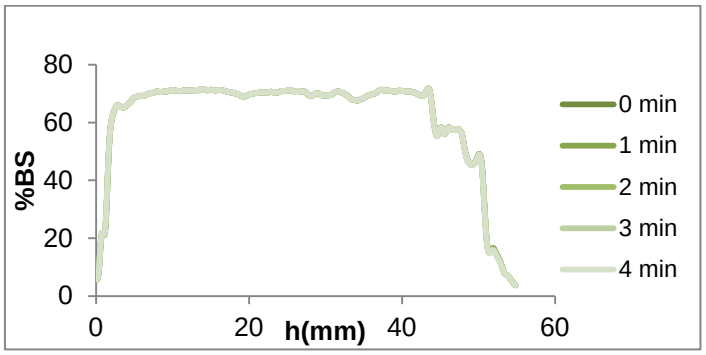

Figure 161: Backscattering profiles before coagulation of sample MM1 final at 5%w/w, measured with Turbiscan^{TM}Lab-2nd test.

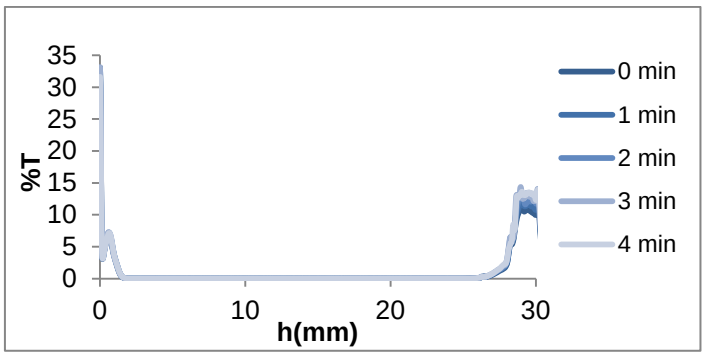

Figure 162: Transmission profiles before coagulation of sample MM2 (5) at 5%w/w, measured with Turbiscan^{TM}Lab.

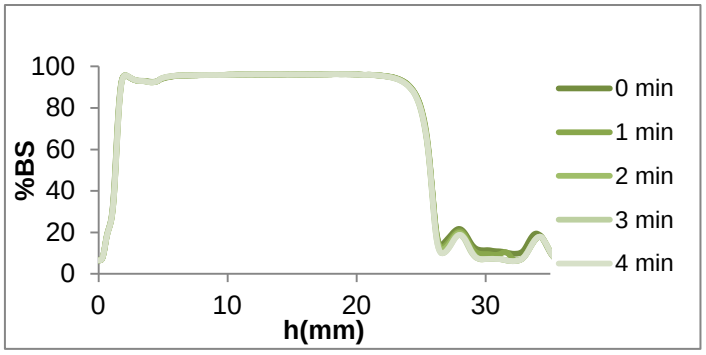

Figure 163: Backscattering profiles before coagulation of sample MM2 (5) at 5%w/w, measured with Turbiscan^{TM}Lab.

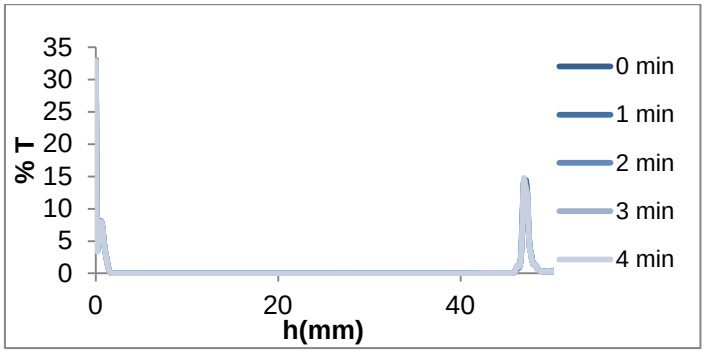

Figure 164: Transmission profiles after coagulation of sample MM2 (5) at 5%w/w, measured with Turbiscan^{TM}Lab.

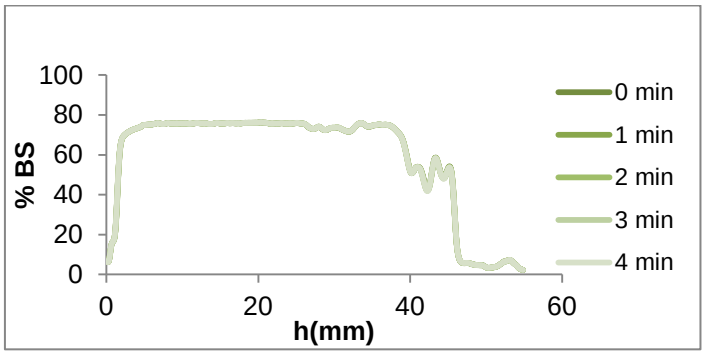

Figure 165: Backscattering profiles after coagulation of sample MM2 (5) at 5%w/w, measured with Turbiscan^{TM}Lab.

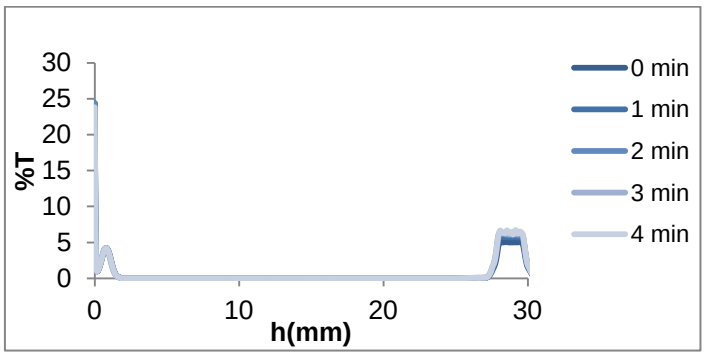

Figure 166: Transmission profiles before coagulation of sample MM1 final cleaned stabilized with [SDS]=1g/L_{water} and with SC=5% w/w, measured with Turbiscan^{TM}Lab.

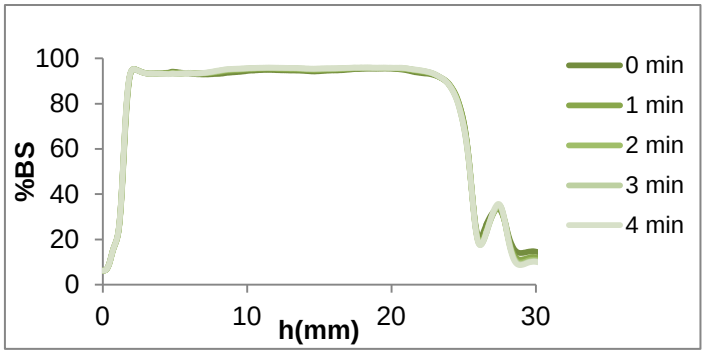

Figure 167: Backscattering profiles before coagulation of sample MM1 final cleaned stabilized with [SDS]=1g/L $_{water}$ and with SC=5% w/w, measured with Turbiscan^{TM}Lab.

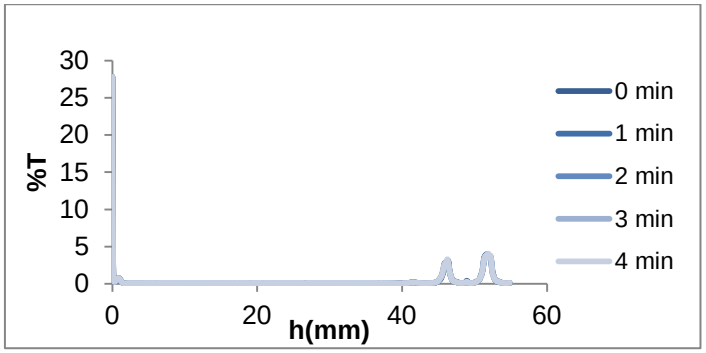

Figure 168: Transmission profiles after coagulation of sample MM1 final cleaned stabilized with [SDS]=1g/L$_{water}$ and with SC=5% w/w, measured with Turbiscan^{TM}Lab.

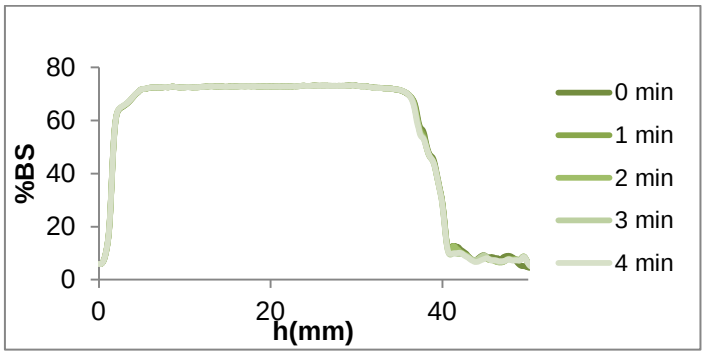

Figure 169: Backscattering profiles after coagulation of sample MM1 final cleaned stabilized with [SDS]=1g/L $_{water}$ and with SC=5% w/w, measured with Turbiscan^{TM}Lab.

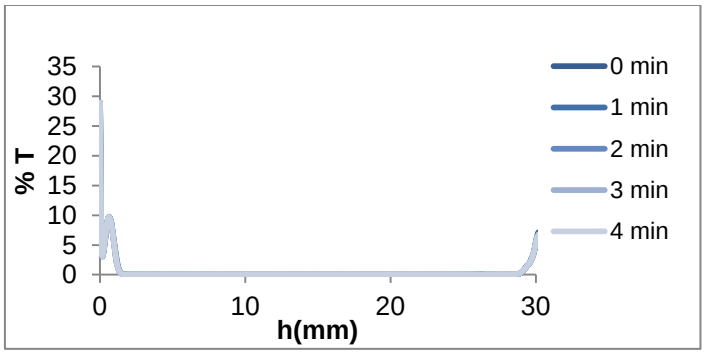

Figure 170: Transmission profiles before coagulation of sample MM1 final cleaned stabilized with [SDS]=2g/L$_{water}$ and with SC=5% w/w, measured with Turbiscan^{TM}Lab.

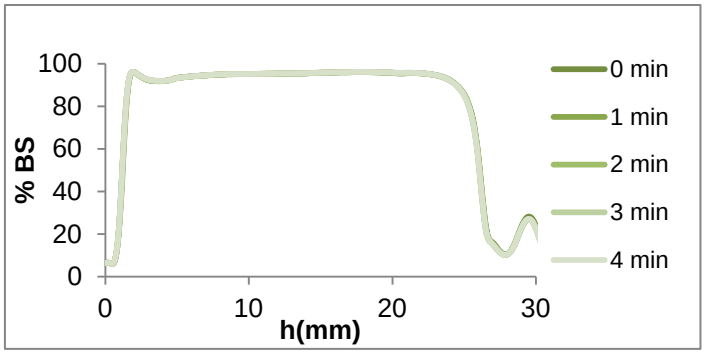

Figure 171: Backscattering profiles before coagulation of sample MM1 final cleaned stabilized with [SDS]=2g/L $_{water}$ and with SC=5% w/w, measured with Turbiscan^{TM}Lab.

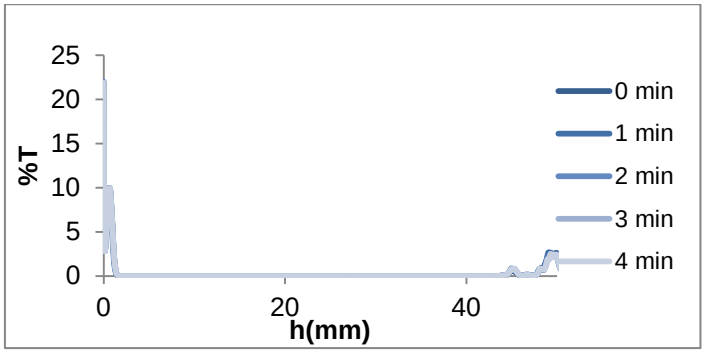

Figure 172: Transmission profiles after coagulation of sample MM1 final cleaned stabilized with [SDS]=2g/L$_{water}$ and with SC=5% w/w, measured with Turbiscan^{TM}Lab.

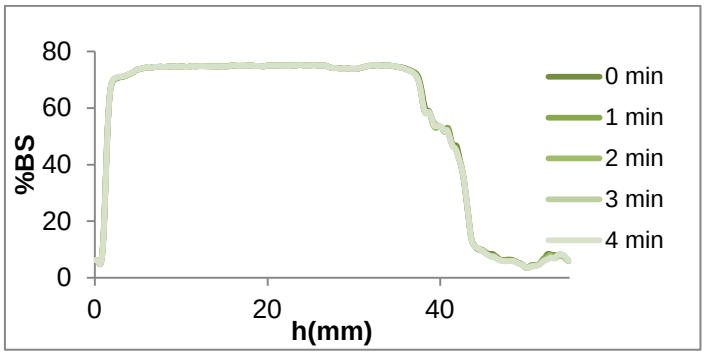

Figure 173: Backscattering profiles after coagulation of sample MM1 final cleaned stabilized with [SDS]=2g/L $_{water}$ and with SC=5% w/w, measured with Turbiscan^{TM}Lab.

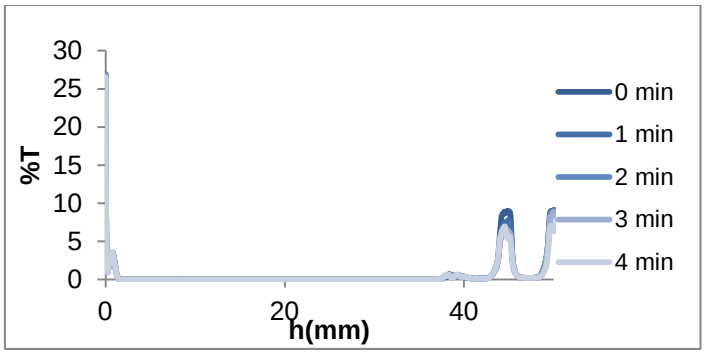

Figure 174: Transmission profiles after coagulation of sample MM1 final cleaned stabilized with [SDS]=2g/L$_{water}$ and with SC=5% w/w, measured with Turbiscan^{TM}Lab- 2nd test.

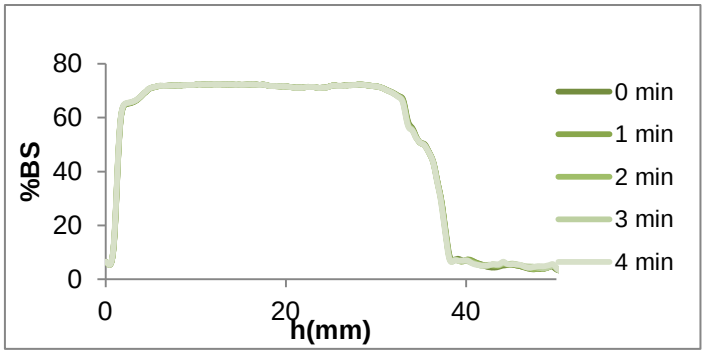

Figure 175: Backscattering profiles after coagulation of sample MM1 final cleaned stabilized with [SDS]=2g/L $_{water}$ and with SC=5% w/w, measured with Turbiscan^{TM}Lab- 2nd test.

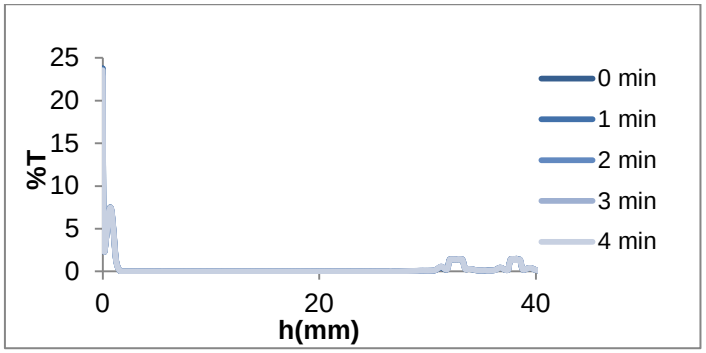

Figure 176: Transmission profiles before coagulation of sample MM1 final cleaned stabilized with [SDS]=3g/L$_{water}$ and with SC=5% w/w, measured with Turbiscan^{TM}Lab.

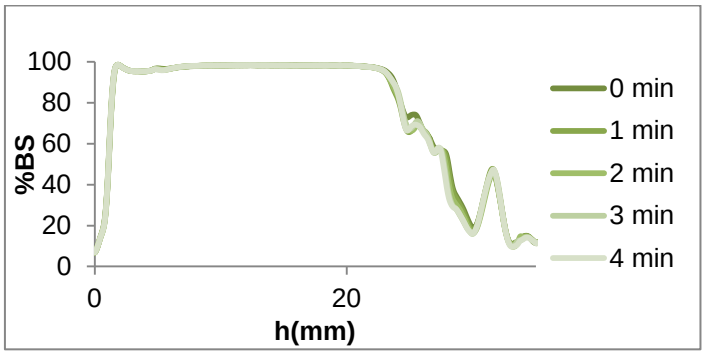

Figure 177: Backscattering profiles before coagulation of sample MM1 final cleaned stabilized with [SDS]=3g/L $_{water}$ and with SC=5% w/w, measured with Turbiscan^{TM}Lab.

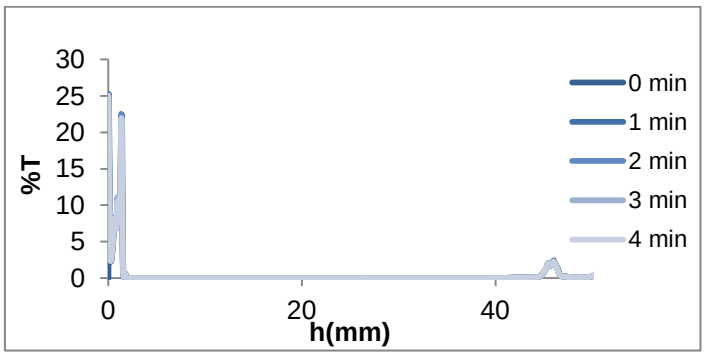

Figure 178: Transmission profiles after coagulation of sample MM1 final cleaned stabilized with [SDS]=3g/L$_{water}$ and with SC=5% w/w, measured with Turbiscan^{TM}Lab.

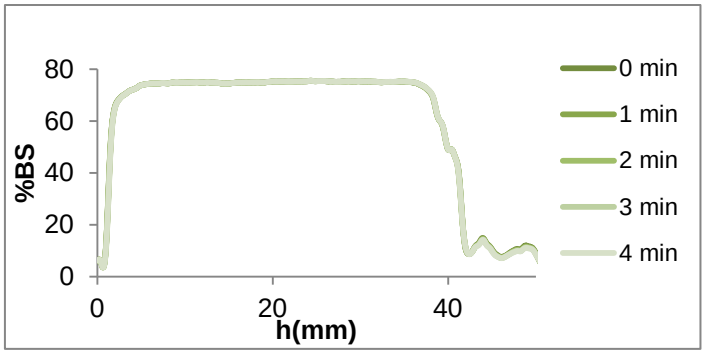

Figure 179: Backscattering profiles after coagulation of sample MM1 final cleaned stabilized with [SDS]=3g/L $_{water}$ and with SC=5% w/w, measured with Turbiscan^{TM}Lab.

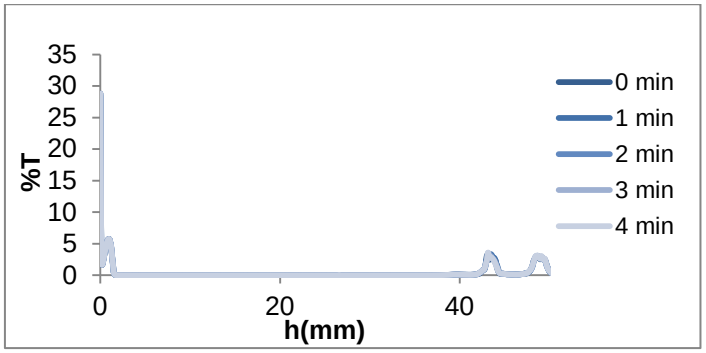

Figure 180: Transmission profiles after coagulation of sample MM1 final cleaned stabilized with [SDS]=3g/L$_{water}$ and with SC=5% w/w, measured with Turbiscan^{TM}Lab- 2nd test.

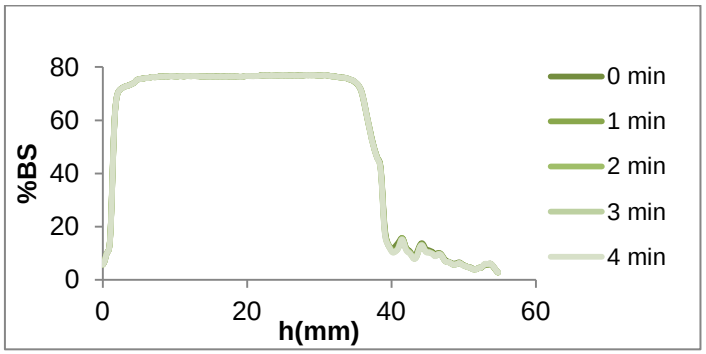

Figure 181: Backscattering profiles after coagulation of sample MM1 final cleaned stabilized with [SDS]=3g/L $_{water}$ and with SC=5% w/w, measured with Turbiscan^{TM}Lab- 2nd test.

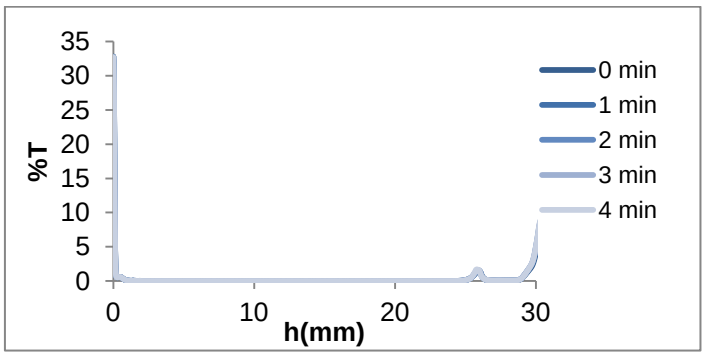

Figure 182: Transmission profiles before coagulation of sample MM2 (5) at 2% w/w, measured with Turbiscan^{TM}Lab.

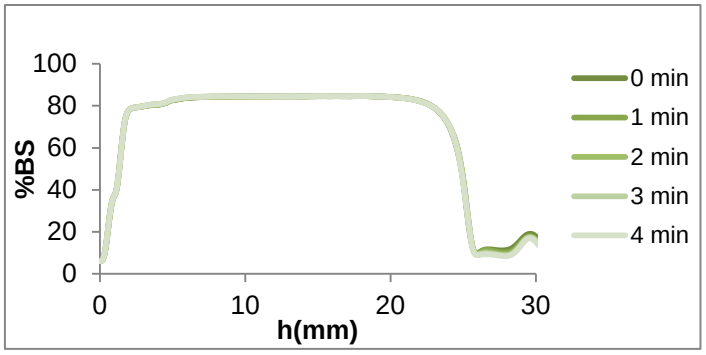

Figure 183: Backscattering profiles before coagulation of sample MM2 (5) at 2%w/w, measured with Turbiscan^{TM}Lab.

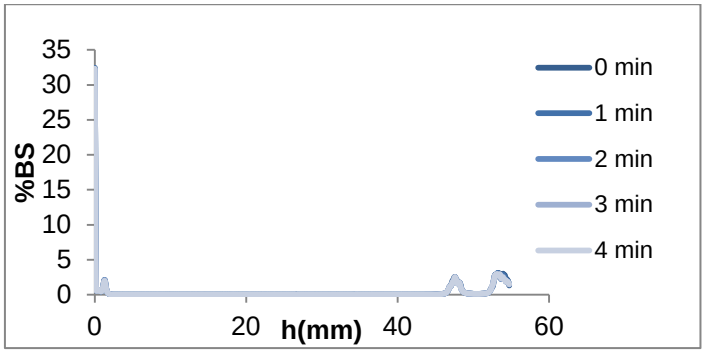

Figure 184: Transmission profiles after coagulation of sample MM2 (5) at 2%w/w, measured with Turbiscan^{TM}Lab.

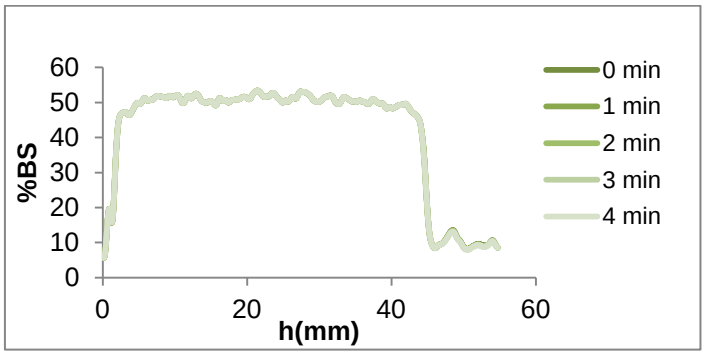

Figure 185: Backscattering profiles after coagulation of sample MM2 (5) at 2%w/w, measured with Turbiscan^{TM}Lab.

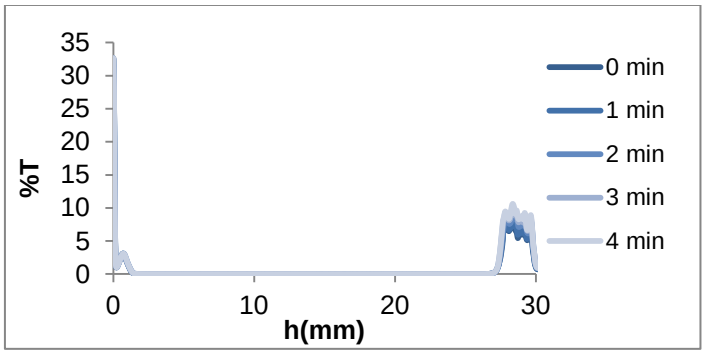

Figure 186: Transmission profiles before coagulation of sample MM2 (5) at 10%w/w, measured with Turbiscan^{TM}Lab.

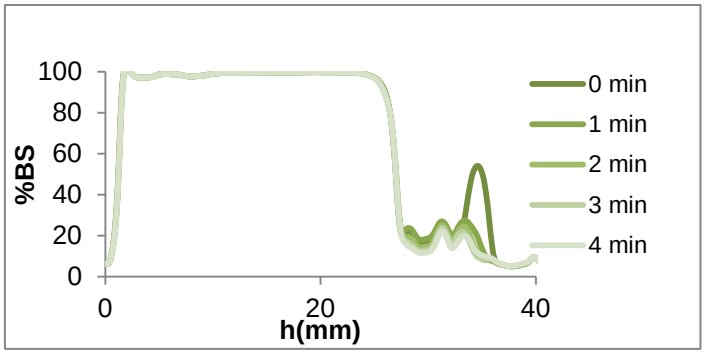

Figure 187: Backscattering profiles before coagulation of sample MM2 (5) at 10%w/w, measured with Turbiscan^{TM}Lab.

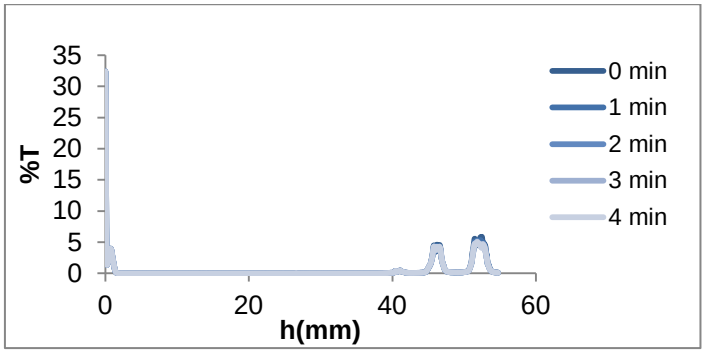

Figure 188: Transmission profiles after coagulation of sample MM2 (5) at 10%w/w, measured with Turbiscan^{TM}Lab.

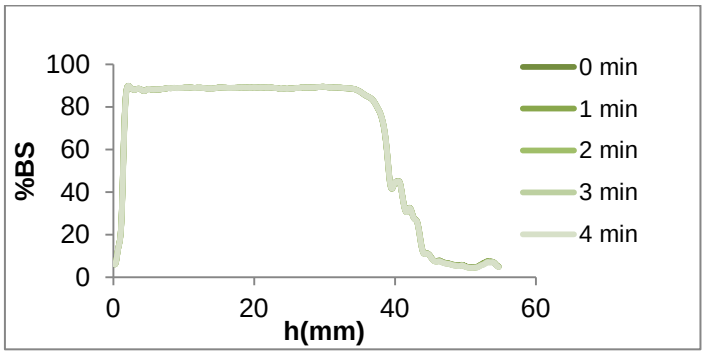

Figure 189: Backscattering profiles after coagulation of sample MM2 (5) at 10%w/w, measured with Turbiscan^{TM}Lab.

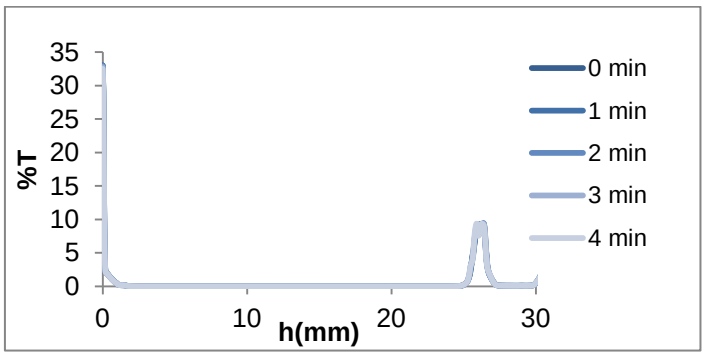

Figure 190: Transmission profiles before coagulation of sample MM2 (2) at 2%w/w, measured with Turbiscan^{TM}Lab.

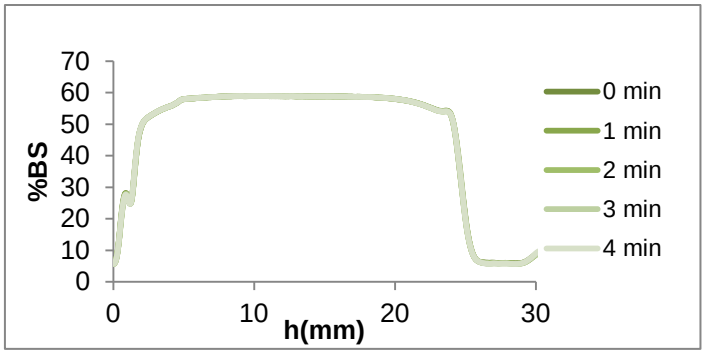

Figure 191: Backscattering profiles before coagulation of sample MM2 (2) at 2%w/w, measured with Turbiscan^{TM}Lab.

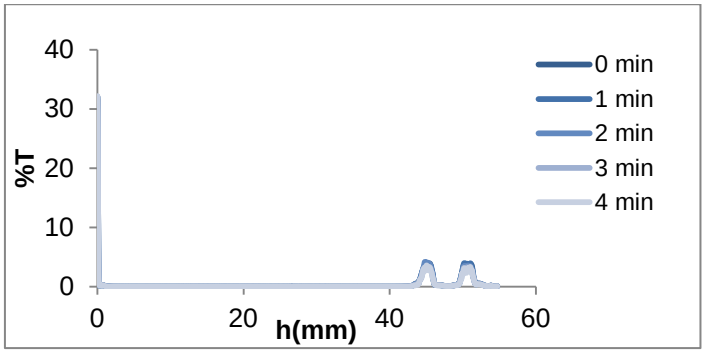

Figure 192: Transmission profiles after coagulation of sample MM2 (2) at 2%w/w, measured with Turbiscan^{TM}Lab.

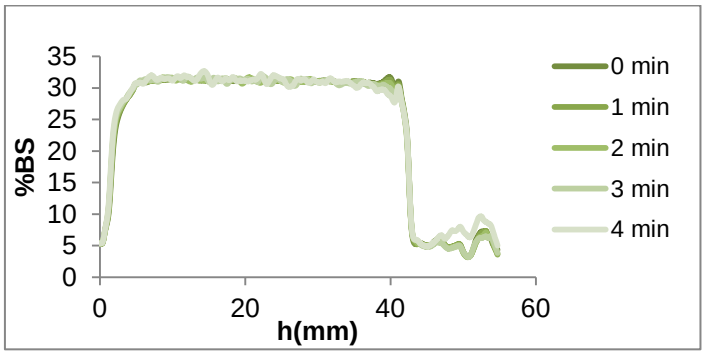

Figure 193: Backscattering profiles before coagulation of sample MM2 (2) at 2%w/w, measured with Turbiscan^{TM}Lab.

❖ **Coagulation profiles**

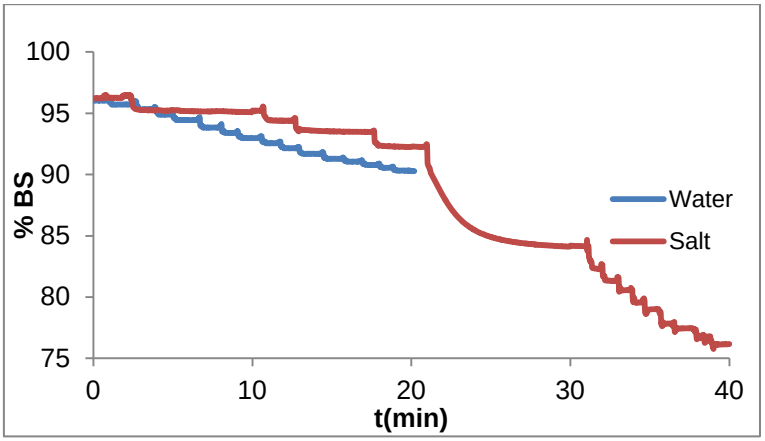

Figure 194: Evolution of backscattering of sample MM2 (5) at 5%w/w during coagulation (red) and addition of water (blue), measured with Turbiscan^{TM}Lab-2nd test. T=26ºC.

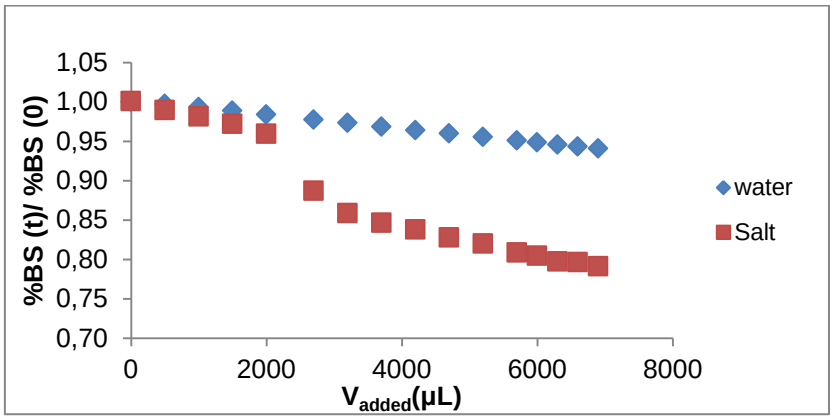

Figure 195: Evolution of backscattering normalized of sample MM2 (5) at 5%w/w, during coagulation (red) and addition of water (blue), measured with Turbiscan^{TM}Lab- Average.

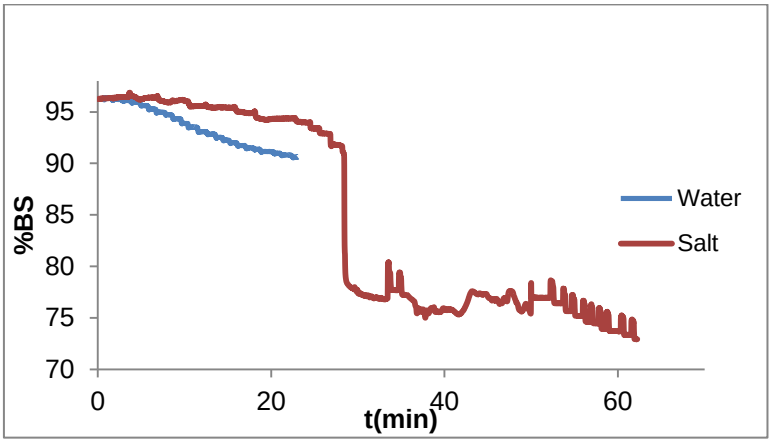

Figure 196: Evolution of backscattering of sample MM1final cleaned, stabilized with [SDS]=1g/L_{water} and with SC= 5%w/w, during coagulation (red) and addition of water (blue), measured with Turbiscan^{TM}Lab. T=25.5ºC.

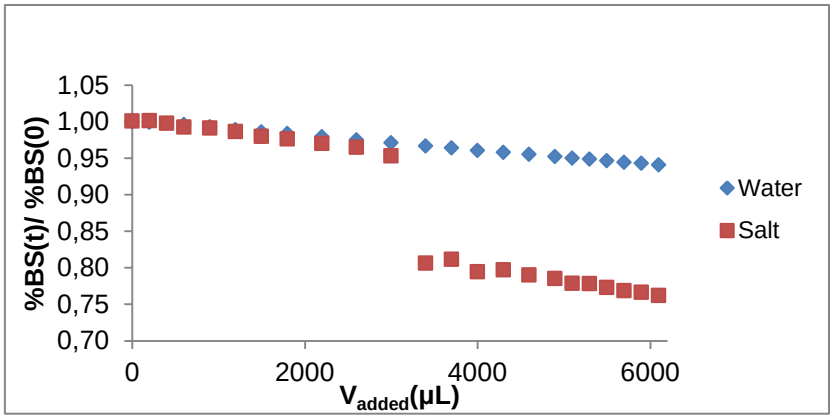

Figure 197: Evolution of backscattering normalized of sample MM1final cleaned, stabilized with [SDS]=1g/L_{water} and with SC= 5%w/w during coagulation (red) and addition of water (blue), measured with Turbiscan^{TM}Lab.

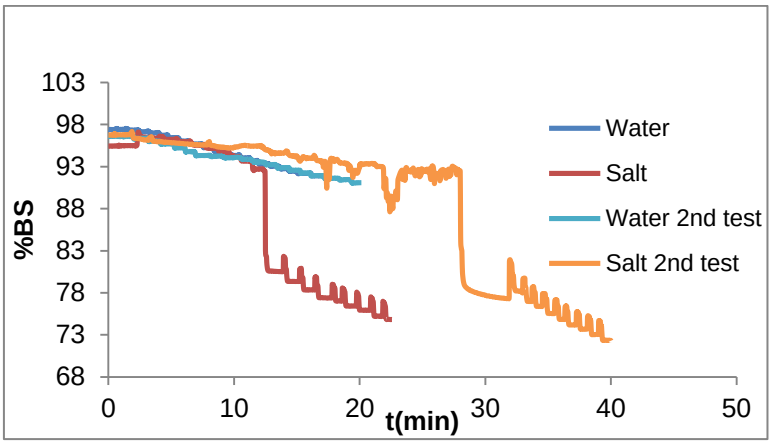

Figure 198: Evolution of backscattering of sample MM1final cleaned, stabilized with [SDS]=2g/L_{water} and with SC= 5%w/w during coagulation and addition of water , measured with Turbiscan^{TM}Lab. T=25.5ºC.

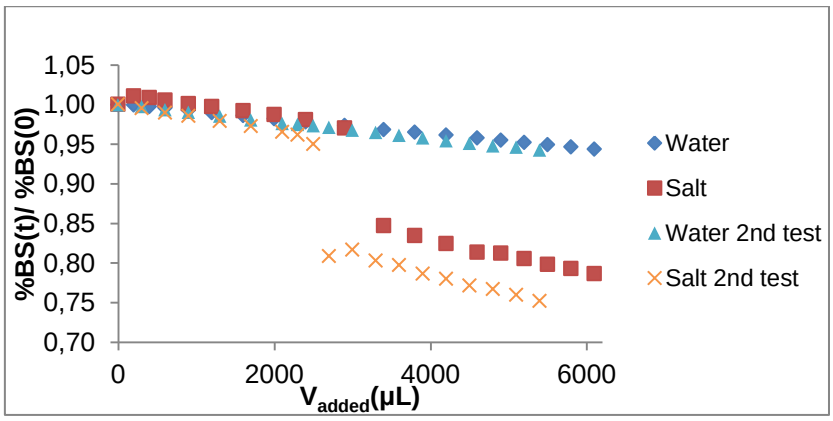

Figure 199: Evolution of backscattering normalized of sample MM1final cleaned, stabilized with [SDS]=2g/L_{water} and with SC= 5%w/w during coagulation and addition of water , measured with Turbiscan^{TM}Lab.

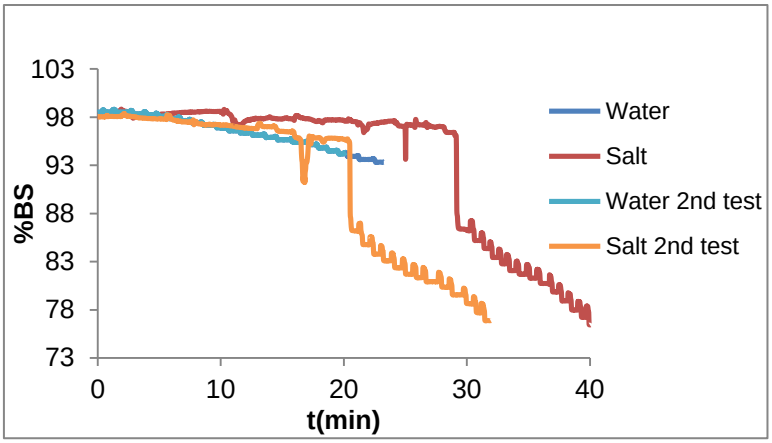

Figure 200: Evolution of backscattering of sample MM1final cleaned, stabilized with [SDS]=3g/L_{water} and with SC= 5%w/w during coagulation and addition of water, measured with Turbiscan^{TM}Lab. T=26ºC.

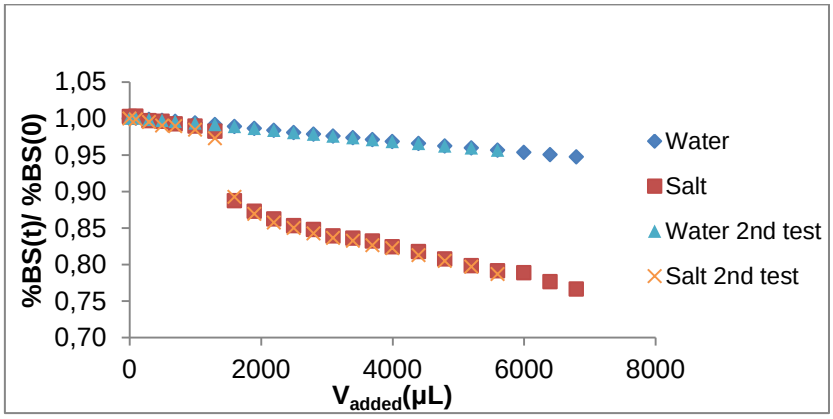

Figure 201: Evolution of backscattering normalized of sample MM1final cleaned, stabilized with [SDS]=3g/L_{water} and with SC= 5%w/w during coagulation and addition of water, measured with Turbiscan^{TM}Lab.

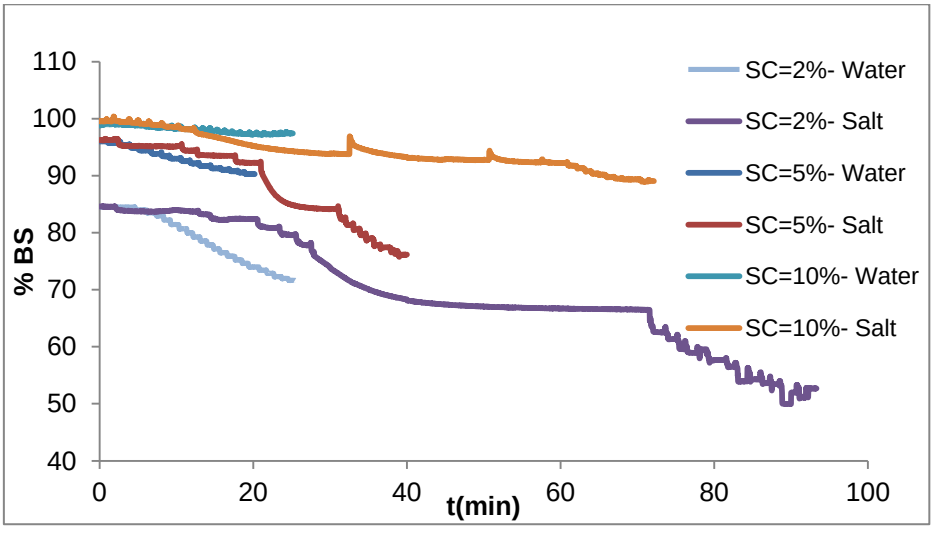

Figure 202: Evolution of backscattering of sample MM2 (5) at different SC during coagulation and addition of water, measured with Turbiscan^{TM}Lab. $T_{SC=2\%}$=25.5ºC, $T_{SC=5\%}$=26ºC, $T_{SC=10\%}$=26.5ºC.

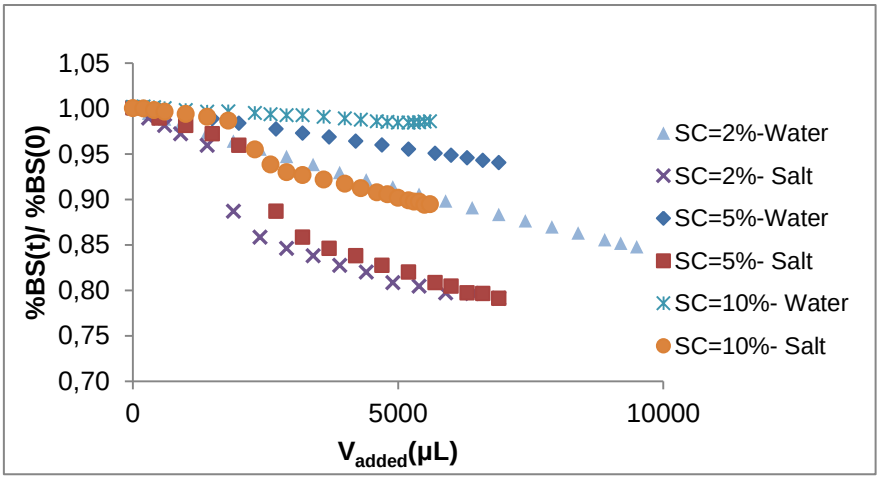

Figure 203: Evolution of backscattering normalized of sample MM2 (5) at different SC during coagulation and addition of water, measured with Turbiscan^{TM}Lab. $T_{SC=2\%}$=25.5ºC, $T_{SC=5\%}$=26ºC, $T_{SC=10\%}$=26.5ºC.

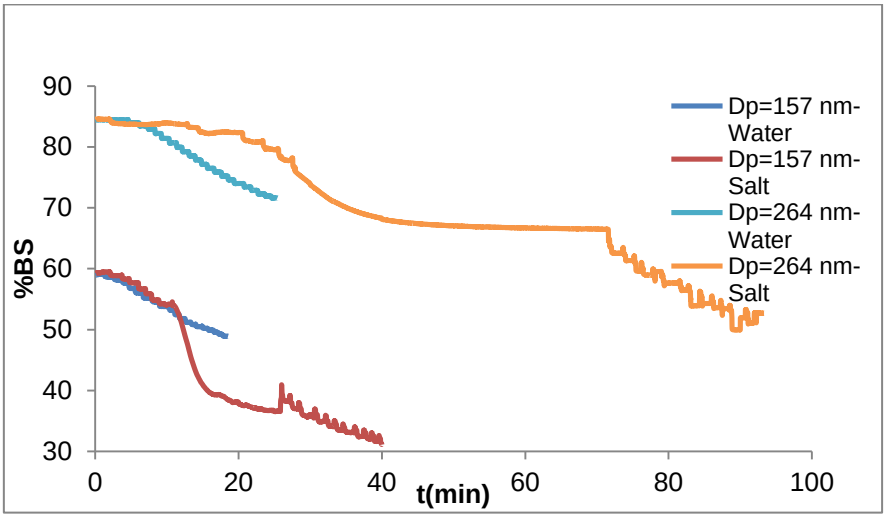

Figure 204: Evolution of backscattering of sample MM2 (5) at 5%w/w and different particle sizes during coagulation and addition of water, measured with Turbiscan^{TM}Lab. $T_{Dp=157nm\ (1st\ test)}$=25.5ºC, $T_{Dp=264nm}$=25.5ºC.

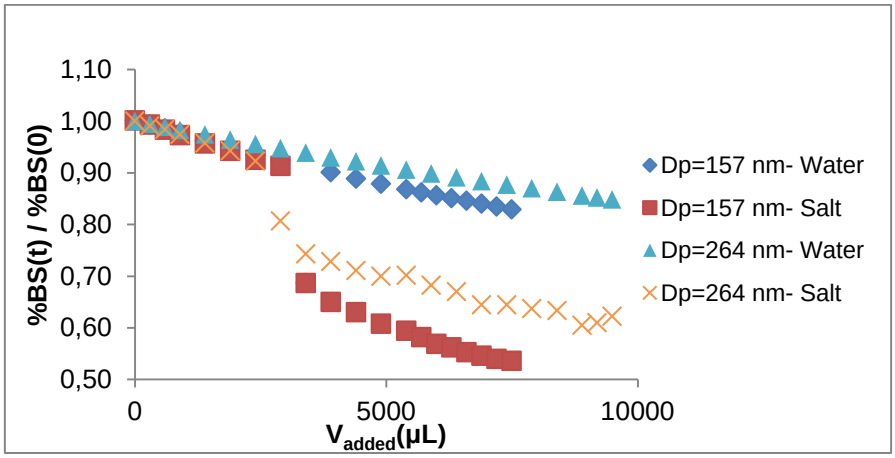

Figure 205: Evolution of backscattering normalized of sample MM2 (5) at 5%w/w and different particle sizes during coagulation and addition of water, measured with Turbiscan^{TM}Lab.

III. Calculations

Applying the equation (23) was possible to calculate the volume fraction. To determine the volume of polymer, $v_{polymer}$, by equation (24), the mass of polymer in latex, $m_{polymer}$, is a necessary value, which can be calculated by equation (26), where the m_{total} corresponds to the total mass of latex. Knowing the mass of polymer, the mass of water in latex, m_{water}, was calculated by equation (27). With this value, the volume of water, v_{water}, was calculated by equation (25).

$$SC(\%\, v/v) = \frac{v_{polymer}}{v_{total}} = \frac{v_{polymer}}{v_{polymer} + v_{water}} \quad (23)$$

$$\rho_{polymer} = \frac{m_{polymer}}{v_{polymer}} \Rightarrow v_{polymer} \quad (24)$$

$$\rho_{water} = \frac{m_{water}}{v_{water}} \Rightarrow v_{water} \quad (25)$$

$$SC(\%\, w/w) = \frac{m_{polymer}}{m_{polymer} + m_{water}} = \frac{m_{polymer}}{m_{total}} \Rightarrow m_{polymer} \quad (26)$$

$$m_{total} = m_{polymer} + m_{water} \Rightarrow m_{polymer} \quad (27)$$

$\rho_{polymer}$ and ρ_{water} correspond to the density of polymer and water, respectively.

To dilute a sample, the equations 28 and 29 are used, where SC_i, SC_f, $m_{polymer}$, m_{water}, m_{total} and $m_{water\ to\ add}$ correspond to the initial SC, final SC, mass of polymer in latex, mass of water in latex, mass of latex to dilute and mass of water necessary to add to have the desired SC_f, respectively.

$$SC_i(\%\, w/w) = \frac{m_{polymer}}{m_{polymer} + m_{water}} = \frac{m_{polymer}}{m_{total}} \quad (28)$$

$$SC_f(\%\, w/w) = \frac{m_{polymer}}{m_{total} + m_{water\ to\ add}} \quad (29)$$